Laser-based investigation of the sooting combustion of additised diesel fuel

Lasergestützte Untersuchung der rußenden Verbrennung von additiviertem Dieselkraftstoff

Der Technische Fakultät

der Friedrich-Alexander-Universität
Erlangen-Nürnberg
zur
Erlangung des Doktorgrades Dr.-Ing.
vorgelegt von
Natascia Palazzo, M.Sc.
aus Torino, Italien

Als Dissertation genehmigt

von der Technische Fakultät

der Friedrich-Alexander-Universität Erlangen-Nürnberg

Tag der mündlichen Prüfung: 29.04.2021

Vorsitzende des Promotionsorgans: Prof. Dr.-Ing. Knut Graichen

1er Gutachter: Prof. Dr.-Ing. Stefan Will

2er Gutachter: Prof. Dr. Rainer Suntz

Acknowledgement

I would like to acknowledge Prof. Stefan Will for his attentive supervision and for all the precious suggestions for my thesis.

I acknowledge Franz and Lars for the valuable professional support and feedback and for the friendly and kind atmosphere they created in my research group.

I acknowledge my colleagues Matthias Koegl for the design of the burner and for his big help, Simon Assmann for the extinction measurements and all his advices and the other people of my fabulous research group Partikelmesstechnik: Bettina Münsterjohann, Florian Bauer, Markus Labus. I acknowledge Sebastian Riess and Andi Peter for the important support during the measurement campaign in the constant volume chamber.

I acknowledge Peter Demmelmeyer, Marius Wesmas-Murgu, Thomas Dressel, Ralf Lindner and Bernd Felske for their valuable technical support.

I would like to acknowledge my students Philipp Bauer and Benjamin Wulf Klevansky for their help during the measurements.

I would like to acknowledge Manu and Mijo, from my project IPPAD, for their collaboration and precious help.

I would like to acknowledge the IPPAD ITN Project - Marie-Curie Innovative Training Network Project, HORIZON 2020, for the financial support.

Abstract

Soot emitted by combustion engines is a dangerous environmental pollutant and it must be kept as low as possible also to meet emission limit regulations. PM reduction strategies include reformulation / modification of existing fuels by the use of fuel additives. The principle goal of the present work is to isolate and comprehend the effect of fuel's additives on particulate emission. During this study a self-designed burner has been implemented and optimized to obtain a laminar diesel flame. Subsequently, the combustion of pure diesel fuels and diesel fuels additised with different ether compounds (oxymethylene dimethyl ethers, OMEs, and tripropylene glycol methyl ether, TPGME), inserted in increasing concentration, has been investigated by optical methods, namely laser-induced incandescence (for evaluation of soot volume fraction), elastic light scattering (for the characterization of soot aggregate size) and two-color pyrometry (for temperature estimation). The optical diagnostics have been combined with a non-optical one, the scanning mobility particle sizer that was employed for particles diameter evaluation. The role of the additives during the soot formation process was investigated on the burner set-up and on spray flames generated in a constant volume combustion chamber (the latest was employed only for soot concentration analysis). The results found show that the production of soot (i.e. soot volume fraction) is inhibited by the addition of oxygenated additives, especially OME with longer molecular chain. The reduction of soot concentration observed, compared to the pure diesel, goes up to a maximum of 36% for the long chain OME-diesel blend and 27% for the TPGME-diesel blend, in the laminar flame conditions. This trend has been confirmed by the measurements on spray flames where the conditions are more similar to a realistic diesel engine. In this case the amount of soot produced by the diesel additised with the oxygenated species decreases up to 88% for OME-diesel blend and 84% for the TPGME-diesel blend, compared to the neat diesel (in both cases the maximum soot drop was observed at higher temperature/pressure conditions). Soot aggregate size is also found to be affected by additives addition. In particular, the soot aggregate size obtained for OME-diesel blend is ~20% smaller than the one obtained for the pure diesel, while TPGME decreases aggregate size of ~13% compared to pure diesel. The same trend has been obtained from scanning mobility particle sizer measurements. On the contrary, soot temperature does not seem to vary significantly when additives are inserted. Overall, the burner implemented and the laminar flame obtained allowed a successful characterization of soot properties by using optical and non-optical diagnostics. Generally, the additive's effect on soot concentration and morphology results to be in most cases proportional to the additive's concentration and the number of C-O bonds in the additive's molecule. Furthermore, the results of this study show that, although the effect of additives is observed during the whole combustion, the maximum reduction of soot concentration and size is achieved at the end of the combustion process. The additives seem to enhance the oxidation process due to their molecular structure that can release oxygen.

Kurzfassung

Der von Verbrennungsmotoren ausgestoßene Feinstaub (PM), der auch als Ruß bezeichnet wird, ist ein gefährlicher Umweltschadstoff und wird so gering wie möglich gehalten, um die Emissionsgrenzwerte einzuhalten. Zu den Strategien zur Reduzierung von PM gehören die Neuformulierung/Modifizierung bestehender Kraftstoffe durch den Einsatz von Kraftstoffadditiven. Das Hauptziel der vorliegenden Arbeit ist es, die Wirkung der Kraftstoffadditive auf die Partikelemission zu isolieren und zu verstehen. Im Rahmen dieser Arbeit wurde ein selbst entworfener Brenner implementiert und optimiert, um eine laminare Dieselflamme zu erhalten. Anschließend wurde die Verbrennung von reinen Dieselkraftstoffen und Dieselkraftstoffen, die mit verschiedenen Etherverbindungen (Oxymethylendimethylether, OMEs, und Tripropylenglykolmethylether, TPGME), die in zunehmender Konzentration zugesetzt wurden, mit optischen Methoden, nämlich laserinduzierter Inkandeszenz (zur Auswertung des Rußvolumenanteils), elastischer Lichtstreuung (zur Charakterisierung der Rußaggregatgröße) und Zweifarb-Pyrometrie (zur Temperaturabschätzung) untersucht. Die optische Diagnostik wurde mit einer nicht-optischen kombiniert, dem Scanning Mobility Particle Sizer (SMPS), der zur Auswertung des Partikeldurchmessers eingesetzt wurde. Die Rolle der Additive während des Rußbildungsprozesses wurde an der Brennereinrichtung und an Sprühflammen, die in einer Brennkammer mit konstantem Volumen erzeugt wurden, untersucht (letztere wurden nur für die Analyse der Rußkonzentration verwendet). Die gefundenen Ergebnisse zeigen, dass die Rußbildung (d.h. der Rußvolumenanteil) durch die Zugabe von sauerstoffhaltigen Additiven, insbesondere OME mit längerer Molekülkette, gehemmt wird. Die beobachtete Verringerung der Rußkonzentration im Vergleich zum reinen Diesel geht unter den laminaren Flammenbedingungen bis zu einem Maximum von 36% für die langkettige OME-Dieselmischung und 27% für die TPGME-Dieselmischung. Dieser Trend wurde durch die Messungen an Sprühflammen bestätigt, wo die Bedingungen einem realistischen Dieselmotor ähnlicher sind. In diesem Fall sinkt die Rußmenge, die von dem mit der sauerstoffhaltigen Spezies versetzten Diesel erzeugt wird, im Vergleich zum reinen Diesel um bis zu 88% für OME-Dieselgemische und 84% für das TPGME-Dieselgemische (in beiden Fällen wurde der maximale Rußabfall bei höheren Temperatur-/Druckbedingungen beobachtet). Es wird auch festgestellt, dass die Rußaggregatgröße durch die Zugabe von Additiven beeinflusst wird. Insbesondere ist die für OME-Dieselgemisch erhaltene Rußaggregatgröße ~20% kleiner als die für reinen Diesel, während TPGME die Aggregatgröße um ~13% im Vergleich zu reinem Diesel verringert. Der gleiche Trend wurde aus den SMPS Messungen erhalten. Im Gegenteil scheint die Rußtemperatur nicht signifikant zu variieren, wenn Additive eingesetzt werden. Insgesamt ermöglichten der eingesetzte Brenner und die erzielte laminare Flamme eine erfolgreiche Charakterisierung der Rußeigenschaften durch optische und nicht-optische Diagnostik. Im Allgemeinen ist die Wirkung des Additivs auf die Rußkonzentration und Morphologie in den meisten Fällen proportional zur Konzentration des Additivs und der Anzahl der C-O-Bindungen im Molekül des Additivs. Darüber hinaus zeigen die Ergebnisse dieser Studie, dass, obwohl die Wirkung von Additiven während der gesamten Verbrennung beobachtet wird, die maximale Reduktion der Rußkonzentration und -größe am Ende des Verbrennungsprozesses erreicht wird. Die Additive scheinen aufgrund ihrer Molekularstruktur, die Sauerstoff freisetzen kann, den Oxidationsprozess zu fördern.

List of contents

0. Symbols and abbreviations

Latin letters

Notation	Parameter	Unit
a	monomer radius	m
$B(t)$	laser irradiance	W/m^2
c	speed of light	m/s
C	Cunningham factor	-
$C_{p,\mathrm{air}}$	heat capacity of air at constant pressure	J/Kg·K
C_v	heat capacity of air at constant volume	J/K
D	distance between two electrodes	m
D_f	fractal dimension	-
d_ae	aerodynamic diameter	m
d_i	inner electrode diameter	m
d_o	outer electrode diameter	m
d_p	primary particle diameter	m
E	electric field	V/m
e	elementary unit of charge	C
$E(m)$	refractive index function for absorption	-
E_n	heat energy	J
f	focal length	m
F_E	electrostatic force	N
f_V	volume fraction	ppm
h	Planck's constant	J·s
H_v	energy for evaporation	J
I	radiation intensity	W/m^2
k	refractive index of soot, imaginary part	-
k_b	Boltzmann's constant	J/K
k_o	proportionality constant of order unity	-
K	constant for non-idealities of bath gas	-
K_λ	extinction coefficient	m^{-1}
l	path length of the beam in the flame	m
L_e	electrodes' length	m
L_z	cylinder length	m
m	complex refractive index of soot	-

M_{LP}	spectral emission of the lamp	W/m^2
n	refractive index of soot, real part	-
N	number of monomers per aggregate	-
N_c	number of elementary charges	-
n_d	number density of clusters	-
N_m	total number of monomers	-
p_v	vapour pressure	Pa
q	scattering vector magnitude	m^{-1}
$\dot{Q}_{abs}$	heating rate due to absorption	W
$\dot{Q}_{ann}$	heating rate due to annealing	W
$\dot{Q}_{cond}$	cooling rate due to conduction	W
$\dot{Q}_{ox}$	heating rate due to oxidation	W
$\dot{Q}_{rad}$	cooling rate due to radiation	W
$\dot{Q}_{sub}$	cooling rate due to sublimation	W
$\dot{Q}_{therm}$	cooling rate due to thermionic emission	W
r_{pos}	radial position where the electric field is calculated	m
R	gas constant	-
R_g	radius of gyration	-
$R_{g,eff}$	effective radius of gyration	m
$S(qR_g)$	structure factor	-
t	time	s
T	temperature	K
U	voltage	V
U_{int}	soot particle's internal energy	J
$\dot{V}_a$	aerosol volume flow	m^3/s
$\dot{V}_{air}$	air volume flow	m^3/s
$\dot{V}_{in}/\dot{V}_{out}$	total volume flow in / out	m^3/s
v_p	particle's velocity	m/s
v_{vol}	velocity of the total volume flow	m/s
W	molecular weight	g/mol
x_{dis}	distance covered by the particle in the x-direction from the moment of its ejection to its deposition	m
Z	electrical mobility	$m^2/V \cdot s$

Greek letters

Notation	Parameter	Unit
α_T	thermal accommodation coefficient	-
α_M	mass-accommodation coefficient	-
β	evaporation coefficient	-
γ	heat-capacity ratio	-
ε	Soot emissivity	-
η	dynamic viscosity	kg/m·s
θ	scattering angle	°
κ_a	thermal conductivity	W/m·K
λ	wavelength	m
λ_{L}	laser wavelength	m
$\mu_{\mathrm{g,eff}}$	median effective radius of gyration	m
σ	standard deviation	-
σ_{abs}	absorption cross section	m^2
τ	detection system sensitivity	-
Φ	equivalence ratio	-

Abbreviations

Notation	Meaning
CCD	Charged Coupled Device
CHRCR	Clustering of hydrocarbons by radical-chain reactions
CPC	Condensation Particle Counter
CW	Continuous Wave
DI	Direct injection
DMA	Differential Mobility Analyser
DME	Dimethyl ether
DMM	Dimethoxymethane
ELS	Elastic Light Scattering
EOI	End of injection
FWHM	Full Width at Half Maximum
HAB	Height above the burner
HACA	Hydrogen abstraction carbon addition
IDI	In-direct injection
IR	Infrared
LIF	Laser-induced fluorescence
LII	Laser-induced incandescence
NTP	Normal Temperature and Pressure
OME_2	Oxymethylene dimethyl ether with two CH_2-O groups
OME_{3-5}	Mixture of Oxymethylene dimethyl ethers containing three to five CH_2-O groups
OMEs	Oxymethylene dimethyl ethers
PAH	Polycyclic Aromatic Hydrocarbons
PM	Particulate Matter
POMDME	Poly oxymethylene dimethyl ethers
RDG-FA	Rayleigh-Debye-Gans theory for fractal aggregates
ROI	Region of interest
RSR	Resonance-stabilized radical
SMPS	Scanning Mobility Particle Sizer
TDC	Top dead center
TPGME	Tripropylene Glycol Methyl Ether
UV	Ultraviolet
WALS	Wide-Angle Light Scattering

Subscripts

Notation	Meaning
a	Aerosol
abs	Absorption
ann	Annealing
agg	Aggregates
c	Charges
cond	Conduction
crit	Critical
dis	Distance
E	Electrostatic
e	Electrode
eff	Effective
g	Gyration
gas	Gas
i	Inner
L	Laser
LP	Lamp
m	Monomers
o	Outer
ox	Oxidation
p	Particle
pos	Position
rad	Radiation
s	Soot
therm	Thermionic
V	Volume
vol	Volume flow
z	Cylinder

1. Introduction

Diesel engines are largely employed in the commercial transportation industry because of their reliability, thermal efficiency, durability, and, consequently, their economical advantage compared to gasoline engines [1]. Furthermore, diesel engines have shown to emit a lower amount of carbon dioxide (known to be a greenhouse gas) [1]. However, diesel engines have several major drawbacks such as the higher emission of particulate matter (PM) and nitric oxides (NO_X). In particular, PM emissions, mainly constituted by soot particles, are a serious concern due to their harmful impact on climate change (soot particles strongly absorb in the visible light influencing cloud formation and accelerating snow and ice melting) and public health. Different studies have shown that diesel exhaust gases are associated with acute inflammation of the lungs and chronic lung function deterioration, lungs cancer, asthma, eye irritation, heavy breathing and wheezing [2-4]. Consequently, public institution in charge of environment and health protection have issued strict PM emission limit regulations, which are going to become even more restrictive in future years. Deeper understanding of PM formation is necessary for fuel engineers and engine designers to develop better fuels and technologies which can reduce emission levels and consequently meet future emission regulations. Soot formation in engines is a complex process which is influenced by various elements such as chemical composition of the fuel, atomization, air-fuel mixture proportion, turbulence level, pressure, injection time and ignition delay [5].

The three main strategies adopted for limiting diesel engine emissions are the reduction of soot directly in-cylinder, the post-treatment of the exhaust (filtering), and fuel modification. Regarding the modification of the fuel, different methods, from complete replacement of the diesel fuel to the insertion of small amounts of additive, have been explored [6, 7]. One of the most effective approach found is the insertion of oxygenated species into the diesel fuel. Indeed, several studies show that a growth of the fuel's oxygen content causes a direct decrease of soot emissions, probably due to the suppression of C-C bonds [8, 9]. The influence of the additive molecular structure on the carbonaceous particulate emitted by engines is also significant. For instance, it has been noted that ethers have a lower sooting tendency than alcohols [10].

The overall objective of this work is the investigation of the effect of oxygenated additives on soot production from diesel combustion. In order to better understand chemical effects of additives, it is necessary to separate the impact of the fuel's chemical composition on soot formation and oxidation processes from other physical factors which could at the same time influence soot emissions. For this purpose, a novel burner for diesel pre-vaporization and

combustion was implemented during this work. The pre-vaporization of diesel allowed to bypass the physical effects mainly connected to the vapour-liquid phase of the spray. The burner implemented generates a diesel laminar diffusion flame where the key steps of soot formation can be examined in simplified conditions by using in-situ optical techniques. Accordingly, the flame obtained was characterized by Laser-Induced Incandescence (LII) and Wide-Angle Light Scattering (WALS) which were employed for the determination of soot volume fraction and radius of gyration of soot aggregates, respectively. Following the characterization of the system, the effect of highly-oxygenated additives on diesel combustion was investigated by LII, WALS and other complementary techniques such as a Scanning Mobility Particle Sizer (SMPS), for particle's diameter characterization, and Two-color pyrometry, for temperature investigation. After a review of the literature concerning oxygenated fuel additives, three ether compounds were selected as additive: Tripropylene Glycol Methyl Ether (TPGME), chemical structure CH_3-OC_3H_6-$(OC_3H_6)_2$-OH, and two poly oxymethylene dimethyl ethers (POMDME or OMEs, chemical structure CH_3-O-$(CH_2$-$O)_n$-CH_3), specifically OME_2 (meaning two CH_2-O groups) and $OME_{3\text{-}5}$ (a mixture of OMEs containing 3, 4 and 5 CH_2-O groups).

The present thesis will first review the state of the art about soot formation and oxidation processes, the properties of soot, its development during diesel combustion and the effect of additives on soot emissions from diesel engines. A detailed description of the novel diesel burner, the spray flame chamber and the in-situ techniques and set-ups employed for soot characterization follows. Finally, the most significant results will be presented. This work shows how the chemical structure of the fuel affect the properties of the soot produced during diesel combustion. Furthermore, this work presents experimental results concerning the influence of highly-oxygenated species on the change of soot concentration and aggregate size in diesel flames, relevant for soot formation models and for developing emission reduction strategies. Moreover, a comparison between the results achieved from experiments on the laminar diffusion flame and measurement data collected in a constant volume combustion chamber (diesel engine-like conditions) are provided. To conclude, an overall comparison within the additives investigated and their effect on soot production are performed and the major outcomes of the study are summarized.

2. State of the art

2.1 Soot

2.1.1 Soot formation and oxidation processes

In order to understand the effect of diesel additives on soot emissions it is necessary to have a closer look into the soot formation process. Soot is produced by incomplete combustion of organic substances. In urban areas the production of soot mostly derives from the fuel-rich combustion of engines. The formation of soot can be described as a gaseous-solid phase reaction which converts hydrocarbon molecules into carbonaceous particles. This process is extremely complex. It has been widely discussed in several papers [8, 11-17]. A schematic diagram illustrating the main steps of the soot formation process is shown in Figure 1. Although many details concerning the chemical-physical interactions behind soot formation are still unclear, there are some main steps generally accepted:

- *Nucleation of particles from precursors*

Large aromatics rings or Polycyclic Aromatic Hydrocarbons (PAH) are commonly recognised as soot precursors [8]. PAH are generally formed through addition of acetylene molecules, originated from fuel's degradation, to single ring aromatics. Subsequently to the formation of precursors, particle inception occurs. The transition from gas-phase hydrocarbons to soot is not well understood and still controversial. Mainly two paths are suggested that can lead to soot inception: a) PAH molecules interact by van der Waals forces to form clusters and b) PAHs join into covalently bound clusters [16]. As for the first mechanism, soot inception usually begins around 1450 K (± 250 K) [16], at which temperature PAHs are mainly constituted by two to five aromatic rings; this means that their volatility is too high to consent nucleation by van der Waals forces. A chemical mechanism that yields to covalent bonds within PAHs is consequently more reasonable. In a recent work Johansson et al. [18] hypothesize a reaction pathway involving radicals. The radicals, by reacting with others hydrocarbons through hydrogen-abstraction and hydrogen-ejection, lead to the formation of covalently bound clusters of PAH. According to Johansson et al. [18] the process is triggered by resonance-stabilized radical (RSR) species. These species have an unpaired electron and consequently high reactivity. First, the RSR's dimension enlarges through acetylene (C_2H_2) or vinyl (C_2H_3) addition, maintaining the unpaired electron. Because of the unpaired electron these species combine easily with others radicals as well as with closed-shell hydrocarbons extending in this

way the conjugation. This foster radical-chain reactions leading to regenerate RSRs. Lastly, a "pool" of resonance stabilized radicals is formed, any of them can generate a 1 nm – 5 nm incipient soot particle. The reaction of radicals on the incipient particles' surface with others hydrocarbons promotes molecular growth and can develop into 10 nm - 50 nm soot particles. This mechanism has been called clustering of hydrocarbons by radical-chain reactions (CHRCR). The nascent soot has a molecular mass of about 2000 atomic mass units (u) [11].

- *Mass growth*

Soot nuclei enlarge by surface reactions with gas species such as acetylene and PAH molecules as well as radicals. It is believed that the reactions develop via hydrogen abstraction carbon addition (HACA) process [15]. The HACA mechanism is promoted by reactive sites originated from soot interaction with H and OH radicals which in turn interfere with C-H bonds located on the soot surface. Consequently, the mass growth is highly influenced by surface properties. Johansson et al [18] proposed that the CHRCR mechanism can also contribute to particle-surface growth under high-temperature conditions. Indeed, larger carbonaceous particles display surface-radical sites similar to RSRs ones.

- *Coagulation*

Another mechanism which significantly contributes to particle growth is coagulation. During this process two or more small particles, by mean of sticking collisions between them, join to form a larger one. The coagulation process significantly increases the particle size while the total mass stays the same. Particle coagulation occurs immediately after particle formation. Two mechanisms mainly contribute to particle growth: aggregation and agglomeration. Primary particles can combine by chemical bonds, in this case aggregates are formed. Both primary particles and aggregates can in turn link via physical bonds maintaining their original shape but creating a larger group of particles; this phenomenon is called agglomeration. Agglomerates are characterized by Van der Waals / physical bonds between particles/aggregates.

- *Oxidation process*

The chemical reaction which converts soot particles' carbon into gaseous species such as CO and CO_2 is called oxidation. This process decreases the mass of soot. Under fuel-rich conditions OH, O and, in less amount, O_2, act as oxidizing elements. On the other hand in fuel-lean flames other species, i.e. H_2O, CO_2, NO_x, could potentially be oxidants. Oxidation takes place on particle surfaces. Consequently, the surface area, together with the concentration of oxidants, affect the oxidation rate [19].

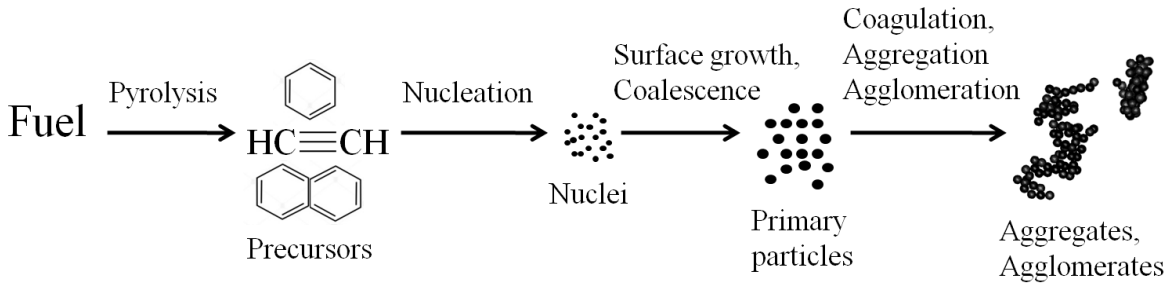

Figure 1. *Schematic diagram of the main steps of the soot formation process. Figure after[20] with additions.*

2.1.2 Influence of fuel chemical composition on soot formation

Several fuel properties are related to particulate emissions from engines: cetane number (indicator of ignition characteristics), fuel density, boiling point, viscosity, etc. Among them, the fuel chemical composition is one of the principal factors governing the sooting tendency of fuels [21]. Starting from pure hydrogen, which does not emit any soot during combustion, as the ratio of carbon to hydrogen increases (C/H ratio), the tendency of a fuel to generate particulates grows. In general, sooting tendencies of hydrocarbons rise following the order: n-paraffins < isoparaffins < naphthenics < aromatics [22]. Moreover, it has been observed that under diffusion flame conditions the trend of aliphatics to generate soot isalkynes > alkenes > alkanes. Indeed, it has been found that during the combustion alkanes are rapidly converted into alkenes. These species are transformed later on to alkynes [23]. The main chain length, the number, position, and length of side chains have secondary effects on soot production. Takatori et al. [24] studied the effect of molecular structure of paraffins on soot formation; they carried out experiments on isomers of hexane and octane (including the ring structure) in a flow reactor (1000 K–1300 K) and in a shock tube (2000 K–2500 K). They noticed that sooting tendencies increase in the order: n-paraffin < 1-branched paraffin < 2-branched paraffin < cycloparaffin. The double bond of carbon (C=C) strongly influences the sooting tendency. It has been observed that cyclohexane (saturated ring) generates more soot than hexane (open chain), but less than benzene (unsaturated ring) [24]. Ultimately, polycyclic aromatic hydrocarbons have shown to be the most prolific sooters. A single-ring aromatic fuel such as benzene expands directly to multiple-ring aromatics by the HACA mechanism.On the other hand an alkane, for example heptane, will produce aliphatic products that must grow to single-ring molecules before they can enlarge to two-ring aromatics. Therefore aromatics have much greater sooting tendencies than alkanes [25].

Consequently, the focus of the majority of the studies on fuels has been related to the role of aromatics. Aromatic fuels are characterised by elevated density and small cetane numbers which in turn affect the liquid length of the injected spray and the ignition delay. It is therefore challenging to decouple the effects of fuel chemical composition from the ones due to physical parameters and engine geometry parameters. Miyamoto et al. [26] studied the effects of the fuel's molecular structure on the exhaust emissions. They inserted various aromatic additives into a mixture of n-tetradecane and heptamethylnonane. The fuels were investigated in both direct injection (DI) and in-direct injection (IDI) single-cylinder engines. The results achieved from the two types of engines were similar. Soot emissions increased linearly with the fuel C/H ratio. The ignition delay and equivalence ratio were constant. Furthermore, the authors observed that di-aromatic fuels had a stronger tendency to produce particulate than mono-aromatic fuels. Accordingly, Tsurutani et al. [27] found that the tendency of aromatics in enhancing PM emissions was mono < di- < tri-aromatics. Bertoli et al.[28] also observed that particulate emission was significantly impacted by di- and tri-aromatics. Bryce et al. [29] measured elevated soot concentrations in diffusion flames and in an IDI engine with increasing amounts of aromatic additive.

Soot production has also been found to be strongly dependent on the ratio of carbon-to-oxygen atoms in the fuel. Böhm et al. [30] estimated that the soot volume fraction in C_2H_4-air flames is proportional to $(C/O - (C/O)_{crit})^n$ with n ranging from 3.5–4. Data in the literature demonstrates that an increased oxygen content in the fuel abates soot particulates [6]. Hallgren and Heywood [31] in their study calculated that soot decreases in a logarithmic way with increasing percentage of oxygen. Indeed, a higher oxygen content in the fuel increases the combustion efficiency and the burn rates as indicated by the reduction of HC, CO and other exhaust pollutants [32]. Mueller and Martin [33] investigated the behaviour of two oxygenated fuels, dibutyl maleate and tri(propylene glycol) methyl ether, in a DI optical engine. The fuels had the same oxygen content but different structure. Flame luminosity was used to compare soot production. The spatially integrated luminosity for dibutyl maleate was higher than the luminosity of tri(propylene glycol) methyl ether, meaning that not only the amount of oxygen but also the molecular structure of the oxygenated fuel influences flame luminosity.

Finally, the presence of sulphur in the fuel increases particulate mass. Sulphur is usually oxidized to SO_2. This specie can combine with unburned hydrocarbons and be absorbed by neighboring soot particles yielding to more soot.

In conclusion, most investigators agree that a higher number of C-C bonds, C=C double bonds and aromatic structures enhance the sooting tendency of the fuel. At the same time, a high percentage of oxygen in the fuel composition generally leads to a reduction of soot formation.

2.1.3 Soot properties

At the end of the combustion process, soot is constituted by roughly eight parts of carbon and one part of hydrogen with a density of about 1.85 g/cm^3[34]. Primary soot particles are nearly spherical. They have diameters ranging from 20nm to 50 nm [35]. These primary particles join to form aggregates which acquire various shapes, from relatively straight chains to more compact clusters. The aggregation process depends on the system itself and how it develops [36]. Consequently, it is of great interest to investigate the properties of the clusters formed. In this study we apply scattering diagnostics to infer morphological properties, and therefore a basic mathematical description of aggregates properties is necessary. Quantifiable parameters that can be utilized to describe aggregates are the radius of gyration R_g, which represents the radius of the overall aggregate (different from the monomer radius and the primary particle diameter d_p), and the fractal dimension D_f [37-39]. In a fractal aggregate the number of monomers per aggregate N can be expressed as

$$N = k_0 \left(\frac{R_g}{a}\right)^{D_f}, \quad (1)$$

where k_0 is a proportionality constant, a is the monomer radius. From equation (1) it is clear that the mass of the aggregate increases (or scales) by increasing the overall size of the aggregate to the D_f power. If, during the formation process, the clusters encounter other clusters through random walk and they link together with almost unity probability, D_f ranges between 1.75 and 1.8 [40]. When the motion of the clusters is limited to be a straight line D_f arise to $\simeq$ 1.9 [41]. Finally, when the sticking probability falls drastically, D_f is found to be between 2.1 and 2.2 [42].

Furthermore, to perform quantitative measurements of soot mass or volume fraction by optical techniques, it is necessary to know or assume physical and optical properties of soot. The most important parameter that describes soot optical properties is the soot emissivity ε. The emissivity ε of the particle is defined as the ratio between the thermal energy radiated by the particle and the thermal energy radiated by a perfect blackbody at the same temperature. E is

dependent on the wavelength λ. Assuming that the emission/absorption of the soot particles is equivalent to the emission/absorption of a comparable volume of isolated primary particles with a primary particle diameter $d_p << \lambda$, the emissivity can be written as [43-45]

$$\varepsilon = \frac{4\pi d_p}{\lambda} E(m, \lambda), \tag{2}$$

where $E(m)$ is a function of the complex index of refraction $m = n_m - k_m i$ and is expressed as

$$E(m) = -\mathrm{Im}\left(\frac{m(\lambda)^2 - 1}{m(\lambda)^2 + 2}\right). \tag{3}$$

2.2 Diesel combustion

2.2.1 Combustion and soot formation processes in direct-injection (DI) diesel engines

The combustion taking place in a conventional direct-injection diesel engine can be assimilated to a spray flame combustion. Diesel combustion is typically divided in three phases [46]:
First, a combustion of air-fuel mixed after the ignition delay. This phase is characterized by high reaction rate and steep pressure rise.
Second, the mixing controlled combustion phase, where the heat release is controlled by the fuel injection system (in classical setups the injector needle is in fully open/maximum lift position and the injection rate is constant; nevertheless, in modern applications the system is more complex).
Third, in the late phase the expansion comes into play and the reaction rate is controlled by the temperature after the so called top dead center (TDC). A sketch of the heat release rate for typical conventional diesel combustion [47] is displayed in Figure 2.

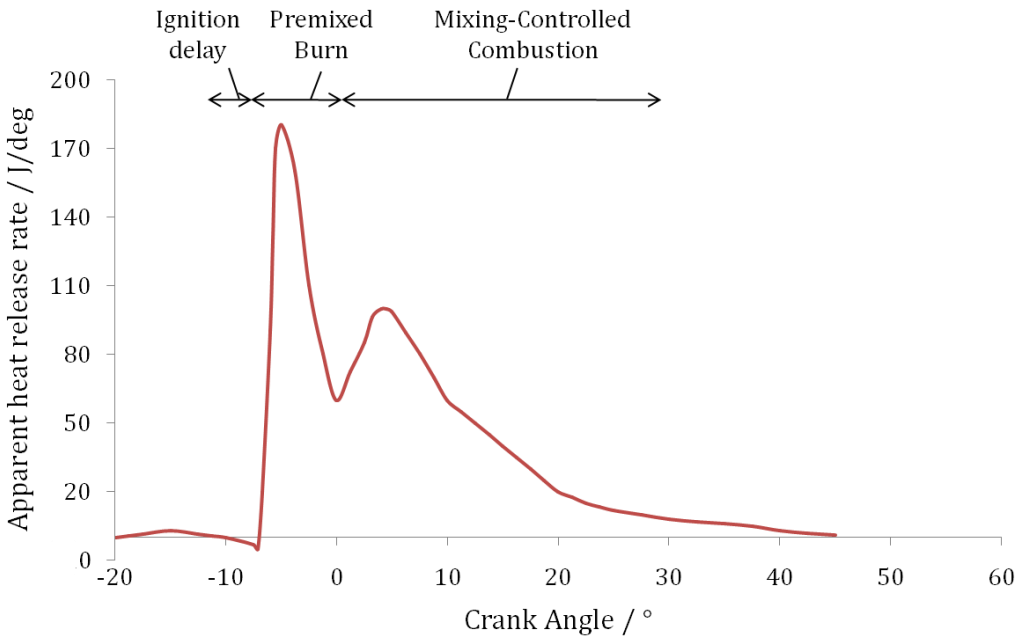

Figure 2. *Schematic draw of the apparent heat release rate for typical conventional diesel combustion. Figure after [47].*

Coming to a more detailed description, the liquid fuel is injected into the cylinder (typically, an engine has six–eight reacting jets in each cylinder) at injection pressures between 35 MPa and 250 MPa. Injection starts close to the end of the compression stroke. Here, temperature and pressure typically range between 850 K –1100 K and 2.4 MPa –12.6 MPa, respectively, corresponding to gas densities of 10 kg/m^3–40 kg/m^3 [48]. As the fuel jet penetrates into the cylinder, it expands into a narrow cone shaped spray entraining the surrounding hot air. The entrained hot air triggers the vaporization of the spray cone. The length of liquid penetration is called the liquid-length [49]. In passenger car applications this value is approximately 20 mm for diesel fuel under the conditions stated above. Beyond the liquid-length there is a vapour region, where no fuel is in the liquid phase. When the fuel/air mixture reaches the ignition temperature, a fuel-rich (in comparison to the globally lean fuel air ratio in the cylinder) combustion reaction occurs. The locally fuel-rich reaction creates soot precursors – poly-aromatic hydrocarbons (PAHs), C_2H_2 – which subsequently yield to the formation of soot. This is the beginning of the quasi-steady phase combustion [47]. In this phase a diffusion flame surrounds the hot products and, after the end of injection (EOI), it moves upstream quickly leaving only some unburned fuel. At this point the jet expands and its structure evolves into a pocket of rich reaction products. The jet reduces in size and breaks into smaller spots as

combustion continues. At the end of the expansion process the temperature decreases until the combustion is quenched.

The distance between the fuel injector and the point where the diffusion flame stabilizes in the stationary phase is called lift-off length. A sketch of the conventional diesel combustion, illustrating the lift-off length, is shown in Figure 3.

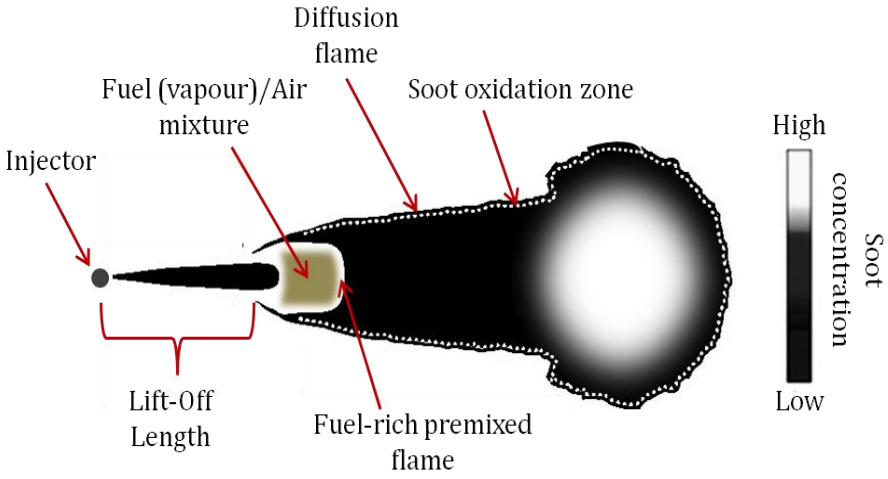

Figure 3. *Sketch of the conceptual model elaborated by Dec et al. [47] for conventional diesel combustion during the quasi-steady period. Figure after[47] with additions.*

The lift-off length is an important parameter for the soot formation process. Fuel and air mix upstream of the lift-off length and react downstream of the lift-off length. The fuel/air mixture formation process, crucial for the subsequent combustion, has been deeply investigated by Riess et al. and Peter et al. [50, 51]. A rich premixed reaction takes place downstream the lift-off length. This premixed reaction releases a significant amount of heat while products like acetylene and ethylene (known as soot precursors) from the unburned or partially burnt fuel are generated. The temperatures in this region range between 1600 K and 1700 K. Radicals like vinyl (C_2H_3), propargyl (C_3H_3), allyl (C_3H_5) and methyl allyl (C_4H_7) are also present [52].Several authors have shown that soot derives partially from this first fuel-rich combustion zone [46, 47]. The lift-off length increases linearly with injection pressure and the percentage of ambient air taken in. Siebers et al. [53] inferred that the flame lift-off length is inversely proportional to the ambient oxygen concentration and dependent on the injection orifice diameter, ambient gas temperature and density.

Other factors which contribute to the creation of soot emissions are the amount of fuel released at the end of the injection, which does not mix completely with air [47], and the quenching of

the final stage of the combustion that yields to incomplete soot oxidation[46, 54]. Two additional mechanisms permit the soot to survive the combustion process: 1) wall and crevice deposition and subsequent removal 2) escape of soot through extinguished regions of the overall diffusion flame [46].

Finally, four parameters emerge as most critical for controlling soot formation in diesel combustion: 1) the lift-off length which is connected to the entrainment of oxygen and therefore the fuel/air ratio in the combustion zone 2) the mass fraction of oxygen in the fuel, 3) the number of C-C bonds (single, double and triple bonds) in the fuel and 4) the temperature in the soot formation region. In particular, the first two parameters control the local equivalence ratio in the fuel-rich premixed zone and appear to influence soot formation massively. It is still unclear if oxygen from the surrounding air is more effective at suppressing soot than fuel bound oxygen or vice versa.

2.2.2 Relevant laboratory diesel flame set-ups

Several works have been carried out on the sooting behaviour of liquid diesel-like fuels, fossil fuel surrogates and biodiesel surrogates under various conditions. The set-ups employed include shock tubes [55, 56], diffusion flames [57-59] and premixed flames [60, 61]. The studies on soot formation in neat diesel flames are restricted to mainly spray flames. Recently, Solero [62] published a study on soot formation in diesel sprays generated by a gas atomizer; diesels were additised with metal oxides nanoparticles such as Al_2O_3. Lemaire et al. [6, 63] in their work compared soot produced by diesel and diesel surrogates. Both authors utilized an atomizer which generated a fuel spray directly vaporized in the flame. Du et al. [64] investigated the influence of injection pressure and nozzle orifice diameter on soot formation. The effect of gas density was also studied [64]. The measurements were performed on a turbulent diffusion diesel flame created in a high-pressure/high-temperature spray chamber where a continuous gas flow was generated. In the study of Matti Maricq [65] a diffusion spray flame for soot investigation from biodiesel and diesel surrogates was achieved by using a syringe pump (for fuel supply) and an injection nozzle. Lemaire et al. [66] implemented a McKenna-Hybrid burner where the classical McKenna burner set-up was coupled with a high efficiency nebulizer for hydrocarbons atomization. The hybrid burner generated a high-speed spray of micro-sized fuel droplets which was subsequently injected in the burner. Recently Tian et al. [67] studied the production of soot from biofuels and biodiesel-diesel blends by employing Laser-Induced

Incandescence (LII) and laser extinction methods. The combustion of the fuels was performed in several co-flow stabilized laminar pool flames.

To specifically investigate only the chemical mechanisms which govern soot production, it is necessary to develop strategies that permit to avoid the effects due to fuel´s physical properties. Within the physical properties of the fuel, the density, viscosity and surface tension of droplets significantly affect the atomization and evaporation time of the gas-liquid aerosol and consequently the combustion itself. One possible solution is to complete pre-vaporize the diesel before the combustion. Nevertheless, due to the high-temperature boiling point of diesels, i.e. around 370 °C, the complete pre-vaporization of this fuel is challenging, considering the low self-ignition temperature (at 210 °C for commercial diesels). Very few examples of non-spray diesel flames have been studied in literature. Gertsmann et al. [68] designed a vaporizing diesel burner for camp stoves and military field kitchens. In the set-up presented the diesel is first vaporized in a vertical tube. Afterward, the diesel is headed toward a super-heater tube. Finally, the fuel is burned on a cylindrical screen flame holder. The flame obtained is not controllable/reproducible, i.e. it cannot be used for soot quantification or morphological studies. The flame is therefore limited to practical applications. Bryce et al. [69] performed measurements on a ~13 mm high diesel flame. The combustion set-up is shown in Figure 4. It is constituted of a vaporizer vessel, a connecting heated tube and a co-flow burner. The vaporizer chamber is kept at 300 °C temperature. The fuel is injected into the burner by means of a needle valve that controls the height of the flame. This system produces a steady flame. However, the injection is not continuous and requires to be monitored to preserve stationary flame conditions.

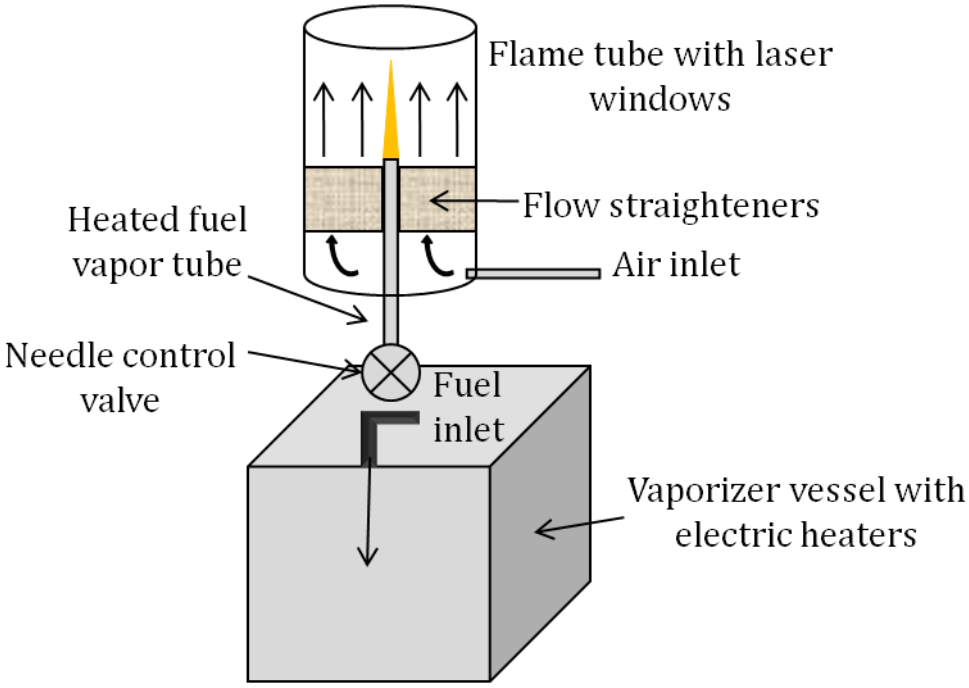

Figure 4. *Sketch of the set-up utilized by Bryce et al. to generate a diffusion diesel flame for quantitative soot investigation. Figure after[69] with additions.*

2.2.3 Effect of additives on soot formation from diesel fuels

The insertion of an additive in the diesel fuel is one of the most used strategies to reduce particulate emissions from combustion [70]. The term “fuel additive” indicates any substance inserted in the fuel that modifies the fuel´s physical and chemical properties [70]. The effect of different kinds of additives on diesel injector flow, spray and soot formation has been investigated in many works [6, 7, 71-73]. Various species have been employed as additives, from water to metal-based additives, detergents and lubricants [72, 73]. For example, detergents (i.e. polyether amines, imidazolines, fatty acid succinimides, polyether amines, etc.) are able to suppress the formation of deposits on the injector and thus decreasing the injector ageing with a consequent reduction of soot formation during long-term operation [73, 74]. Recently, it has been noted that oxygenated species such as mono-alkyl esters, long-chain fatty acid, n-butanol, methanol, etc. have a lowering effect on soot emissions [6, 75, 76]. In fact, numerous studies indicate that an increment of the number of oxygen atoms in the fuel’s molecular structure/blend composition suppresses soot emissions [8, 9]. This phenomenon is probably connected to the reduction of C-C molecular bonds which leads to a drop of soot precursors. Moreover, a growth of oxygen supplies more oxidants for carbon oxidation. On the other hand, the insertion of

biodiesel or in general different alcohol and esters structures seem to slightly increase the amount of NO_x emissions [77, 78]. Imtenan et al. [79] correlated the additive's oxygen content with PM/smoke production. They estimated that the correlation between the additive's capability of decreasing particulate and its oxygen content is up to 95%. Hallgren and Heywood [31] inserted several oxygenated agents to an ultra-low sulphur diesel fuel in a DI diesel engine. They observed that the species added were able to lessen soot. The reduction depended on the percentage of oxygen as well as the type of functional group. Many studies have shown that besides the amount of oxygen inserted, the chemical structure of the additive plays an important role on the overall emissions. The impact of oxygenated additives with various molecular structures or functional groups on soot formation from diesels has been topic of a number of studies. A general overview of the works performed on the effect of oxygenated additives is given here following a classification based on the type (i.e. molecular structure) of additive used.

a) Esters

Ester groups are typically present in biodiesel fuels. The influence of a rapeseed methyl ester, employed as additive, on particulate matter was studied by Lemaire et al. [6]. By using optical methods they measured soot emission from a low sulphur diesel where the methyl ester was inserted in different concentrations (from 10 % vol. to 100 % vol.). The results showed that the insertion of the ester leads to a significant drop of soot amount as well as soot precursors quantity. Tian et al. [67] investigated, by using optical diagnostics, soot emissions of three biodiesels containing methyl esters. The measurements were compared with the pure diesel. They found that particulate matter from pure biodiesels decreased up to 67% compared to the total amount of soot produced by pure diesel. They also observed that the quantity of soot produced correlates directly with the degree of unsaturation of the additised diesels. Several works show that the ester structure of biodiesel-diesel blend leads to relatively higher smoke emissions than alcohol-diesel or ether-diesel blends [71, 80].

b) Alcohols

Various researches report significant PM reduction when ethanol-diesel and dimethylglyoxime-ethanol-diesel blends are employed [71, 81-84]. Also alcohol fumigation into the inlet manifold was proved to be a good soot suppression strategy [85-87]. Cheng et al. [88] traced carbon isotopes in ethanol and demonstrated that carbon from ethanol is about 50% less likely to contribute to soot formation with respect to the carbon from diesel fuel.

c) Ethers

Two-color measurements for temperature estimation in a DI diesel engine by Donahue and Foster [32] displayed that both oxygen enhancement of the intake air as well as oxygenation of the fuel with a ether compound decreased pyrolysis and enhanced oxidation, shortening the combustion duration and reducing particulate matter production. PM reduction effects on exhaust emissions were also found by Beatrice et al. [89] who tested three blends of diglyme-diesel (10 %, 20 % and 30 % in volume) in a commercial DI diesel engine.

Liotta and Montalvo [90] compared PM emissions from ethers and alcohols finding that ethers were more effective than alcohols in reducing PM. A substantial drop of PM emissions was observed in the case of dimethyl ether (DME)-diesel blend combustion[91, 92]. DME performances were tested under different engine operating conditions. In all cases PM emissions were lower. The decrement was correlated to the chemical structure of DME which does not contain any C-C bonds. Many others works followed to that. Ether-based species with raised oxygen content, less C-C bonds and longer C-O chain(s) have been investigated as additives leading to promising results [93, 94]. In particular, two ethers-based species emerged as powerful soot reducer, i.e. Tripropylene Glycol Methyl Ether (TPGME) and poly oxymethylene dimethyl ethers (POMDME or OMEs). OMEs and TPGME were selected in the present study as additives for investigations in a laminar diffusion flame. They will be further described in sections 2.2.3.1 and 2.2.3.2.

Finally, many insights about how the chemical structure of the additive influences the soot produced can be achieved through soot formation models. Kinetic modeling concerning methanol, ethanol, dimethyl ether, dimethoxymethane and methyl butanoate, employed as additives to n-heptane, showed that these compounds lower the concentrations of ignition products (and soot precursors) such as acetylene, ethylene, 1,3-butadiene and propargyl and vinyl radicals [52]. Calculations by Flynn et al. [46] suggested that the formation of particulate precursors is almost completely inhibited at an oxygen-to-fuel mass ratio of 25%. The addition of oxygenated species, beside reducing the production of soot precursors in the fuel-rich premixed zone, increases the concentration of O, OH and HCO, which promotes the oxidation of hydrocarbons to CO and CO_2. Furthermore, higher concentrations of OH in the post-premixed flame region also suppress soot particle inception by oxidizing aromatics and limiting PAH growth.

Lastly, it should be considered that oxygenated compounds, when inserted into diesel fuel, not only modify the oxygen content but also other properties like the cetane number, density or viscosity. All these parameters could affect the fuel ignition time and the distribution of the injected fuel into the chamber which could in turn have an influence on PM emissions.

2.2.3.1 Tripropylene glycol methyl ether

A recent work by Mueller et al. [93] explores soot precursor characteristics and soot emitted by various oxygenated fuels. The study was conducted by carrying out numerical simulations and experiments. The experiments were performed in a constant-volume combustion chamber and in a single-cylinder DI diesel engine. The outcomes of this work highlighted that some oxygenated species were able to lower PM emission. In particular, one of the species investigated, tripropylene glycol methyl ether or TPGME, displayed a significant capability of decreasing soot that was higher compared to other oxygenates. The chemical structure of TPGME is shown in Figure 5. A chemical kinetic model released by Westbrook et al. [95] further investigated the mechanism behind particulate reduction by oxygenated additives. The compounds studied, at diesel engine conditions, included TPGME. The model revealed that the soot drop is due to the decrement of soot precursors. Indeed, the authors showed that adding oxygenated species in the diesel blend causes an abatement of hot products in the fuel-rich diesel ignition zone.

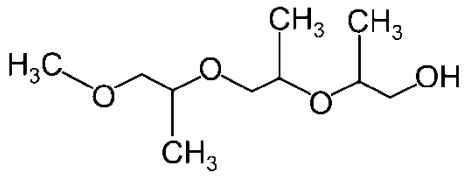

Figure 5. *Molecule of Tripropylene glycol methyl ether (TPGME). Figure from [96]*.

2.2.3.2 Poly oxymethylene dimethyl ethers

The chemical structure of OMEs (also called POMDME) is displayed in Figure 6. In general, OMEs species have a formula CH_3-O-$(CH_2$-O$)_n$-CH_3, where n can range between 1 and 6. Starting from dimethoxymethane or DMM (molecule CH_3–O–CH_2–O–CH_3) all the other molecules of this class are obtained by adding-CH_2-O- groups. The mass fraction of oxygen in OMEs can go up to 50%. Kenney et al. [97] and Sirman et al. [98] report results concerning PM emissions measured in a direct injection diesel engine where 15% DMM-diesel blend was burned. They show that the insertion of DMM suppresses soot emissions considerably at any

speed/load condition tested and at the exhaust. Nevertheless, they state that the replacement of diesel with DMM is not advisable because of the different physical properties between DMM and normal diesel. In fact, DMM has a lower boiling point (42°C), cetane number (=30) and viscosity than a standard diesel. Therefore, a complete substitution would entail a modification of the fuel system of the existing engine. A suitable alternative is the utilization of oxymethylene dimethyl ethers with longer chain. Indeed, long-chain OMEs have properties similar to diesels i.e. a higher boiling point and viscosity. For example, the molecules CH_3-O-(CH_2-O)$_n$-CH_3, where n varies between 2 and 5 and it is written $OME_{2\text{-}5}$, can be employed for diesel blending in any percentage without modification of the engine's injection system. According to Pellegrini et al. [99], who estimated the PM concentration of neat OMEs and OMEs-diesel blends in a Euro-2 diesel passenger car engine, the particulate emitted by a 10% OMEs-diesel blend is 18% less than pure diesel. In the case of neat OMEs, soot production drops by about 77% compared to that from pure diesel. They remarked though that the neat OMEs caused an increase of CO, NO_x and formaldehyde emissions. Iannuzzi et al. [100] investigated soot production from pure OMEs, DMM and several OMEs-diesel blends. They carried out measurements in a constant-volume cylindrical cell by using optical diagnostics. The results obtained show that the soot concentration falls during the soot formation dominated phase and the early start of oxidation. Subsequently, they studied the emission performance of 5% and 10% OMEs-diesel blends [101] in a single-cylinder heavy duty diesel engine. These further measurements revealed a reduction of soot emissions compared to commercial diesel of more than 10% for the 5% OMEs-diesel blend. Furthermore, the suppression of soot for the 10% OMEs-diesel blend was up to 35%.

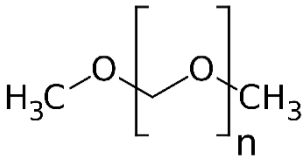

Figure 6. *General chemical structure of OMEs. Figure from [96].*

2.3 Objectives

The principal objective of the present study is the investigation of the effect of diesel additives, specifically oxygenated additives, on soot formation and soot properties. From the review above the importance of discerning the impact of the fuel's chemical composition on soot formation from the physical properties connected to spray and engine characteristics comes to light. Consequently, this work has three main objectives:

- An initial milestone is the implementation of a burner that permits to isolate the influence of the fuel chemical composition on soot formation. The system developed should completely vaporize the fuel in order to avoid a liquid-vapour mixture whose characteristics significantly affect PM emissions. A laminar flame, easy accessible for in situ measurements, is also desirable. Basically the novel burning system should have the capability of a) highlighting the role played by fuel additives during soot formation and b) being suitable for the application of optical techniques (further discussed in section 3.).
- A second milestone is the investigation of the impact of TPGME and OMEs, selected as additives, on soot concentration and particle size. On this purpose optical diagnostics will be employed while the novel burner realized will be used as combustion system. In particular, the aggregate size of the particles emitted governs the uptake of aerosols by the human respiratory system and thus has a major influence on health hazards. The size of the aggregates generated from additive-diesel blends has not been widely explored yet. The investigation of the additive's effect on soot temperature will also be carried out. The knowledge of the temperature has a key role because additives could affect the flame's temperature which can in turn influence soot production.
- A final milestone is the comparison between the results obtained in the laminar flame and the ones achieved on spray flames in a constant volume chamber where the overall conditions are more similar to real engines. This comparison will help to comprehend whether the additive's effect is insignificant, the same or enhanced under engine-like conditions. Furthermore, these measurements will underline the effect of the fuel's chemical composition within the whole physical, chemical and mechanical effects.

3. On-line techniques used for soot investigation

For the investigation of particulate matter numerous off-line and on-line analytical techniques are used. Within the off-line techniques we can mention electronic microscopy, X-ray diffraction, Raman spectroscopy, and thermogravimetric analysis. Also infrared spectroscopy, soot reactivity towards O_2 and NO, UV–Visible spectroscopy, size exclusion chromatography and fluorescence spectroscopy are off-line techniques commonly employed for soot characterization [102]. During the combustion itself, soot development is mostly studied by on-line techniques which avoid particle sampling and the directly connected perturbation of the combustion conditions (i.e. the flame). Within the on-line techniques, laser-based techniques are preferred due to the possibility of in situ measurements [103]. Furthermore, these techniques have the desirable capability of a temporally and spatially resolved visualization of soot. In the present work we chose to utilize two well-established laser-based methods: Laser-Induced Incandescence (LII) for the investigation of the soot concentration and Elastic Light Scattering (ELS) for the characterization of the aggregate size of the particles. The background of these techniques is described in paragraphs 3.1 and 3.2. Furthermore, two non-laser based methods are employed for further soot characterization, namely Scanning Mobility Particle Sizer (SMPS) analysis, for the measurement of particles' mobility diameter, and Two-color pyrometry, for the evaluation of the soot particles temperature. These two techniques are described in the paragraphs 3.3 and 3.4.

3.1 Laser-Induced Incandescence

For the Laser-Induced Incandescence (LII) technique a high-power laser (either constant wave, CW, or pulsed) is employed to heat (usually) carbonaceous particles up to a temperature high enough to have sufficient radiation signal, which often corresponds to the temperature of sublimation (i.e. beyond 3000 K). The absorption of the laser energy by the soot particle and the consequent rapid temperature rise causes the emission of enhanced thermal radiation, i.e. the Planck radiation or incandescence. Theoretical and experimental studies have demonstrated that the LII signal peak, detected right after the laser pulse, is roughly proportional to the soot concentration while the signal's decay time leads to the estimation of the primary particle's size [104]. The typical LII signal decay over time after the laser pulse, together with the temperature development, is shown in Figure 7.

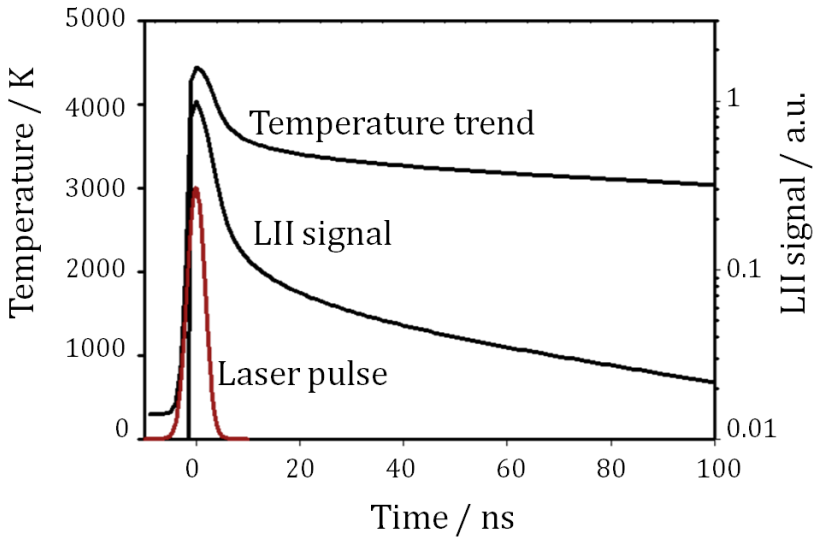

Figure 7. *LII signal and temperature decay over time after the laser pulse.*

When the laser pulse hits the soot particle, different phenomena occur: absorption, radiation, conduction, sublimation, annealing, thermionic emission are some examples. Accordingly, the particle's internal energy U_{int} changes as described by

$$\frac{dU_{\mathrm{int}}}{dt} = \dot{Q}_{\mathrm{abs}} + \dot{Q}_{\mathrm{rad}} + \dot{Q}_{\mathrm{cond}} + \dot{Q}_{\mathrm{sub}} + \dot{Q}_{\mathrm{ox}} + \dot{Q}_{\mathrm{ann}} + \dot{Q}_{\mathrm{therm}}. \quad (4)$$

In this relation the change in internal energy U_{int} over time t is equal to the sum of the heating rate due to absorption $\dot{Q}_{\mathrm{abs}}$,the cooling rate due to radiation $\dot{Q}_{\mathrm{rad}}$, the cooling rate due to conduction $\dot{Q}_{\mathrm{cond}}$, the cooling rate due to sublimation $\dot{Q}_{\mathrm{sub}}$, the heating rate due to oxidation $\dot{Q}_{\mathrm{ox}}$, the heating rate due to annealing $\dot{Q}_{\mathrm{ann}}$ and finally, the cooling rate due to thermionic emission of electrons $\dot{Q}_{\mathrm{therm}}$. The Eq. 4 represents the energy balance of the soot particle during irradiation with laser light and allows to infer the time evolution of particles temperature.
Considering Eq. 4, it becomes clear that different competitive processes contribute to influence the particle's internal energy during the laser irradiation. Since the incandescence signal derives from the radiative emission generated by the heated particle, the most relevant step for the LII process is the initial absorption of the laser light by the particle and the consequent heating. The absorptive-heating rate can be easily calculated by

$$\dot{Q}_{\mathrm{abs}} = \sigma_{\mathrm{abs}} B(t), \quad (5)$$

where $B(t)$ is the time dependent irradiance of the incident laser with wavelength λ_L (much bigger than the particle diameter) and σ_{abs} is absorption cross section expressed as

$$\sigma_{abs} = \frac{d_p^3 \pi^2 E(m)}{\lambda_L}. \quad (6)$$

σ_{abs} takes into account the area of the particle ($\pi \cdot d_p^2$), which is assumed to be spherical, and the absorption efficiency ($d_p \cdot E(m)$).

Particle heating is balanced by the cooling process. The radiative-cooling rate of the particle can be formulated as [104]

$$\dot{Q}_{rad} = \frac{198.97\pi^3 d_p^3 \ (k_b \cdot T)^5 \cdot E(m)}{h(hc)^3} \quad (7)$$

where h is Planck's constant, c is the speed of light, k_b is the Boltzmann constant. In this expression appears the refractive-index function $E(m)$ which is dependent on the incident wavelength. Since lasers operate on a fixed wavelength, we could use a constant value for $E(m)$ (in our case the value selected was 0.3 [105, 106], see below). If other incident sources of radiation are employed (non-laser sources with different wavelengths), more complex equations need to be used [107]. Furthermore, two other phenomena limit the temperature rise of the particles: heat conduction and, especially at high fluences, sublimation.

If we want to describe the conductive-cooling rate during LII we have to introduce first the thermal accommodation coefficient α_T. This parameter describes the thermal energy exchanged between the soot particle surface and a colliding gas molecule. It can be expressed as

$$\alpha_T = \frac{T_{gas,0} - T_{gas}}{T_s - T_{gas}} = \frac{E_{n,gas,0} - E_{n,gas}}{E_{n,s} - E_{n,gas}}, \quad (8)$$

in Eq. 8 T_s is the soot particle temperature, T_{gas} is the temperature of the colliding gas stream, $T_{gas,0}$ is the initial temperature of the bath-gas and $E_{n,s}$, $E_{n,gas}$ and $E_{n,gas,0}$ are the corresponding energies. The value of the thermal accommodation coefficient has been widely investigated and found to lie between α_T = 0, 24 and α_T = 0, 44 [108]. The uncertainty concerning α_T makes the modelling of the conductive-cooling rate quite challenging. A typical expression employed to describe $\dot{Q}_{cond}$ is [109]

$$\dot{Q}_{\mathrm{cond}} = \frac{2\kappa_a \pi \mathrm{d_p^2}}{d_p + GL}(T - T_0), \tag{9}$$

where T_0 is the ambient temperature, κ_a is the thermal conductivity of surrounding gas, L is the mean free path of the molecules and G is a function of the heat-capacity ratio $\gamma = C_{p,\mathrm{air}}/C_{\mathrm{v}}$, ($C_{p,\mathrm{air}}$ is the heat capacity of air at constant pressure while C_v is the heat capacity of air at constant volume). G contains the term α_T as can be seen in the following

$$G = \frac{2(9\gamma - 5)}{\alpha_T(\gamma + 1)}. \tag{10}$$

The particle cooling due to conduction is still under investigation. In particular, the impact of polydispersity, bridging between primary particles, aggregate size and morphology and particle maturity on LII-signal decay rates are still under study [104, 110-112].

A critical phenomenon for the modelling of the particle energy and mass balance during LII, especially at high fluences, is the sublimation process, as the mass loss results in a decrease of LII signal. This process is still to be fully understood, nevertheless various models for the estimation of the cooling rate due to sublimation have been developed[113, 114]; one way to assess $\dot{Q}_{\mathrm{sub}}$ is [114]:

$$\dot{Q}_{sub} = \frac{\Delta H_v}{W_v} \cdot \left(\frac{dM}{dt}\right)_{sub}, \tag{11}$$

Here W_v denotes the average molecular weight of soot vapour, ΔH_{v} is the energy required to evaporate a mole of carbon and $\left(\frac{\mathrm{d}M}{\mathrm{d}t}\right)_{\mathrm{sub}}$ can be expressed as:

$$\left(\frac{\mathrm{d}M}{\mathrm{d}t}\right)_{\mathrm{sub}} = \frac{\pi d_p^2 W_v \alpha_M p_v}{RT}\left(\frac{RT}{2\pi W_v}\right)^K. \tag{12}$$

Eq. 12 describes the loss of mass over time due to sublimation $\left(\frac{\mathrm{d}M}{\mathrm{d}t}\right)_{\mathrm{sub}}$. Here R is the gas constant, p_v is the vapour pressure of soot, α_M is the mass-accommodation coefficient while K is a constant that accounts for the non-idealities of bath gas and it ranges between 0.4 and 0.5 [104].

When soot reaches its maximum temperature during laser irradiation, the maximum LII signal detected in the visible wavelength range allows the determination of the soot volume fraction f_V [104]. For the evaluation of f_V the system needs to be calibrated. The calibration is usually performed by laser extinction on a sooting "reference" lab flame [115] or directly on the flame under investigation [116].

By measuring the ratio between the beam intensity before (I_0) and after (I) passing the flame, and knowing the path length of the beam in the flame l, it is possible to calculate the extinction coefficient K_λ by:

$$K_\lambda = \ln\left(\frac{I_0}{I}\right)\frac{1}{l}. \tag{13}$$

With K_λ we have all the parameters for the determination of the soot volume fraction f_V:

$$f_V = \frac{K_\lambda \lambda}{6\pi E(m)}. \tag{14}$$

where $E(m)$ is a function of the complex index of refraction already seen in the section 2.1.3. The value for $E(m)$ has been investigated in several studies [106, 117, 118] and it is still under discussion in the scientific community. In this study the value 0.3, typically used [105, 106, 118], has been selected. The value of $E(m)$, and consequently the absolute value of f_V, is influenced by soot particles characteristics which might be slightly different between the burner used for calibration and the diesel burner (as well as within the diesel burner itself). Consequently, when we compare soot properties in the diesel burner some minimal differences due to the influence of soot type and composition are expected although the formation conditions are similar [104]. Furthermore, the measurements may be affected by the scattering process. When a light beam passes through a soot volume, its intensity will diminish due to both absorption and scattering. Sorensen [36], by using the albedo, that is the ratio of scattering to total extinction, showed that the scattering process in case of aggregates > 200 nm usually accounts for 20%-25% of the total attenuation (monomer size 20 nm – 40 nm).

Furthermore, it should be taken into account that the LII signal is nonlinear with laser fluence [104]. At low fluences the signal increases by increasing the fluence until it reaches a plateau; at this point a further increment of the fluence does not cause an increment of the signal but, on the contrary, the signal slightly decreases because of mass loss due to sublimation. Ideally, the

fluence used for the measurements should be adjusted in order to be at the beginning of the plateau region; in this way it is barely affected by the laser's energy fluctuations and, at the same time, the sublimation effects are limited (although they are already present). Consequently, a fluence optimization should be carried out before [104]. Another application of LII (not used in the present study) is the evaluation of the soot primary particle size. Particles cooling after irradiation exhibits a size-dependent signal decay behaviour. This can be exploited for the determination of primary particle size [119]. The signal decay rate depends on a variety of influencing parameters. The major ones are the local gas temperature and composition which strongly influence the heat transfer from the laser-heated nanoparticles and thus the resulting particle cooling [120].

Since soot absorbs in a large spectral region (from ultraviolet to infrared) many laser wavelengths for LII measurements can be chosen. However, IR wavelengths are usually preferred to avoid interference from laser-induced fluorescence of polycyclic aromatic hydrocarbons and C_2-radicals resulting from photo-fragmentation of molecules.

LII is suitable for soot characterization and it has been employed for the evaluation of soot concentration in different types of flames. In particular, laminar premixed [119], laminar diffusion [121, 122] and jet-diffusion flames [123] have been deeply studied by LII. For jet-diffusion flame investigations two-dimensional LII is usually selected. The influence of buoyancy and fuel type on the soot produced in premixed and non premixed laminar diffusion flames has been also explored by using Laser-Induced Incandescence [124, 125]. Finally, the application of LII has been extended to particle characterization inside the cylinder of a diesel engine, at the exhaust and in a combusting diesel jet [126-128].

3.2 Elastic Light Scattering

Primary soot particles tend to coagulate/aggregate into bigger clusters. The aggregation process significantly affects the LII signal [36]. Aggregate size and morphology can be expressed by two parameters, namely radius of gyration R_g and fractal dimension D_f. The root mean square of the lengths between each primary particle and the mass centre of the aggregate corresponds to R_g while D_f describes the morphology of the aggregate and its typical value ranges between 1.5 and 1.9 [129-131]. The values of R_g and D_f can be determined by elastic light scattering (ELS) measurements [36].

In the ELS technique the intensity of the light scattered by the soot aggregates after laser light irradiation is used to achieve information about aggregates size. The ELS experimental set-ups

can be of two types: in the first kind of set-up a scanning goniometer is employed [132]. This approach allows for two-dimensional measurements [133], nevertheless a major drawback is that the sequential measurement procedure is too slow for the investigation of moving samples, limiting the application to only stationary objects. In the second approach the scattering signal is collected by several detectors [134-136]. It is therefore possible to acquire the scattering light at diverse angles simultaneously. The limited number of detectors yields to a reduction of the angular resolution. An implementation of ELS was employed by Oltmann et al. [137]. The novel method presented is called wide-angle light scattering (WALS). Oltmann et al. were able to achieve a high angular resolution, coupled with a fast measurement procedure, by using an ellipsoidal mirror. Basically, the aggregates are first irradiated with polarized light. The light scattered within a plane is collected by the ellipsoidal and imaged onto a planar detector. The intensity of the scattering signal varies depending on the detection angle and the size of the particles. From the image on the detector a scattering diagram with high resolution (<1°) can be obtained. The theory of Rayleigh-Debye-Gans for fractal aggregates (RDG-FA) is usually utilized for the estimation of aggregate size from WALS data [36]. If we assume that primary particles scatter independently, the intensity of the scattered light I_{sca} in case of monodisperse aggregates is directly proportional to the structure factor $S(qR_g)$. Here q represents the magnitude of the scattering vector. The scattering vector $\vec{q}$ stands for the difference between the incident and the scattered wave vector. The magnitude of q can be calculated by

$$q = \frac{4\pi}{\lambda} \sin\left(\frac{\theta}{2}\right) \tag{15}$$

where λ is the wavelength and θ the scattering angle. The scattering intensity signal varies with q as depicted in Figure 8:

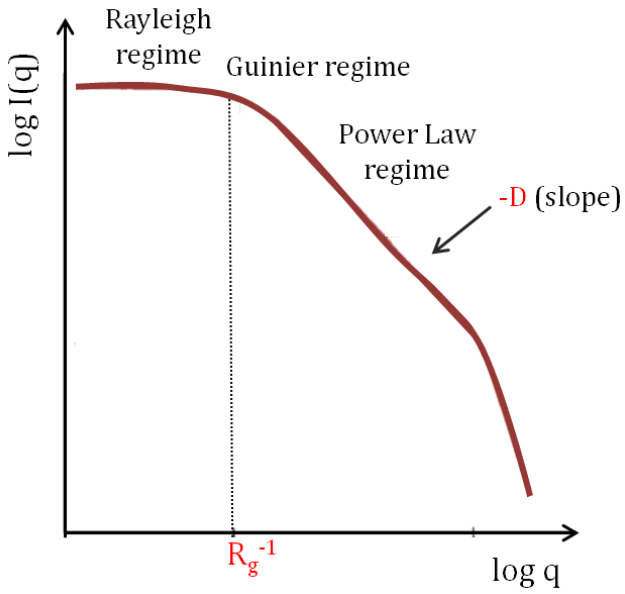

Figure 8. *Double logarithmic plot of the scattered light intensity I(q) versus q. Figure after [36].*

From Figure 8it is possible to observe that the functional behaviour of the structure factor $S(qR_g)$ can be described for the regimes [36]:

$$S(qR_g) \approx 1, \qquad qR_g \ll 1 \qquad \text{Rayleigh regime} \tag{16}$$

$$S(qR_g) \cong 1 - q^2R_g^2/3, \qquad qR_g \leq 1 \qquad \text{Guinier regime} \tag{17}$$

$$S(qR_g) \cong C(qR_g)^{-D_f}, \qquad qR_g \gg 1 \qquad \text{Power law regime.} \tag{18}$$

R_g is inferred from the Guinier regime. This leads to:

$$\frac{I_{sca}(0)}{I_{sca}(q)} = \frac{S(0)}{S(qR_g)} \cong 1 + \frac{1}{3}q^2R_g^2. \tag{19}$$

The radius of gyration is obtained by plotting the inverse scattering intensity $I_{sca}^{-1}(q)$ against q^2. The R_g calculated in this way will be an effective value which depends on size distribution since real particles ensemble are polydisperse. R_g obtained is strongly dominated by large aggregates. Sorensen et al. [132, 138] explored the influence of polydispersity on the measured radius of gyration while Huber et al. [131] derived size distribution parameters from WALS-

measurements. WALS technique has been implemented for non-stationary flame studies as well as for investigations on premixed laminar flames [137, 139].

3.3 Two-color pyrometry

The two-color pyrometry (2-CP) technique has been widely employed for soot temperature measurements in different types of flames (laminar, diffusion, co-flow diffusion, turbulent flames) and in engines [140-145]. In this technique the soot temperature is obtained from the ratio of the spectral radiance of soot acquired at two different wavelengths. The intensity of the soot radiation $I_{s\lambda}$ emitted at a certain wavelength λ is expressed by Planck's law:

$$I_{s\lambda}(\lambda, T_s) = \varepsilon(\lambda) \frac{2\pi hc^2}{\lambda^5 \left(e^{\frac{hc}{\lambda k_b T_s}} - 1 \right)}. \quad (20)$$

In the equation above ε is the soot emissivity, already described in paragraph 2.1.3, h is Planck's constant, c is the speed of light, k_b is the Boltzmann constant and T_s is the soot temperature.
The detection system has to be calibrated previously. This can be made by measuring the radiation emitted by a calibrated tungsten lamp in the same spectral range of acquisition of the two-color pyrometry measurements. The emission intensity of the calibrated lamp, $I_{LP\lambda}$ can be expressed as:

$$I_{LP\lambda}(\lambda, T_{LP}) = \tau(\lambda) M_{LP}(\lambda, T_{LP}). \quad (21)$$

In Eq. 21, M_{LP} (λ, T_L) describes the spectral emission of the lamp (known) at the lamp temperature, while $\tau(\lambda)$ is an optical parameter specific of the detection system and represents the detector sensitivity at the detection wavelength selected. This parameter takes into consideration the collection efficiency and solid angle. The relative sensitivity $\tau_{1/2}$ is calculated from the ratio $I_{LP\lambda_1}/I_{LP\lambda_2}$:

$$\tau_{1/2} = (I_{LP\lambda 1} M_{LP\lambda 2})/(I_{LP\lambda 2} M_{LP\lambda 1}). \quad (22)$$

Soot temperature can be evaluated, for example, by applying Wien's law [143] or by using a spectral radiance-temperature look-up table. In this work the second method mentioned was

employed. It must be pointed out that the detected emission $I_{S\lambda}$ results from the soot emission radiation integrated over the thickness of the sample facing the detection system. In the case of flames, the soot is usually not uniformly distributed, meaning that the values of temperature calculated are an average of the overall soot present along the thickness of the flame. The use of tomographic methods allows the evaluation of local soot temperature values [146-148]. On the other hand, for axially symmetric flames, the radial distribution of soot radiation is determined through an Abel inversion procedure [142, 145].

3.4 Scanning Mobility Particle Sizer

The Scanning Mobility Particle Sizer performs a size selection of charged particles depending on the particles electrical mobility (i.e. mobility of charged particles in a electric field). This property depends mostly on particle size and charge. It follows that the particles have to be as uniformly charged as possible. The homogenization of the charges is done by a neutralization source. The neutralization source consists of a radioactive conditioner where ions are created by radioactive decay of Krypton-85. When Krypton-85 decays to the non-radioactive Rubidium-85 it emits electrons by a process called beta-minus decay. The electrons emitted carry high kinetic energy, capable of ejecting electrons out of other atoms within the aerosol. As a result, the atoms impacted by the free electrons lose in their turn an electron, acquiring a positive charge. In addition, the electron emitted as a consequence of the beta-minus decay may be absorbed by another atom, which charges negatively. This bipolar ionic environment allows the soot to charge and discharge itself through Brownian molecular movement. After enough time, the particles will reach an equilibrium charge state, called the Boltzmann equilibrium. The bipolar diffusion charge distribution is described by Wiedensohler et al. [149].
The particles, after being uniformly charged thanks to the neutralization source, are guided through a cylindrical tube, called Differential Mobility Analyzer (DMA), where an electric field is applied. The DMA includes an inner and an outer electrode (the inner electrode is constituted by a wire along the cylindrical tube axis). The velocity of the particles (vertical and radial directions) changes depending on the electrostatic force F_E,

$$F_E = N_c e E, \tag{23}$$

where N_c is the number of elementary charges, e is the elementary unit of charge and E is the electric field intensity. The electric field strength E inside the cylindrical tube can be described

by [150]

$$E = \frac{\Delta U}{\mathrm{r_{pos}} ln\left(\frac{d_0}{d_\mathrm{i}}\right)} \tag{24}$$

With ΔU the difference in voltage between the electrodes, d_o/d_i the diameter of the outer electrode divided through the diameter of the inner electrode and r_{pos} the radial position where the field is calculated. Generally, the electrical mobility describes the ability of charged particles (in this case soot) to move through a fluid (in this case air) in response to the force applied by the electric field. The velocity of the particles v_p with a diameter d_{ae} is then calculated by Eq. 25:

$$v_\mathrm{p} = \frac{N_c e E C}{3\pi\eta d_\mathrm{ae}}. \tag{25}$$

In this expression η is the dynamic viscosity of air (the fluid through which the particles are moving) and C is a correction factor experimentally determined called Cunningham factor [151] that depends on particle surface and fluid characteristics [152]. Knowing the intensity of the electric field E and the particle velocity v_p, the electrical mobility Z is obtained by:

$$Z = \frac{v_\mathrm{p}}{E} = \frac{N_c e C}{3\pi\eta d_\mathrm{ae}}. \tag{26}$$

In Eq. 26 is clear that the particle diameter has a direct influence on the electrical mobility. If the electrical mobility of the particle is known, the voltage can be adjusted in order to control the particle's trajectory. In this way, particles with a selected diameter can be guided outside the cylinder to a detector. On the other hand, particles with a different diameter will have a different trajectory which leads them to impact on the wall of the cylinder. Figure 9 shows a sketch of a capacitor (similar to the one usually employed in the SMPS technique), which acts as a simple electrical mobility analyser.

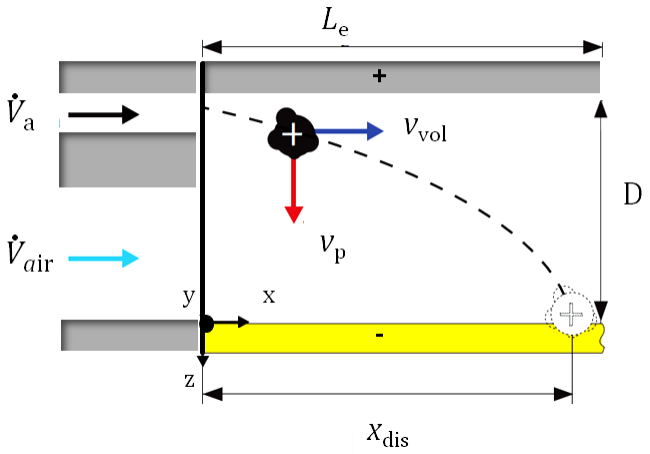

Figure 9. *Side view of the two dimensional cut-out of the capacitor or electrical mobility analyser. The trajectory of a positively charged soot particle inside the capacitor section is displayed.*

In Figure 9, $\dot{V}_a$ is the volume flow of the aerosol, $\dot{V}_{air}$ is the volume flow of air, and v_{vol} is the velocity of the resulting volume stream $\dot{V}_{in} = \dot{V}_a + \dot{V}_{air}$.The dashed line is the trajectory of the soot particle, x_{dis} is the distance covered by the particle in the x-direction from the moment of its ejection to its deposition, D is the distance between the two electrodes and L_e is the length of the electrodes.

Finally, the voltage corresponding to a specific electric mobility can be expressed as:

$$U = \frac{\dot{V}_{in} D}{L_e Z x_{dis}}, \tag{27}$$

which relates voltage, electric mobility, and volume flow.

Finally, the size classification is followed by the particles counting performed by the Condensation Particle Counter or CPC. In the CPC the nanoparticles are transported by a carrier gas saturated with butanol to a condenser. Here the butanol condenses on the nanoparticles and forms µm-sized droplets which are detectable by optical light scattering. Finally, after this process, the particles reach the optical sensor for the concentration measurement.

4. Experimental apparatus and approach

4.1 Novel vapour diesel burner design and implementation

The implementation of a system capable to completely pre-vaporize and combustion of diesel fuels in a laminar flame is quite challenging due to the prompt self-ignition of diesel. The temperature required for complete pre-vaporization of all diesel components is 633 K, while the self-ignition temperature of diesel is 483 K. Pei et al. [153] and Roubaud et al. [154] studied the auto-ignition behaviour of different aromatic compounds with chemical characteristics similar to the diesel's components or used as diesel surrogates. As shown in Figure 10 from Roubaud et al. [154] at the temperature of diesel's complete vaporization (red circle) the self-ignition delay time is less than 150 ms, meaning that if the hot diesel vapours, heated up to 633 K for fostering the vaporization, mix with air, the combustion will immediately start. If this happens already inside the vaporization system, an uncontrollable combustion will begin with obvious safety risks.

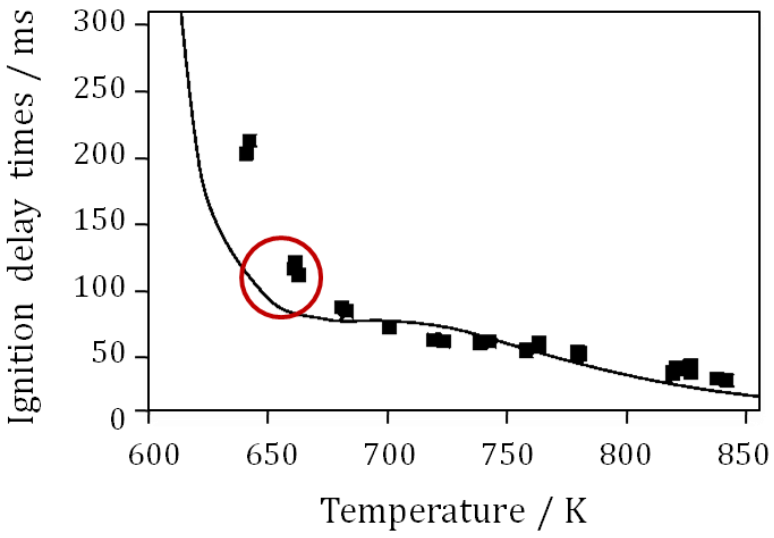

Figure 10. *Auto-ignition delay-times of n-butyl benzene. Measurements carried out in a rapid compression machine at pressure above 14 bar, equivalence ratio Φ = 1, [O_2]/[inert] = 0.37. Figure after Roubaud et al. [154] with additions.*

Consequently, the vaporization must be carried out only using nitrogen as carrier gas and the system has to be impenetrable to air. Moreover, the system should perform a uniform heating of the diesel while the fuel-nitrogen ratio, and consequently the flow, has to be adjusted in a way that allows a laminar diffusion combustion at the exit of the system. A laminar diffusion flame is desirable because it is easy accessible by the laser beam, it ensures steadier flame conditions than a turbulent flame and, above all, it prevents from self-ignition of diesel inside the vaporization-burning device (as mentioned above) since the blending between the diesel fuel and the air occurs outside the vaporization-burning system (the ambient surrounding air is involved in the combustion reaction, no air is inserted before like in pre-mixed combustion). Furthermore, it should be taken into account that an elevated percentage of nitrogen inhibits the combustion. Starting from these considerations and after a deepened literature review [64, 69, 154], the novel burner has been designed.

A first concept of the burner, shown in Figure 11, considered a modular structure composed of a vaporization zone, positioned in the lower part of the construction, and a mixing zone. In the vaporization zone the fuel is inserted and heated up to the diesel vaporization temperature. After this first section the fuel passes through a metallic porous set that facilitates the vaporization and enters in the mixing zone where it is diluted with pre-heated nitrogen. The mixing zone is constituted of five units forming a cylinder. The units can be easily assembled and disassembled making the system easy to clean when the fuel has to be changed. The mixing zone includes five thermocouples for temperature monitoring. The thermocouples measure the temperature of the flow in the centre of the cylinder. A ceramic porous set combined with a flow homogenizer is inserted in the final part of the burner for better blending and homogenization. This first prototype exhibits some disadvantages, for example high heat loss due to the flanges between the units. This disadvantage was solved by employing a single unit as mixing section. Furthermore the position of the fuel inlet above the heating elements is not optimal because the fuel does not have enough time for vaporization; This shortcoming has been overcome by placing the inlet downward within the heating elements. In this way the fuel crosses the entire vaporization zone, spending more time in this section.

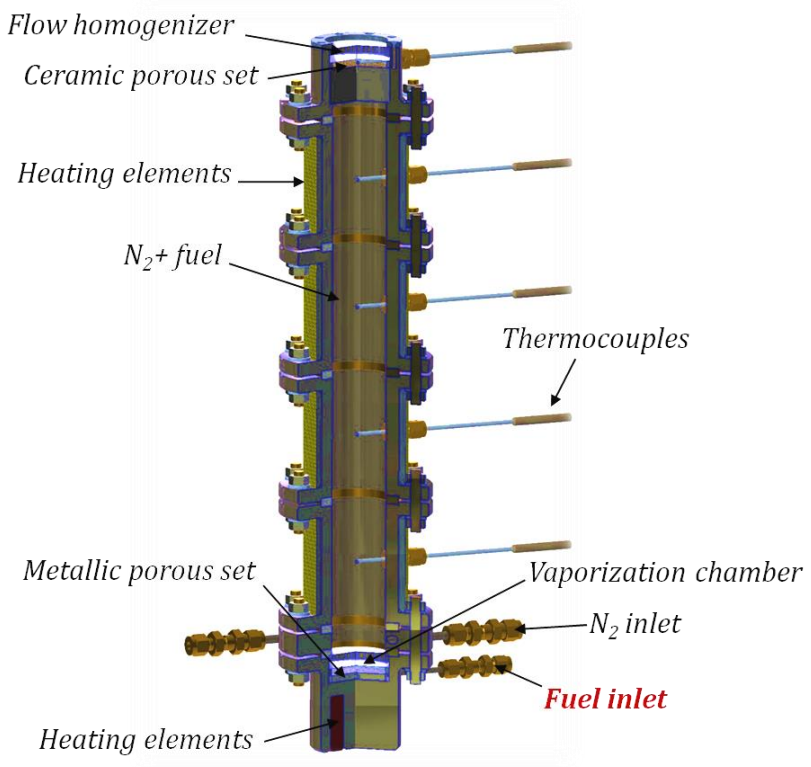

Figure 11. *Liquid fuel burner for Diesel study application, first concept.*

A second prototype, which was finally adopted, is described in [155] and it is shown in Figure 12 (details in [155]). The second burner considers again different zones for vaporization and mixture. The vaporization zone, 100 mm in length, is similar to the previous one, but in this case the fuel inlet is moved down in the centre of the lower surface. Here the fuel is inserted and pumped upward by a gear pump (Manufactured by HNPM, type mzr®-2921). The diesel is simultaneously pre-vaporized thanks to five heating elements which surround the inlet tube (4 mm diameter). The five heating elements allow a constant inner temperature of 653 K. The temperature set is slightly higher than the diesel vaporization temperature, ensuring the complete vaporization of all diesel components and, at the same time, minimizing pyrolysis [156]. The accuracy of the thermocouple, namely the measurement error on the temperature, is $\pm$1.5 K. After leaving the vaporization zone, the vapour fuel passes through a metallic grid coupled with a metallic porous set and finally reaches an intermediate zone where it merges with N_2. N_2 is pre-heated up to 653 K before entering the intermediate zone. The N_2 flow is 0.3 l/min at 653 K. For homogenization purposes the carrier gas is introduced radially from opposites sides of the burner, in the area between the vaporization zone and the mixing section, creating a swirling flow. At this point, the vapour fuel, 0.175 l/min gas volume flow at 653 K

corresponding to 0.45 g/min, diluted with nitrogen, enters the mixing chamber (180 mm total length). The flow rates of the fuel and N_2have been chosen taking into account the stability of the flame, the flow meter sensitivity and the N_2 percentage (in volume) in the blend; since a percentage of N_2 > 80% would not have allowed the ignition of the flame at the burner outlet, the N_2 percentage was kept at ~ 60 % vol. Around the mixing section a heating jacket is placed that keeps the temperaturebetween 643 Kand 653 K. Also in this case the temperature range is selected in order to guarantee the complete evaporation of every diesel component while the pyrolysis, which mainly occurs between 673 K and 1073 K [156], is suppressed. At the end of the mixing section prior to the flame zone, a flow homogenizer as well as a ceramic porous set are inserted to better homogenise and stabilise the flame. The inner flow temperature is constantly monitored by two thermocouples positioned at the end of the vaporization and mixing sections. The diameter of the inner tube of the mixing section is 45 mm; this diameter permits, due to the large area and the increased diffusion time of the blend, a uniform mixture of the N_2 – fuel blend. Finally, at the end of the mixing zone, a conical nozzle is positioned to stabilize the flame; the conical nozzle reduces the diameter up to 2.5 mm. The Reynolds number at the burner outlet is approximately 100. Furthermore, a co-flow of air, 20 l/min volume flow, is added in order to efficiently shield the flame from external perturbations due to draughts. Also in this case the air is pre-heated up to 653 K and introduced from both sides in a cylinder around the nozzle. To obtain a homogeneous distribution of the co-flow air, the co-flow cylinder, which surrounds the nozzle, is filled with glass spheres of 5 mm diameter. The burner implemented during this work produces a laminar flame with height of about 95 mm and a width of 8 mm. A summary of the burner's working settings is displayed in Table 1.

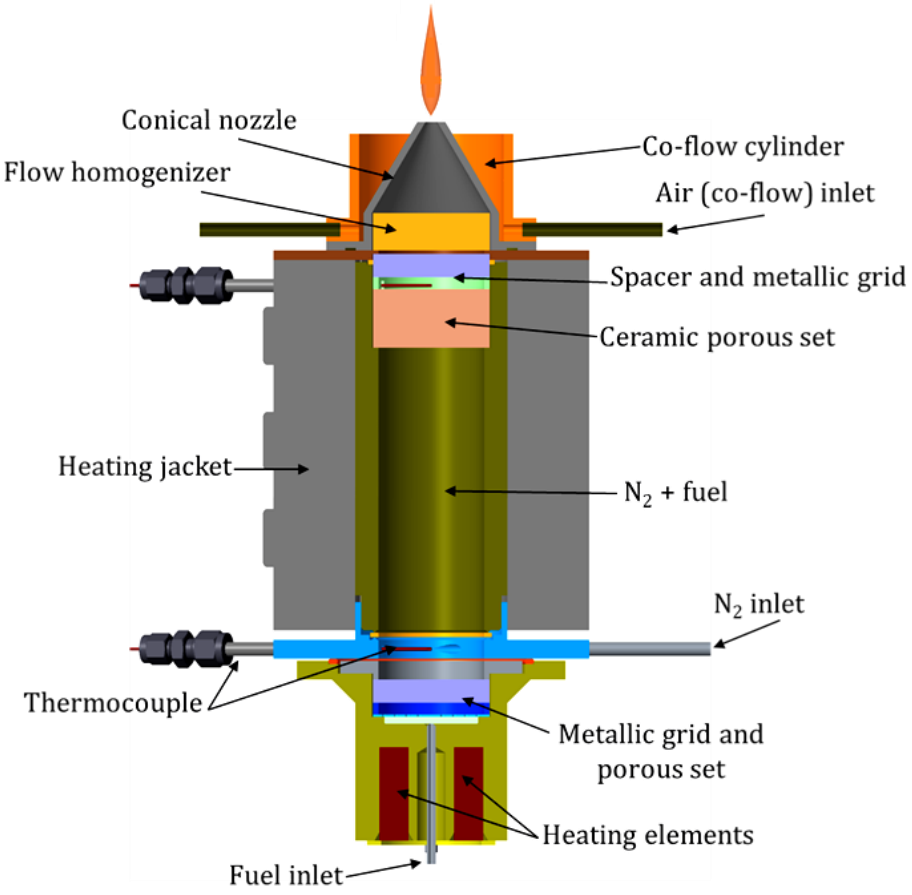

Figure 12. *Final design of the vapour diesel burner implemented. (Figure from[155]).*

Table 1. *Diesel burner working parameters.*

Diesel (vapour) volume flow	0.175 l/min
N_2 volume flow	0.3 l/min
Diesel + N_2 flow rate	170 cm/s
Air (Co-flow) volume flow	20 l/min
Outlet diameter	2.5 mm
Reynolds Number	~100

4.2 Constant volume chamber

The effect of oxygenated additives on soot production was studied also under (similar) diesel engine conditions (i.e. high pressure and temperature) for comparison with the results obtained from the burner's set-up. In this case the flame investigated was a diffusion spray flame. The spray flame measurements were carried out in a high temperature and high pressure injection and combustion chamber called "OptiVeP" (Figure 13) [50]. The chamber consists of a

constant-volume vessel with an inner volume of 10 litres. A gas flow, with composition variable from air to pure nitrogen, is introduced in the chamber from the top corners (after being heated electrically) and reaches the bottom corners; here the gas cools down thanks to water cooler jackets. The gas temperature and pressure inside the chamber can be adjusted independently up to 1000 K and from 30 kPa to 10 MPa, respectively. The gas flow velocity is approximately 30 $mm \cdot s^{-1}$ (in the measurement plane, namely the plane where the laser sheet lies). Although the gas flow is fast enough to scavenge the injected fuel before the next injection, during the measurements the spreading velocities of the fuel spray is much higher than the ambient gas flow in the chamber so that it can be considered static compared to the spray velocity. The chamber is constituted of a cubic metal body. It houses five window flanges where quartz glass windows with an optical accessible diameter of 125 mm are installed. Only the bottom side does not contain a window but instead a flange with the injector and an intercooler system. The injector employed in all the experiments was a piezo-driven servo hydraulic common rail injector equipped with a special research nozzle. The nozzle has three holes at an elevation angle of 45° arranged equidistantly (in terms of angle) around the nozzle axis. This allows to observe a single fuel jet isolated (if the nozzle had more than 3 holes, for example 4, there would be more than one plume in the measurement plane, which means that, for example, a nozzle with 4 holes would produce 4 plumes, 2 of them would be along the path of the laser sheet since the laser sheet lies in the measurement plane). The hole diameter is 115 µm with a length-to-diameter ratio of 6.5. The fuel's injection frequency is 1 Hz, therefore it is possible to assume that there is no shot to shot influence affecting consecutive injection events. The temperature of the fuel in the nozzle tip is varied between 243 K to 373 K by a thermostat while the injection pressure can be increased up to 250 MPa in a common rail system. Finally, a fully programmable electronic drive unit is used for triggering and injection timing.

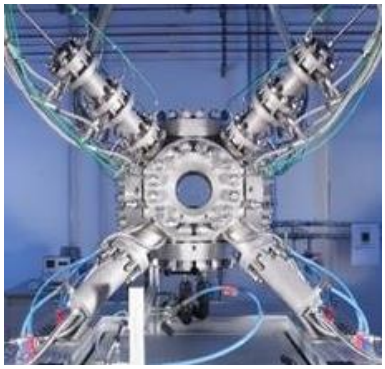

Figure 13. *The high temperature - high pressure injection and combustion vessel "OptiVeP".*

4.3 Laser-Induced Incandescence set-ups

The LII technique was employed to measure soot production on both laminar diffusion flame (at normal temperature and pressure, NTP, which corresponds to 293.15 K and 1 atm) and spray flame (high temperature and pressure, see section 4.2). The LII set-up used was basically the same for both combustion devices, the only difference was the detection system. Figure 14shows the one used for the measurements carried out on the self-designed burner set-up. For heating up the soot particles we utilized a Q-switched pulsed Nd:YAG laser (Quantel, Q-smart 850), with a repetition rate of 10 Hz and a pulse width of 5 ns. The fundamental wavelength, 1064 nm, was chosen to avoid interferences with laser-induced fluorescence (LIF) which is emitted by polycyclic aromatic hydrocarbons after excitation with shorter wavelengths (i.e. typically 266 nm, 355 nm and 532 nm). Shortly behind the laser exit a half-wave plate and a thin film polarizer are placed for adjusting the laser energy. To perform two dimensional LII measurements, a laser sheet is created by using a combination of three cylindrical lenses. The first lens, f_1 = -50 mm, expands the beam vertically while the second lens, f_2 = 200 mm, collimates it. The last lens, f = 1000 mm, focuses the beam into the flame. Finally, right before the burner (or the chamber), a 30 mm aperture is arranged. The aperture is used to cut the beam edges which are usually not uniform. The thickness of the aperture, 20 mm, is much larger than the laser sheet thickness (0.6 mm), therefore diffraction effects are largely avoided. In this way a top hat beam profile is achieved. The final laser sheet results to be 30 mm high and has a thickness of 0.6 mm. The laser sheet exhibits a homogeneous profile, as shown in Figure 15; the strong dips in the vertical direction are due to intrinsic characteristics of the laser employed. The image displayed in Figure 15 has been collected by the beam profile camera SP620U Spiricon, OPHIR Photonics. Regarding the burner measurements, for the detection of the LII images an intensified CCD camera (Andor USB iStar model DH334T-18F-E3, 16 bit) with a resolution of 354 x 301 pixels (maximum resolution 1024 x 1024 pixels) and a repetition rate of 10 Hz was used. The gate width of the intensifier has been adjusted in order to detect the maximum LII signal intensity (while avoiding to saturate the camera's chip), and finally set to 20 ns. In front of the objective lens of the camera a band-pass filter at 425 nm with 50 nm FWHM is placed. This wavelength was selected in accordance with the camera's spectral sensitivity as well as to reduce the soot luminosity signal that increases by increasing the wavelength in the visible region. Furthermore, the band-pass filter at 425 nm ± 50 nm allows to avoid interference from Swan bands.

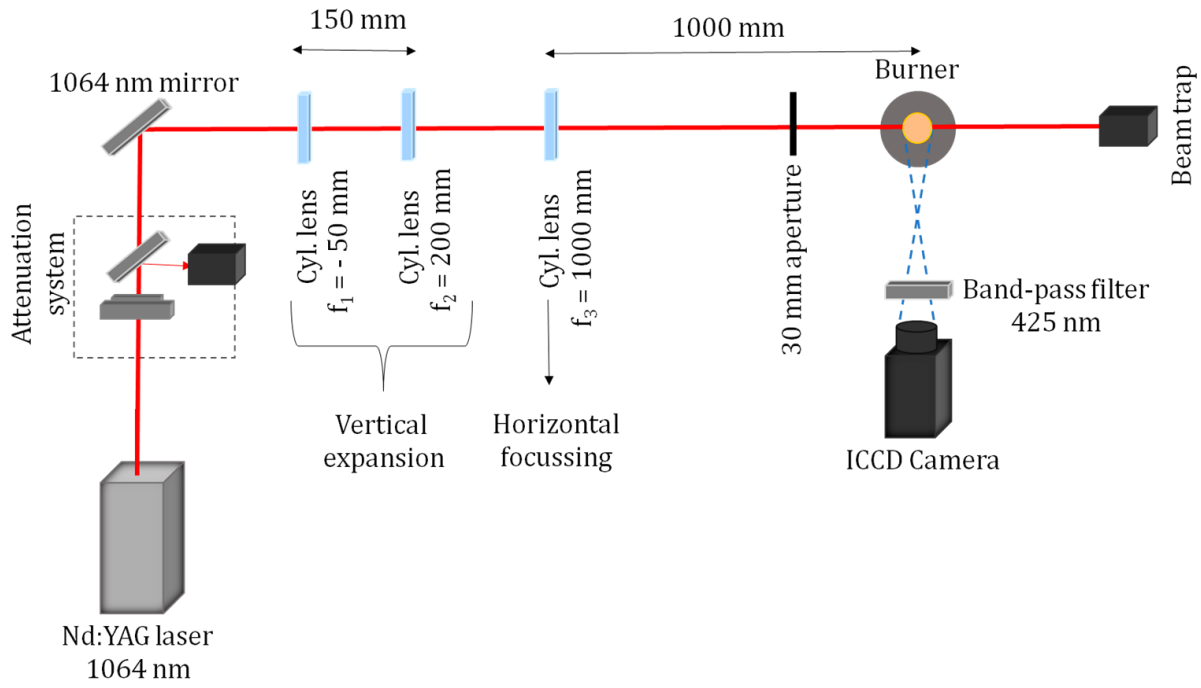

Figure 14. *Laser-Induced Incandescence set-up used for investigation of the diesel burner flame. (Figure from [155]).*

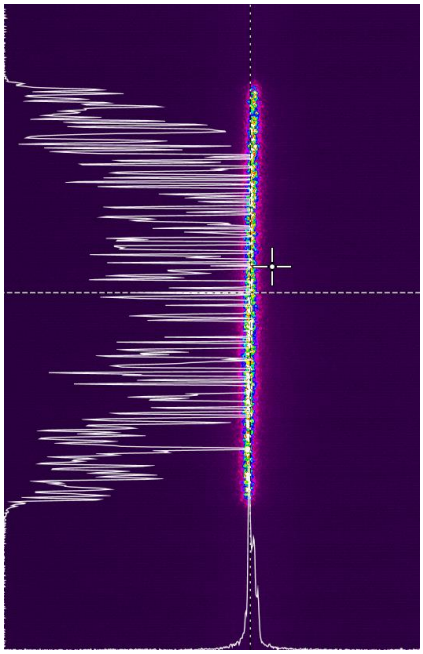

Figure 15. *Beam profile of the laser sheet (30 mm high, 0.6 mm thick) used for 2D LII measurements on the laminar diffusion flame, collected by the beam profile camera SP620U Spiricon, OPHIR Photonics. (Figure from [96].)*

The calibration of the LII signal for soot quantification was performed by extinction measurements. On this purpose, the beam intensity of a CW laser at 532 nm wavelength was measured before and after passing a premixed ethane flat flame produced by a McKenna burner. Figure 16 shows a single shot extinction image of the ethene flame.

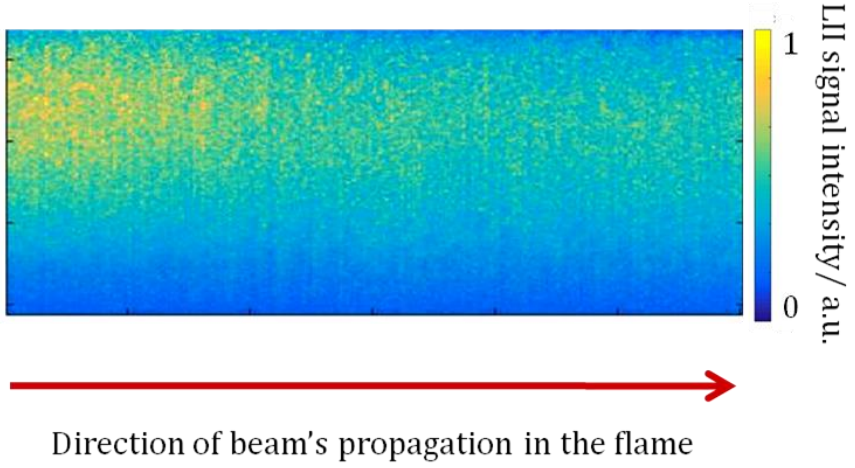

Figure 16. *LII-signal image of the McKenna burner flame used for calibration of LII in which extinction effects can be observed.*

The LII set-up employed for the measurements on spray flames is illustrated in Figure 17. As mentioned before, it is similar to the one utilized for the burner measurements, i.e. same laser type, attenuation system and set of lenses (only the height of the aperture was increased to 50 mm), but it differentiates in the detection system.

The visualization system in this case is composed of a PCO DiCam Pro camera (12 bit, 1280x1024 pixel) equipped with a band-pass filter (425 nm with 50 nm FWHM). The recording frequency and exposure time, adjust with respect to laser and injection, are set at 1 Hz and 20 ns, respectively.

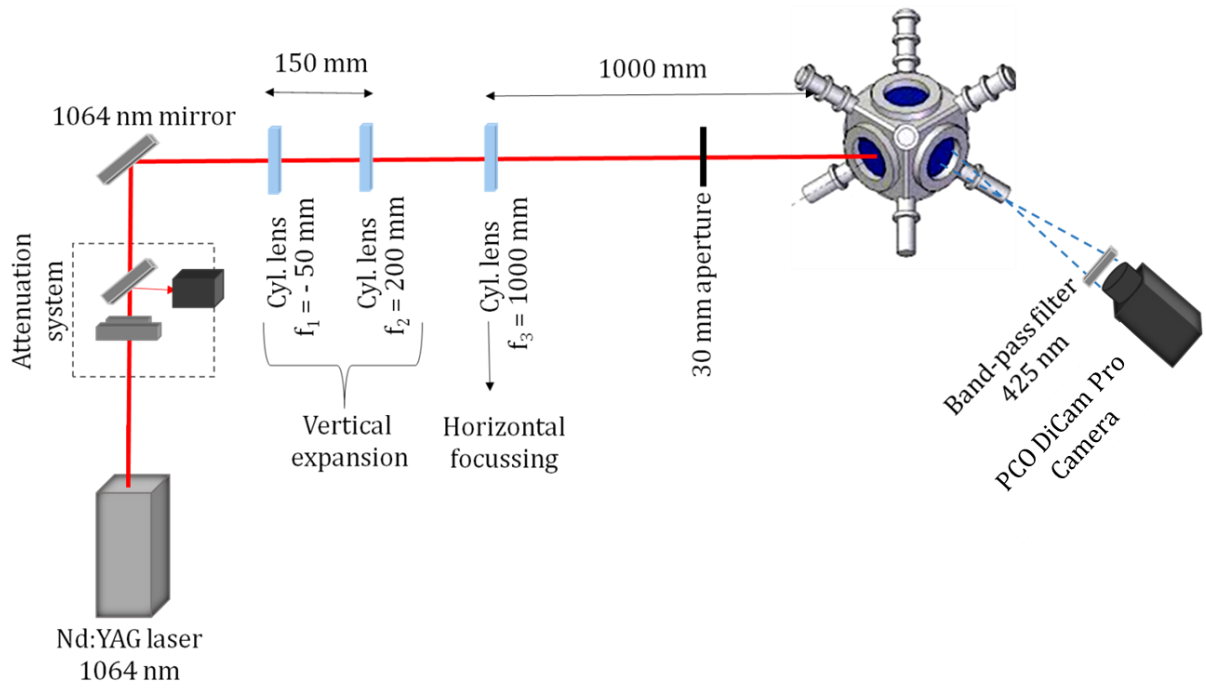

Figure 17. *Laser-Induced Incandescence set-up used for investigation of spray flames.*

4.4 Wide-Angle Light Scattering set-up

Apart from LII, all the other techniques, including WALS, have been employed only for the measurements on the diesel burner which is easy accessible to complex optical objects such as the ellipsoidal mirror. The most important element of the WALS set-up, illustrated in Figure 18, is the ellipsoidal mirror. This is basically a slice cut out of a 32 mm height spheroid. The mirror consists of an aluminium body covered with a reflective surface, used to collect the scattered light, where an amorphous nickel plating has been applied. The mirror has two focal points at a distance of $\Delta f = 600$ mm. The focal points lie in a plane of 250 mm diameter, i.e. the diameter of the slice. At the two opposite sides of the mirror two slits of 10 mm width are cut, facing each other, in a way that permits the beam to pass through. The light source is a continuous wave (CW) laser (Qioptiq Nano-250) at 532 nm wavelength and 200 mW power (only 35 mW are used for measurements). The beam polarization is filtered by a Glan-Taylor prism to achieve a clean vertically polarized light relatively to the mirror plane. Afterward the beam is focussed into the flame by a f=300 mm lens. The focal point of the lens coincides with the measurement volume; this corresponds in turn to the first focal point of the ellipsoidal mirror. The laminar diffusion flame is specifically located in the first focal point of the ellipsoidal mirror (the mirror structure is positioned above the burner, as depicted in Figure 19).

The scattered light from the first mirror's focal point is collected and imaged by the mirror itself onto the CCD-camera (AV PIKE F-100B, 1000 x 1000 pixels, 16 bit). In front of the camera's lens a bandpass filter at 535 nm wavelength is positioned. This wavelength was chosen to compensate the blue-shift of the tilted illumination under 12.5°. The filter serves to minimize ambient light and light from soot luminescence. The aperture of the camera coincides with the second focal point of the mirror. The size of the measurement volume is therefore defined by the camera's aperture and the laser beam's diameter in the focal point. The camera's aperture is f/5.6. The exposure time of the camera used for the measurements is 43 µs while for calibration the exposure time is raised to 3 s. The mirror, together with the camera, is installed in a flexible construction capable of gyrating. Consequently, the mirror-optics-camera system, as it is shown in Figure 19, can be rotated by 15° angle with respect to the vertical axis of the burner which has a fixed position. In this manner the signal is not blocked by the burner (without the tilt of the mirror-optics-camera system the scattered light collected by the whole mirror would be reflected on the burner which would be placed exactly between the ellipsoidal mirror and the camera). Thanks to the tilt the scattered light acquired by one half of the mirror can be imaged into the camera, meaning that we are able to collect the scattering light intensity at every angle from 0° to 180°. The image of the other half of the mirror cannot be detected by the camera, nevertheless, this data is redundant since one half of the mirror carries the same information of the other half (the intensity of the scattered light from 0° to 180°).

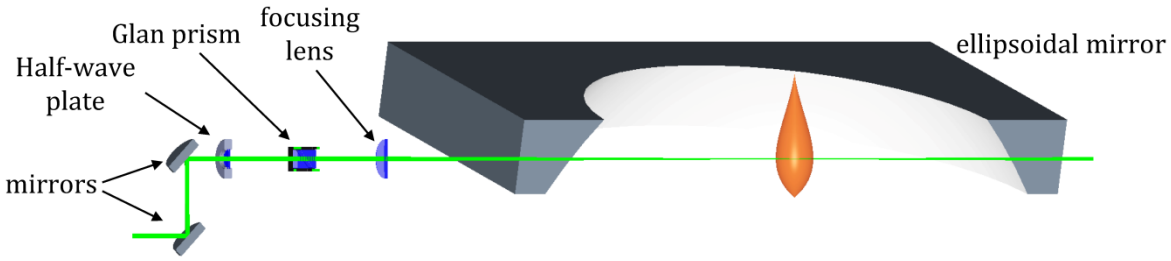

Figure 18. *Optical set-up used for WALS measurements, side-view.(Figure from [155].)*

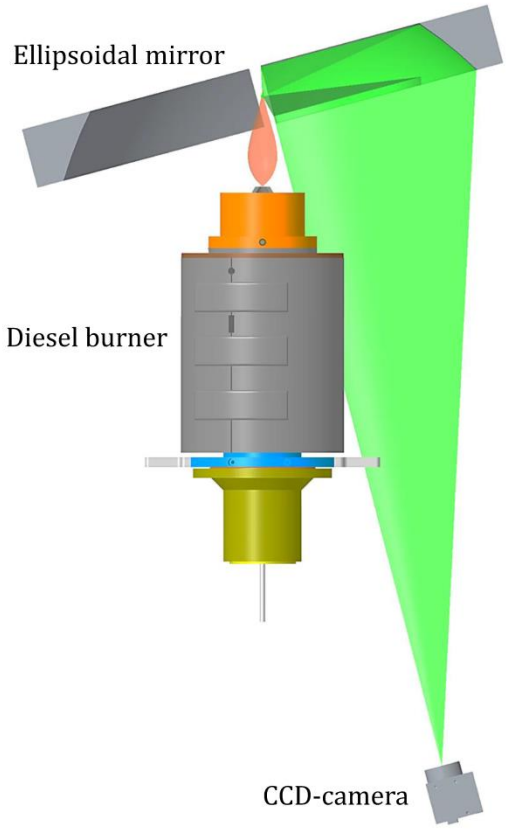

Figure 19. *Burner inserted in the rotatable camera-mirror system tilted by 15° with respect to the vertical axis of the burner. (Figure from [155]).*

In order to take into consideration the measurement volume size dependence ($1/\sin(\theta)$) and the aberrations due to the mirror's surface it is necessary to calibrate the optical set-up. The calibration has been performed by detecting the scattering signal of nitrogen gas molecules. N_2 typically scatters in the Rayleigh regime, hence the scattering is expected to be isotropic in the scattering plane. The calibration with nitrogen required an increment of the laser-power and exposure time that were set to 200 mW and 3 s respectively. These settings guarantee sufficient scattering signal as well as constant conditions during a single camera exposure preventing from signal blurring. A ring shaped calibration image generated from the scattering of nitrogen molecules is shown in Figure 20.

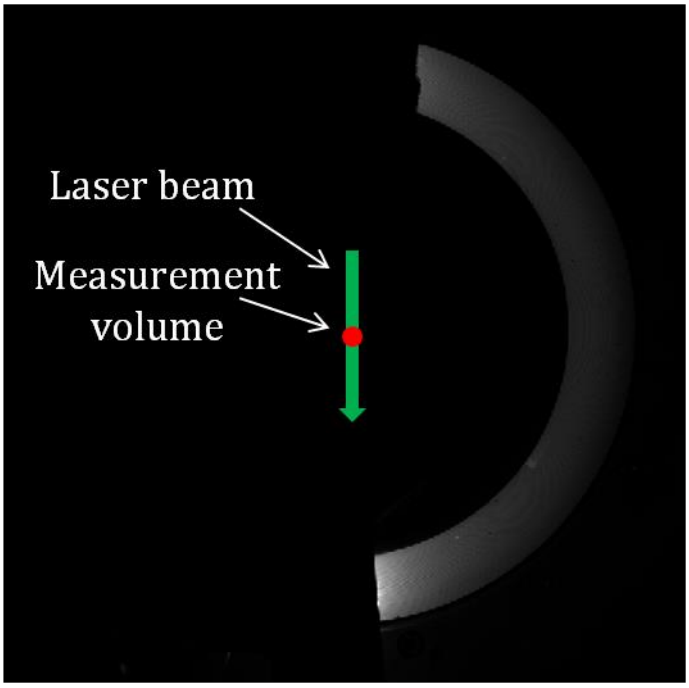

Figure 20. *Ring shaped scattering calibration image of nitrogen molecules.*

4.5 Scanning Mobility Particle Sizer set-up

The Scanning Mobility Particle Sizer set-up (PALAS GmbH) is constituted of three principal components: a neutralisation source, a Differential Mobility Analyser (DMA), and a counting unit, the Condensation Particle Counter (CPC) (See section 3.3 for more details on the background mechanisms). The SMPS set-up is depicted in Figure 21. Furthermore, a sampling probe has been used to suck the aerosol out of the burner flame. The sampling probe is based on the principle of the Venturi nozzle. The particles in the flame are sucked through a 1 mm diameter glass capillary (50 mm long). One extremity of the capillary is placed directly into the flame while on the other extremity, the glass capillary is connected to a nozzle. The diameter of the nozzle is 1 mm at the connection with the glass capillary and increases up to 3 mm moving away from the glass capillary connection (basically the nozzle presents a decreasing diameter moving towards the glass capillary connection).A stainless steel case surrounds the nozzle. On one side of the stainless steel case there is a inlet through which compressed air free of soot particles is inserted; the compressed air moves through the case and enters inside the nozzle. The compressed air serves to create the vacuum at the point where the glass capillary is connected to the nozzle. In addition to this, the compressed air also dilutes the aerosol. A dilution is strictly necessary to operate the SMPS since the DMA employed may only be

operated with a maximum particle concentration of 10^7 particles per cubic centimetre. Particle concentrations may vary depending on fuel or pressure, however, in an ethylene flame for example, the concentration is typically above 10^{10} particles per cubic centimetre [157]. In addition, the dilution quenches chemical reactions within the aerosol, preventing the particles from further size growth after sampling [157].

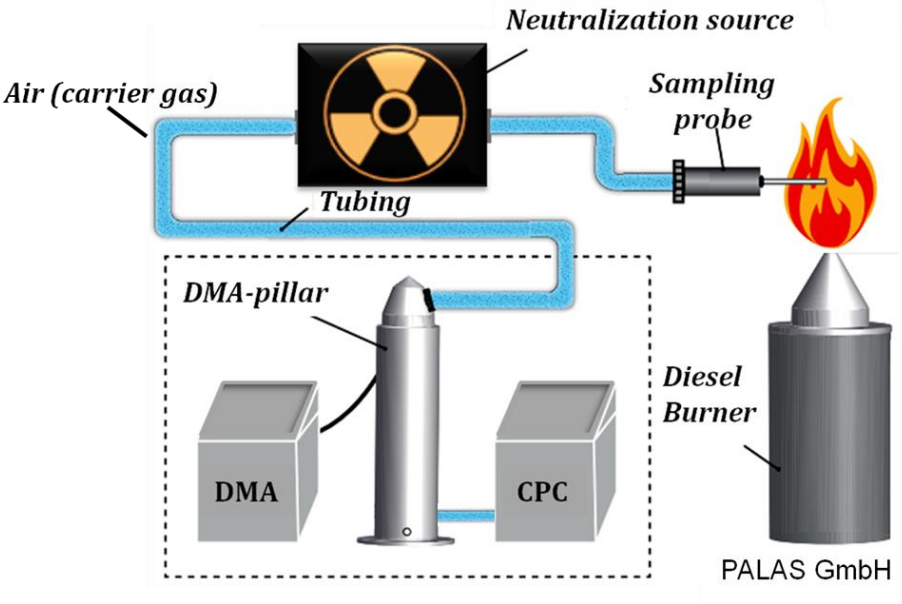

Figure 21. *Scanning Mobility Particle Sizer set-up (PALAS GmbH). Figure after Zhao et al. [157].*

Following to the sampling, soot particles have to be uniformly charged (as already mentioned, the SMPS technique relies on the classification of particles that, when subjected to an electric field, have different trajectories according to their size and charge.); this is done in the radioactive conditioner, i.e. the neutralization source (see section 3.3). The radioactive conditioner is placed between the sampling probe and the DMA-pillar and it is connected to both by a plastic tube. As this tubing may alter the charge distribution of the particles, which is especially critical after the radiation source, a minimal length of the tube (20 cm) has been employed.

After the uniformly charged particles leave the neutralization source, they enter the DMA-pillar (PALAS GmbH, type DEMC 2000, column SN5470), that is where the actual size classification of the soot particles takes place. Immediately before the entrance of the DMA an impactor is placed to discard the particles which are too large to be sorted based on their electrical mobility.

The aerosol is then guided downwards the DMA pillar by a laminar air flow. In the path inside the DMA pillar the aerosol passes through the electrical field formed between an inner electrode, where the voltage is applied, and the walls of the cylinder that constitute the outer electrode. This accelerates the particles towards the outlets with different velocities depending mainly on the size (since the charge is uniform). The voltage of the inner electrode is varied in order to select the size of the particles that will exit through the exit of the pillar connected to the CPC, while the others will exit through the "waste" outlet. In the present study both up-scans voltage (the voltage starts low and then rises) and down-scans (the voltage starts high and then falls) have been performed. The selected nanoparticles enter the CPC where they are counted. The CPC used in this study is the UF-CPC 200 model. The UF-CPC 200 is able to detect up to $2 \cdot 10^6$ particles/cm^3.

4.6 Two-color pyrometry set-up

In the two-color pyrometry experiments two images of the flame taken at the same time but at different wavelengths are collected on a CCD. The set-up is very simple and comprises an intensified CCD camera (Andor, model iStar sCMOS18F63, 16 bit), with a resolution of 1024 x 1024 pixels (2 µs gate width, 8 Hz repetition rate) and an image doubler (LaVision GmbH). The image doubler is basically a stereoscope that projects an image pair onto the camera. Two band-pass filters at 600 nm and 750 nm, with 50 nm FWHM, are mounted in front of the image doubler. We selected these two wavelengths because of 1) the higher emissivity of soot in this region of the visible spectra with respect to the soot emissivity at lower λ and 2) a good spectral sensitivity of the camera employed. We chose the detection wavelengths as far away as possible, within the limit imposed by the condition stated above (higher soot emissivity and high camera sensitivity), to increase the accuracy of the measure [158]. Furthermore, since we collected on the CCD two images at different wavelengths, the depths of field could vary slightly, namely the two images could be focussed on different planes. Nevertheless, considering the small difference between the wavelength regions and the quite high f-number used (f/5.6), the variation of the depth of field was negligible.

For the calibration of the detection system a tungsten-ribbon spectral calibration lamp (Ocean Optics, model HL-3-CAL), was employed. The calibration lamp was placed exactly at the same position of the flame, therefore the optical path lengths from the flame to the camera and from the lamp to the camera were exactly the same (100 cm).

5. Results

5.1 Diesel burner characterization

The diesel burner implemented has been initially characterized by using two reference diesels, CEC RF-06-03 and CEC RF-79-07, which have known chemical composition. In the present work the fuel CEC RF-79-07 will be called “baseline” while we will refer to the other one, diesel CEC RF-06-03, by calling it “reference” for simplicity. The two fuels selected are typically employed for laboratory investigations of emission performances. In particular, the fuel CEC RF-79-07, “baseline”, is used as base fuel for insertion of additives. These two diesels have a similar chemical composition which differs slightly for the content of aromatic species, as displayed in Table 2. The fact that the concentration of aromatic species differs slightly between the two fuels is desirable because in this way we can verify whether we are able of measuring a different soot concentration when the chemical composition of the fuel changes lightly (this is, for example, the case of additives insertion).In fact, as already reviewed in chapter 2.1.2, the polycyclic aromatic hydrocarbons are the species that most increase the amount of soot produced; consequently, only a small increment of these species in the fuel will enhance soot emissions. The sooting behaviour just described was verified by carrying out LII and WALS measurements on the burner’s laminar diffusion flame; this allowed to reveal differences in soot concentration and size between the two fuels. It should be remarked that, although the flame obtained from the novel burner is laminar and sufficiently stable for soot characterization, it has minor fluctuations of ±0.7 mm from the central position in the radial direction, which implies that a considerable number of LII and WALS images have to be collected to have meaningful results.

Table 2. *Comparison of the chemical composition of the two reference diesels tested, i.e. CEC RF-79-07, "baseline", on the left, and CEC RF-06-03, "reference", on the right[159]. The total aromatics content is highlighted with red colour.*

		BASELINE DIESEL (CEC RF-79-07)			REFERENCE DIESEL (CEC RF-06-03)		
Feature	Units	Results	Limits Minimum	Limits Maximum	Results	Limits Minimum	Limits Maximum
Cetane number	-	53.3	52.0	54.0	52.4	52.0	54.0
Density at 15°C	kg/m^3	833.8	833.0	837.0	834.0	833.0	837.0
Flash point	°C	84	62	-	87	55	-
Viscosity at 40°	mm^2/s	2.9	2.3	3.3	2.8	2.3	3.3
Aromatics, total	% w	21.6	-	-	24.4	-	-
Aromatics, Mono	% w	16.9	-	-	20.2	-	-
Aromatics, Poly (2+3)	% w	4.7	3.0	6.0	4.2	3.0	6.0
Sulfur	mg/kg	< 1.0	-	10	1.8	-	10

5.1.1 Volume fraction

During LII measurements, 5000 images were collected for every fuel under study; nevertheless, due to the flame's fluctuations, some of the images collected could not be considered during the evaluation process. A Matlab filter was specifically implemented to select the images which were suitable for evaluation. The selection was based on a symmetry criterion, i.e. in a diffusion flame the soot formed is usually uniformly disposed in the external layer of the flame, called annular region. Therefore, in a two-dimensional LII image the soot should be equally visible on both external sides of the flame, while the central part does not display a strong soot region (therefore is darker). However, when the flame is tilted the soot is not equally visible on both external sides (sometimes, also the central part of the flame displays high soot concentration) as shown in Figure 22. The Matlab filter implemented check the distance between the two external layers of soot along the flame's height (especially within the first seven centimetres);

if the distance within the soot layers is between 6 mm and 8 mm (the width of the flame) in the first 7 cm height, the images pass the filter, otherwise they are rejected. To distinguish between the "dark" pixels (no soot/very low soot concentration, i.e. the dark region between the soot layers) and the "bright" pixels (high soot concentration, i.e. the soot layers) the Matlab filter scans the entire image for the area that contains the 10 (neighbour) pixels with the highest value (that corresponds to the maximum LII signal intensity) and calculates the average value of these pixels. Subsequently, the filter scans the image a second time checking the pixels' value. All pixels which have the value lower than 1/10 of the average value calculated before (the maximum LII signal) are considered as "dark" and will be set to "0", while all the others are considered as "bright" and are set to "1". Subsequently, the filter scans the entire binary image line per line counting the "0" and "1" values. When the filter detects a sequence of "0" values between two sequences of "1" values it recognizes the dark region between the two bright soot layers. The pixels are then converted into millimetres to find the width of the dark region between the soot layers; this is finally compared with the threshold set for the layers' distance, i.e. 6 mm - 8 mm. Eventually, around 1000 - 1200 LII images for every measurement condition were selected and used for soot distribution quantification. Furthermore, before every measurement set 100 background images of the flame were collected and averaged; during the recording of the background images the laser was turned off so that the averaged background image obtained accounted for the natural background flame luminosity, ambient light and thermal noise of the camera.

Some examples of LII single-shot images of the flame (selected by the Matlab filter), baseline and reference diesel, are shown in Figure 23.

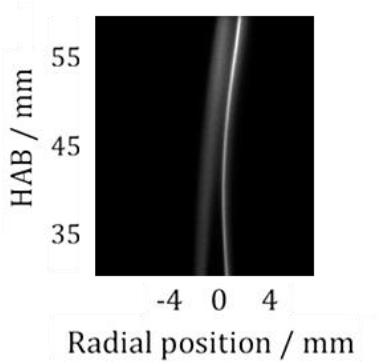

Figure 22. *LII single-shot image of the tilted laminar diffusion flame which does not pass the Matlab filter. The image shows the flame (baseline diesel) between 30 mm and 60 mm height above the burner (HAB).*

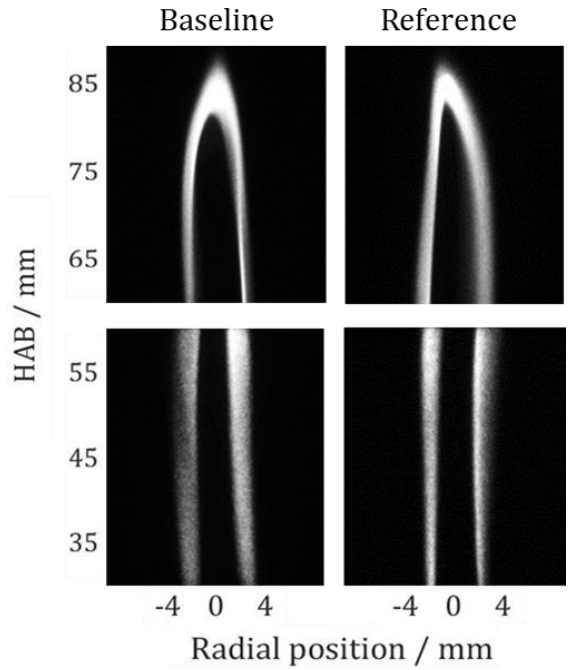

Figure 23. 2D *LII single-shot images of the laminar diffusion flame (which passed the Matlab filter), baseline (on the left) and reference (on the right) diesel. The lower images show the flame between 30 mm and 60 mm HAB while the upper images show the flame between 60 mm and 90 mm HAB. Recording two different images, one for the lower part of the flame and one for the upper part, was necessary due to 1) the fixed distance between the camera and the flame, dictated by the focal length of the objective lens (we could not move the camera backward to detect a larger portion of the flame) 2) the limited Region of Interest (ROI) of the camera employed. (Figure from [155]).*

From the ~1000 images selected by the filter an averaged image was created and used for the determination of soot volume fraction after calibration. The averaged images of the baseline and reference flame are shown in Figure 24.

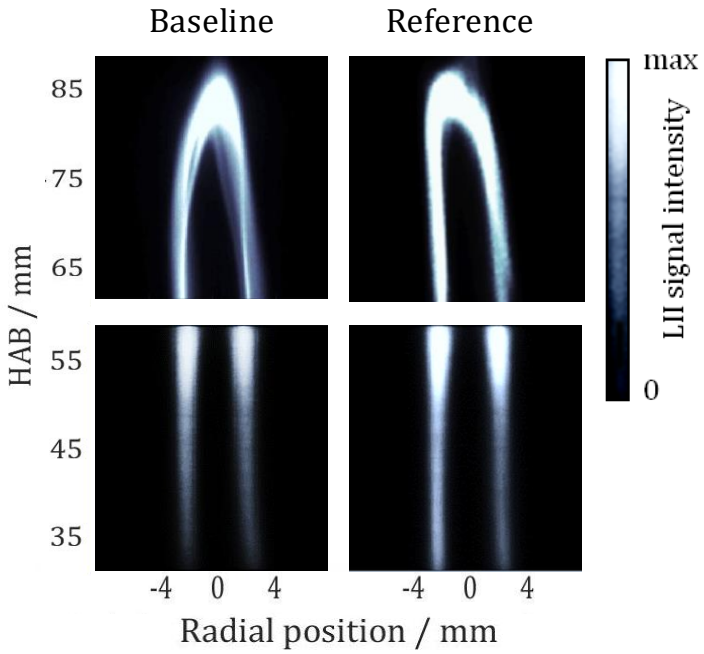

Figure 24. 2D *LII images, average of ~1000 single-shot images (selected by the filter), of the laminar diffusion flame. On the left: resulting images of the LII measurements on the baseline diesel; On the right: resulting images of the LII measurements on the reference diesel. (Figure from [155]).*

Before starting the measurements, the laser fluence has to be optimized to minimize effects of fluence fluctuations. For pulsed LII applied on flames, typically LII signal rises by rising the fluence until it saturates when the sublimation temperature is reached [160] (see section 3.1). The measurements for the LII peak signal-fluence curve were carried out in the burner diesel flame at 50 mm height above the burner; the curve is shown in Figure 25. In this case around 500 single shot images were filtered and evaluated for a fluence range between 0.05 J/cm^2 and 0.3 J/cm^2. After the visualization of the LII signal-fluence curve, the value 0.15 J/cm^2 was selected for being used for the following quantitative soot measurements. At this fluence, corresponding to the start of the plateau region of the curve, the LII signal is barely dependent on the fluence.

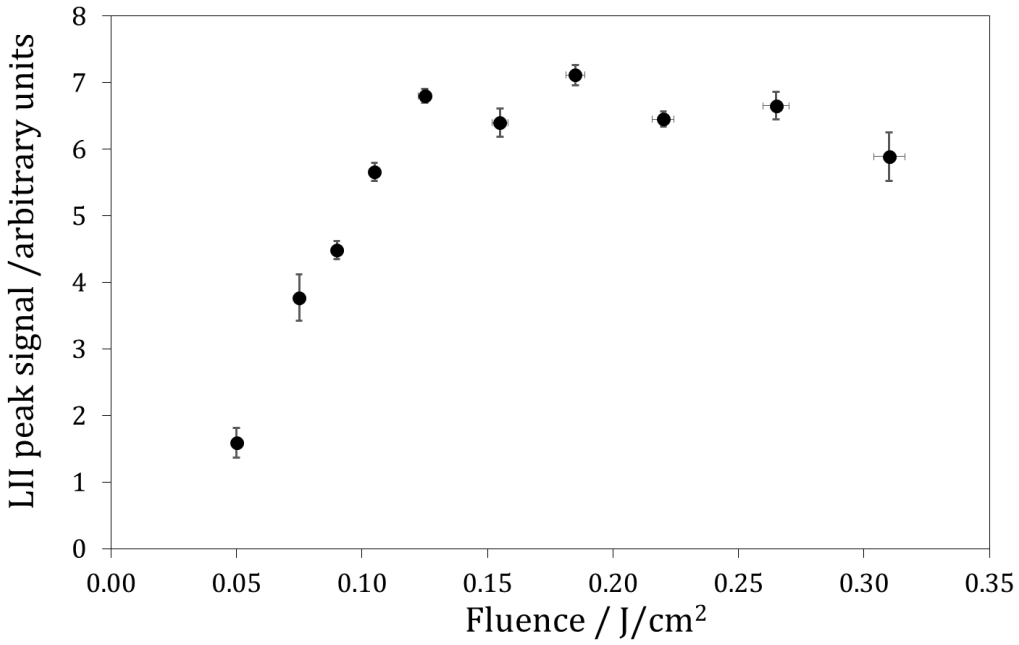

Figure 25. *LII peak signal-fluence curve. The standard deviation of the laser fluence fluctuation is used to determine the horizontal error bars while the vertical error bars result from the standard deviation of the selected LII single shot images (1000). (Figure taken from [155]).*

The radial profiles of the soot volume fraction distribution were estimated from the 2D LII images (average of ~1000 single-shots) shown in Figure 24. Although the full image could be used for soot quantification, the evaluation of soot f_V at specific HAB for both fuels simplifies the comparison between them and consequently the comprehension of the effects of fuel chemical composition on soot. The data were evaluated from 30 mm to 90 mm height above the burner (HAB), in steps of 10 mm. The soot volume fraction f_V found at 30 mm, 50 mm, 70 mm and 90 mm above the burner surface is shown in Figures 26 and 27 for the baseline and reference diesel flames respectively.

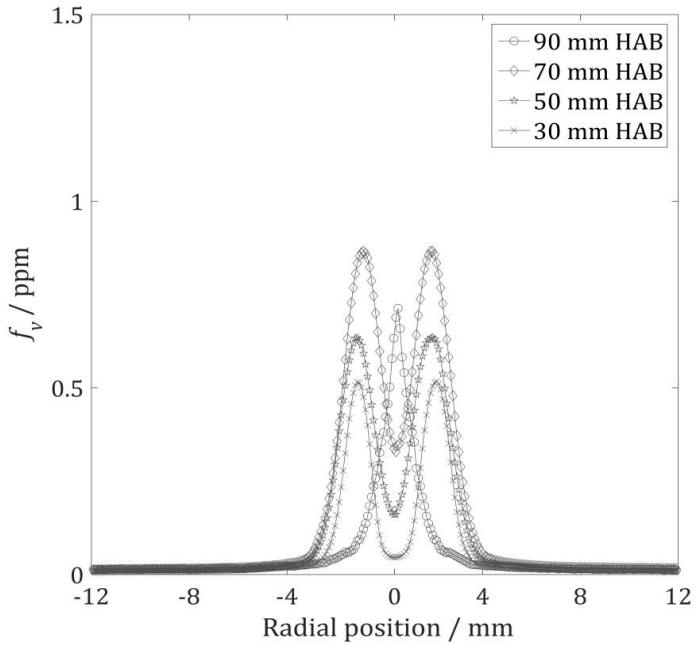

Figure 26. *Soot volume fraction (f_V) trend over the radial profiles at 30 mm, 50 mm, 70 mm and 90 mm HAB for the baseline diesel. (Figure taken from [155]).*

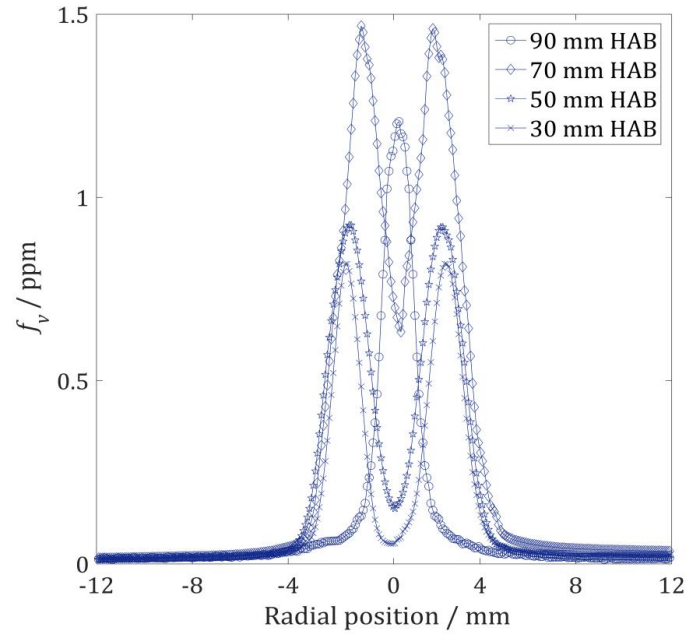

Figure 27. *Soot volume fraction (f_V) trend over the radial profiles at 30 mm, 50 mm, 70 mm and 90 mm HAB for the reference diesel. (Figure taken from [155]).*

Generally, from 30 mm to about 75 mm above the burner the soot radial profile of the diffusion flame exhibits two side areas where the soot volume fraction is higher, corresponding to the flame's annular region. In the central part of the flame the soot volume fraction drastically drops. This trend is characteristic of diffusion flames [161]. The reason of this peculiar behaviour is the diffusion of the air's oxygen from outside toward the middle of the flame. Accordingly, two different regions are formed: a fuel-rich area where soot is generated and a stoichiometric region. After 75 mm HAB the two soot peak regions spread horizontally and join, covering also the centre of the flame.

Moreover, from Figures 26 and 27, as well as from Table 3 (below), emerges that soot concentration grows with increasing HAB until ~80 mm HAB, due to the continuous soot formation, while at 90 mm the soot volume fraction decreases again. Indeed, higher in the flame, in this case above 80 mm HAB, soot oxidation, which is always present during the combustion, becomes dominant, yielding a reduction of the amount of soot produced. The trend just described is observable for both baseline and reference diesel and it is in agreement with other works in literature [161-163].

For a better comparison between the fuels, the mean and maximum f_v of every HAB along the radial line (sampling points every 10 mm steps) were calculated for every single-shot image. The values were subsequently averaged. They are reported in Table 3 with the standard deviation calculated taking into account the variation within the single-shot images. The maximum f_v is observed at 80 mm HAB and is about 1.8 ppm for the reference diesel and about 1.5 ppm for the baseline diesel.

Table 3. *Maximum f_v estimated along the flame's height and the corresponding standard deviations. (Table from [155]).*

	BASELINEDIESEL (CEC RF-79-07)				REFERENCEDIESEL (CEC RF-06-03)			
HAB / mm	$f_{v,max}$ / ppm	σ ($f_{v,max}$) / ppm	$f_{v,mean}$ / ppm	σ ($f_{v,mean}$) / ppm	$f_{v,max}$ / ppm	σ ($f_{v,max}$) / ppm	$f_{v,mean}$ / ppm	σ ($f_{v,mean}$) / ppm
30	0.54	0.02	0.17	$1.3\cdot10^{-4}$	0.73	0.04	0.30	$4.9\cdot10^{-3}$
40	0.52	0.01	0.19	$3.3\cdot10^{-4}$	0.69	0.02	0.31	$2.1\cdot10^{-3}$
50	0.68	0.02	0.24	$1.5\cdot10^{-4}$	1.02	0.05	0.43	$3.0\cdot10^{-3}$
60	0.67	0.02	0.29	$1.5\cdot10^{-3}$	1.09	0.09	0.50	$4.9\cdot10^{-3}$
70	0.87	0.03	0.41	$9.0\cdot10^{-4}$	1.45	0.14	0.72	$6.8\cdot10^{-3}$
80	1.47	0.09	0.77	$2.5\cdot10^{-3}$	1.76	0.11	0.84	$3.7\cdot10^{-3}$
90	1.06	0.08	0.15	$9.0\cdot10^{-3}$	1.27	0.11	0.28	$2.0\cdot10^{-2}$

The maximum soot volume fraction found at every HAB for the reference and the baseline diesel are compared in Figure 28. It is noticeable that the combustion of the reference diesel generates significantly more soot than the baseline diesel. Specifically, the baseline diesel emits between 17% and 40% (depending on the HAB) less soot compared to the reference diesel. This data is meaningful also when we take into account the error bars (in average 9%). The error bars are calculated from the standard deviation of the single-shot images. The higher content of aromatic hydrocarbons in the reference diesel, about 3% (mainly mono-aromatics), might be the reason of the different sooting behaviour of the two fuels investigated. A further explanation can be inferred when we consider the phenomenological models of soot formation [15]. According to the model the formation of soot from hydrocarbons is controlled mainly by the rate of incipient soot nucleation. The nucleation of a soot particle can occur by three major paths: 1) cyclization of straight chain molecules into rings 2) dehydrogenation of aromatic rings and consecutive formation of polycyclics (it usually takes place at low temperatures) and 3) breakup and subsequent recyclization of rings, usually at higher temperatures. Consequently, an higher amount of aromatic hydrocarbons in the fuel causes a growth of the number of soot nucleation paths yielding to more soot particles.

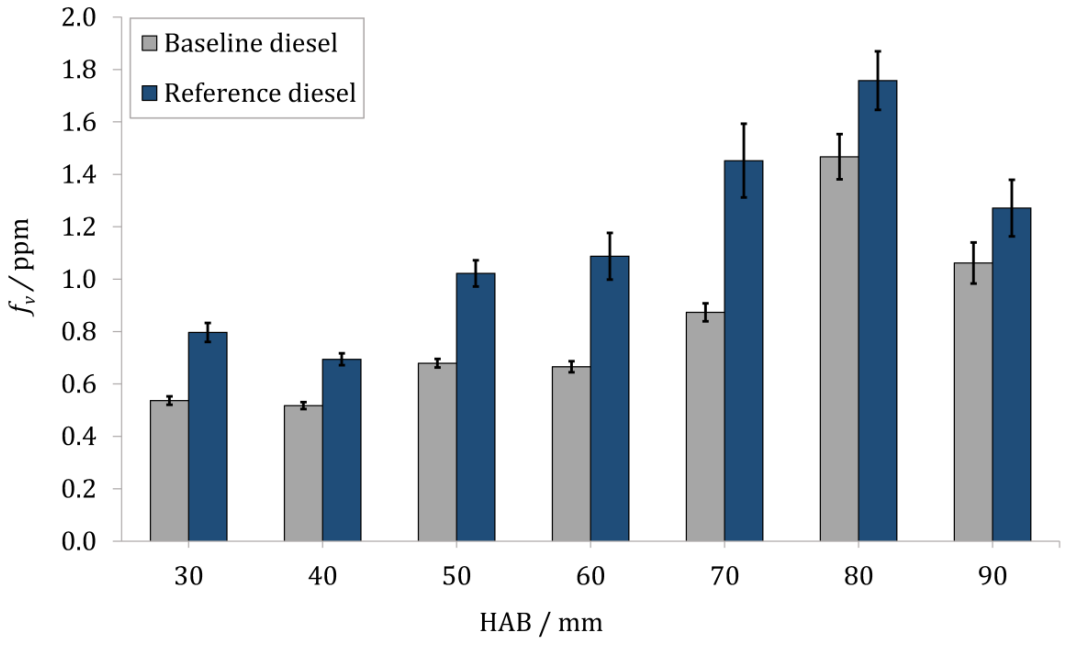

Figure 28. *Comparison of f_v maximum between reference and baseline diesel. (Figure taken from [155]).*

5.1.2 Radius of gyration

We performed WALS measurements along the flame's height every 10 mm from 30 mm to 80 mm above the burner surface. The point-wise measurement volume was situated in the flame's annular region, in correspondence with the f_v maximum. The position of the measurement volume was chosen according to the following procedure: WALS images along the radial profile of the flame were collected; the measurement volume was then set in the point where the scattering signal was higher along all the mirror (for all the angles). Because of flame's flickering, especially in the upper part, at 90 mm HAB the signal-to-noise ratio was too low, not allowing the evaluation. Therefore, this point was not considered. For every measurement point, 5000 images of the WALS mirror were captured by the CCD camera. The angular resolution of the scattering data was 1°. Figure 29 shows one single-shot ring shaped scattering image (calibrated) flanked by the corresponding normalized (by the maximum) intensity – angle chart. The intensity – angle chart was obtained by integration of the scattering intensity over the radial thickness of the mirror, for every degree. Figure 29 clearly depicts that the forward scattering, i.e. between 10° and 90°, is predominant over the backward scattering, between 90° and 170°. Consequently, calibrated scattering data from fractal aggregates plotted over the angle typically exhibit a monotonous negative slope when the angle increases (that is what occurs in Figure 29). In this study the data with positive slope were discarded by a self-made Matlab filter. The positive slopes were caused by the flickering of the flame. As mentioned, the position of the measurement volume was set on the f_V maximum. Nevertheless, if the flame slightly moves during the measurement, the region where soot is more concentrated moves away from the measurement volume and it is replaced by a zone where soot is less concentrated. Sometimes, in the flame zone that accidentally replaces the one chosen for measurements, the soot aggregates are very low concentrated and their scattering signal is not detectable (it is too weak). This leads to an image that is either black or has some random illumination from the flame. Consequently, the intensity-angle curve achieved from these images shows both rising and decreasing slopes. Although we implemented the burner system in order to minimize fluctuations, some minor movements of the flame could not be avoided, therefore the Matlab filter for images selection was required. Furthermore, to guarantee measurements conditions as uniform as possible, the size of the measurements volume was reduced by decreasing the camera's aperture to *f*/5.6. The filter rejected the scattering data that displayed growing normalized intensity over the angle. Since the forward scattering influences predominantly the R_g-evaluation, between 10° and 90° a very rigid criterion was used, allowing only five data-

point to be slightly higher than the previous one. For the backward scattering a larger number of non-decaying data-points (i.e. ten) were permitted.

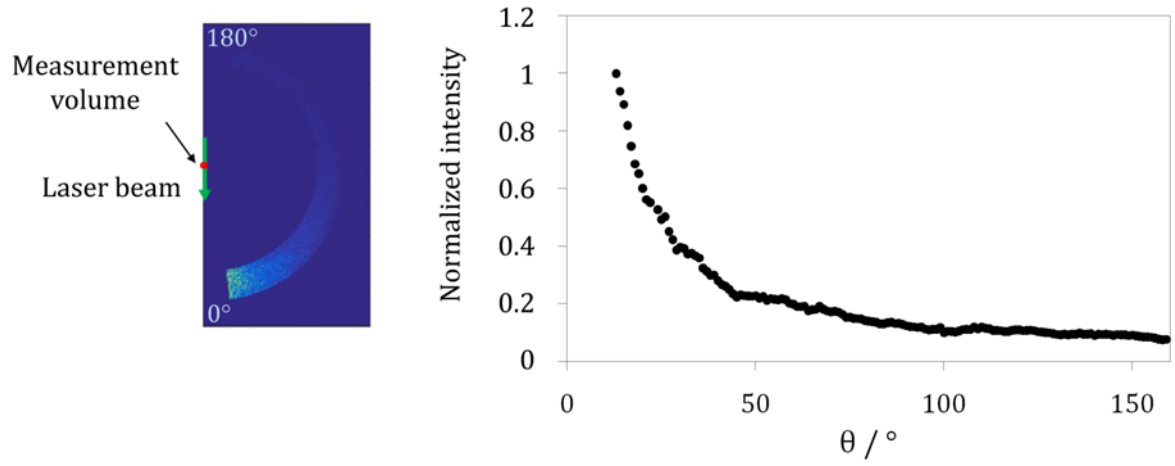

Figure 29. *Left: Ring shaped WALS scattering data, generic calibrated single-shot image of half (0° -180°) of mirror acquired at 50 mm HAB (baseline diesel). Right: Normalized scattering intensity over the angle obtained from the image on the left. (Figure taken from [155]).*

About 200 images out of the 5000 single-images detected passed the filter. The data were evaluated in the Guinier regime. The effective radius of gyration $R_{g,eff}$ has been obtained from the intensity $I(q)$ of the acquired scattering data through the formula [36]:

$$\frac{1}{I(q)} = \frac{1}{I(0)} + q^2 \frac{R_{g,eff}^2}{3I(0)}. \tag{28}$$

For the determination of $R_{g,eff}$,1/$I(q)$ is fitted linearly against q^2 (within the limit of the Guinier regime $I(q)/I(0) \leq 2$ [36]). This yields to the estimation of $I(0)$ and the slope $m = R_{g,eff}^2/3I(0)$ is used for the subsequent calculation of the effective soot aggregate size. The $I(q)/I(0)$-$qR_{g,eff}$ curves (single-shots) for different heights in the flame (baseline diesel) are displayed in Figure 30.

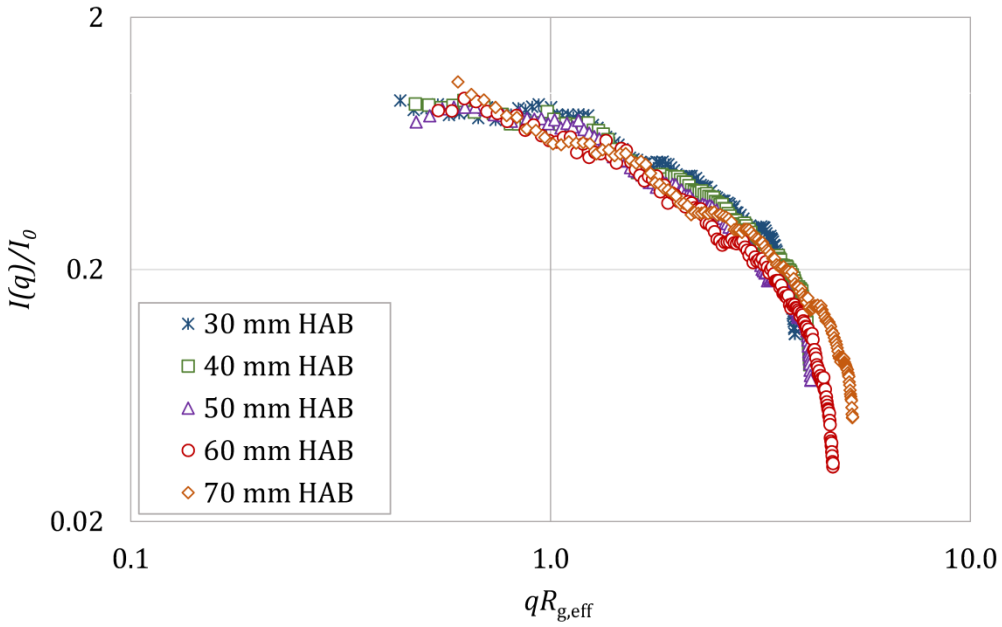

Figure 30. *Single-shot scattering data as a function of* $qR_{g,eff}$. *(Figure taken from [155]).*

The statistical distribution of the radii of gyration, extrapolated from the evaluation of WALS data at every flame's height, are shown in Figures 31 (baseline diesel) and in Figure 32 (reference diesel). The $R_{g,eff}$ distribution has a lognormal shape; the same was found by Oltmann et. al [139] in barely turbulent flames. From the $R_{g,eff}$ distribution a median value symbolized by $\mu_{g,eff}$ was determined with the aim of comparing the corresponding measurement points of the two fuels. Considering the median $\mu_{g,eff}$ for the different heights, a general slight increment of the median radius of gyration with increasing HAB is noticeable. The slight increment probably occurs because of the increasing aggregation time of the particles. The median $\mu_{g,eff}$ estimated for the baseline diesel ranges between 168 nm at 30 mm above the burner and 207 nm at 70 mm HAB. In the case of the reference diesel, the variation of $\mu_{g,eff}$ between the lowest height measured (178 nm) and the upper one (211 nm) is approximately 33 nm.

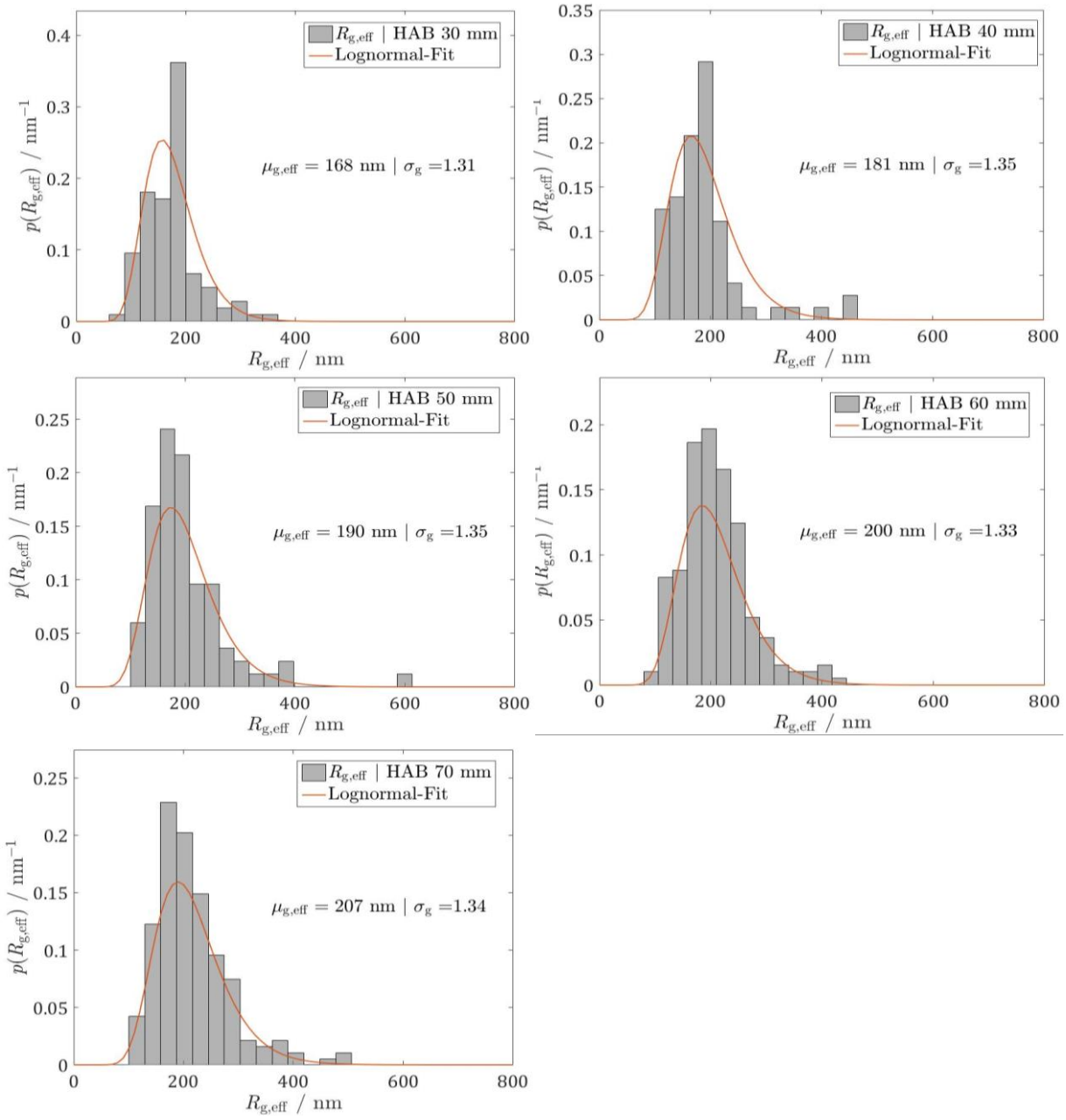

Figure 31. *$R_{g,eff}$ distribution from 30 mm to 70 mm HAB for the baseline diesel. (Figure taken from [155]).*

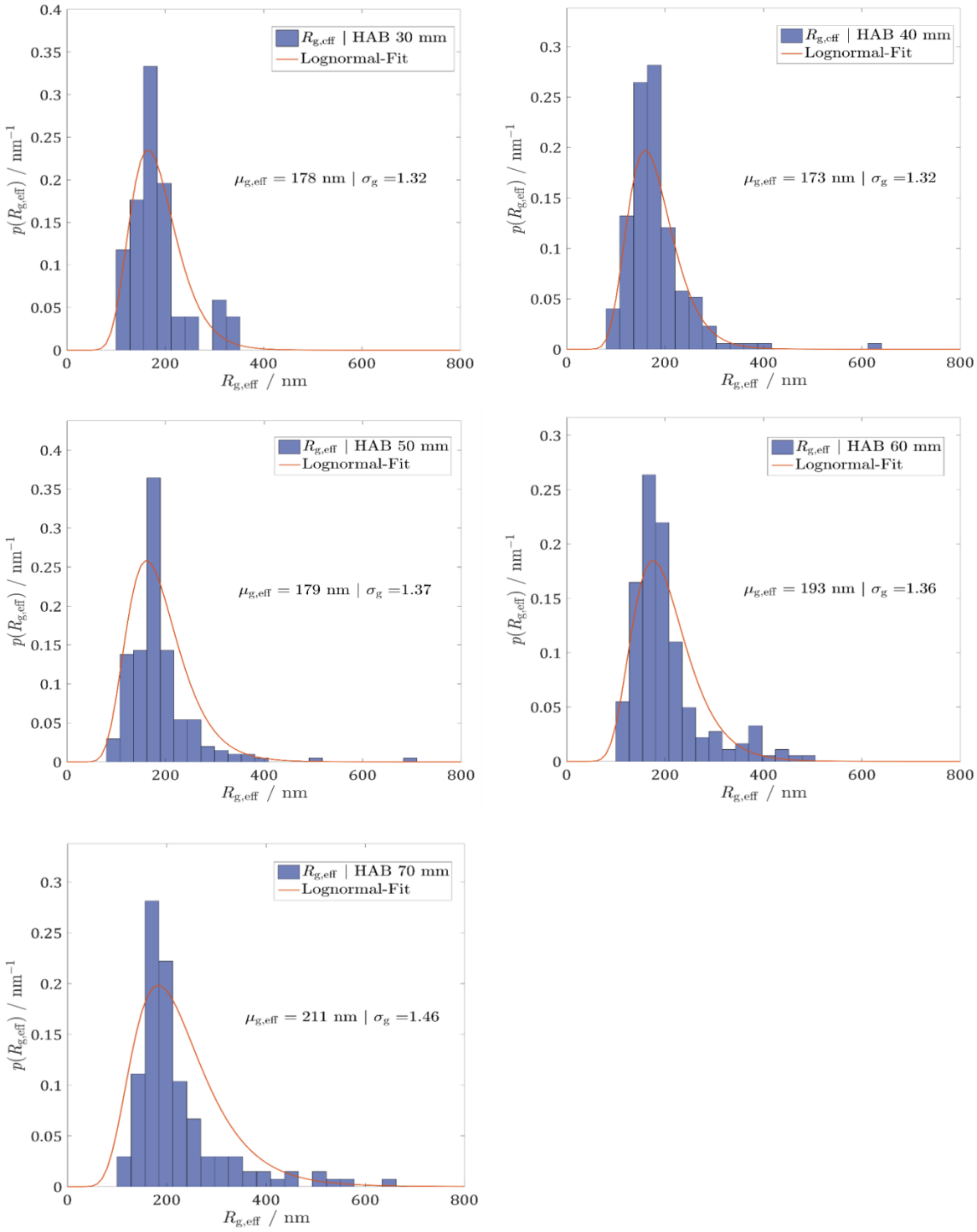

Figure 32. *$R_{g,eff}$ distribution from 30 mm to 70 mm HAB for the reference diesel.(Figure taken from [155]).*

A direct comparison of the median $\mu_{g,eff}$ values between the two diesels (at various heights) is shown in Figure 33. The error bars are determined from the standard deviation of the 200 images that passed the Matlab filter. This leads to an averaged measurement error of about 7 nm. The

median radii of gyration of the baseline appear to be slightly higher compared to the ones of the other fuel under study. Nevertheless, when we consider the statistical uncertainty of the results, it is not possible to infer whether the soot aggregate size between the reference and the baseline diesel actually differs.

Overall, on one hand LII measurements allowed to detect a reduction of soot concentration when the amount of aromatics content was lower; on the other hand the soot aggregation process itself, as WALS measurements have shown, does not seem to vary during the combustion of the two fuels. Eventually, the combustion system was characterized; it allowed to highlight the impact of the fuel's chemical composition of soot properties.

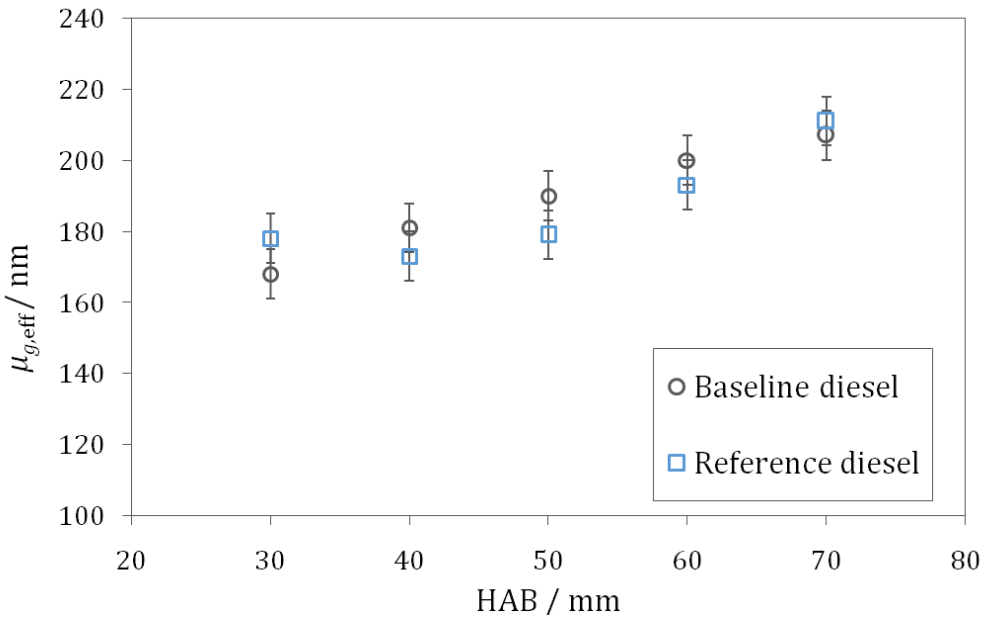

Figure 33. *Comparison of $\mu_{g,eff}$ over the height above the burner. (Figure taken from [155]).*

5.2 Additive effect on soot properties

LII and WALS were employed for investigation of fuel's chemical composition effects on soot formation. For the study of additives' impact on soot properties besides LII and WALS, which were used as main detection tools, two supporting techniques, i.e. SMPS and two-color pyrometry, were applied. In particular, two-color pyrometry was used to evaluate soot temperature changes. Indeed, additives could affect the flame's temperature which can in turn influence soot production. The additives investigated are TPGME, OME_2 and $OME_{3\text{-}5}$; the OME_2 has n=2 (n is the number of -CH_2O- groups in the molecule) while the $OME_{3\text{-}5}$ is a

mixture of OMEs with n varying from 3 to 5, specifically the blend used contains about 10 % of OME_3, 80 % of OME_4 and 10% of OME_5 (percentage in m/m). The additives are inserted in the neat baseline diesel (CEC RF-79-07) in three different concentrations, i.e. 1%, 3% and 9% in volume. The data obtained for the additised fuels are always compared with the baseline's ones. All the measurements were carried out in the annular region of the flame as displayed in the false colour soot luminosity image (average of 200 single shot images collected with 750 nm band-pass filter, 50 nm FWHM) in Figure 34. In Figure 34 the 2D-LII and two-color pyrometry measurement areas are indicated with red rectangles (the red rectangles correspond to a 2 mm x 2.4 mm area i.e. 20 pixels x 24 pixels), while the WALS measurement points are symbolised by the grey dots.

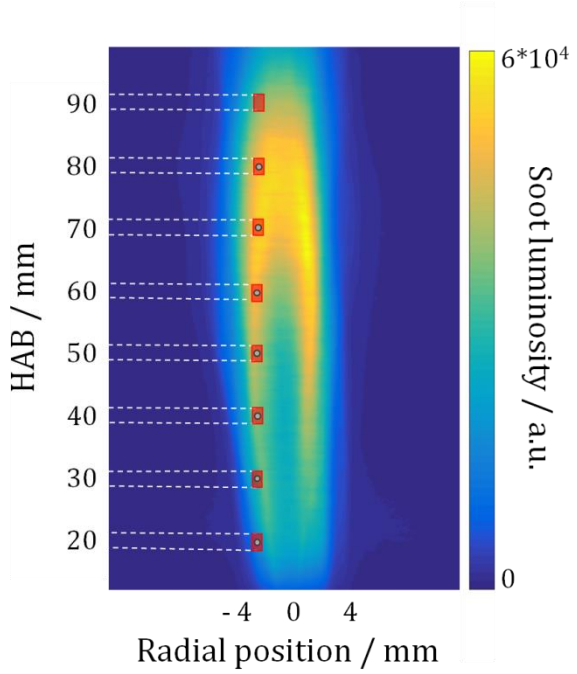

Figure 34. *Soot luminosity image of the laminar diffusion flame (baseline diesel), false colour. The red rectangles stand for the LII and two-color pyrometry evaluation area while the grey dots symbolize the WALS measurement points. (Figure from [96].)*

5.2.1 Volume fraction

The same evaluation procedure already employed for the burner's characterization, which implies the acquisition of 5000 single-shot LII images subsequently filtered and averaged to obtain a final one used for f_V determination, was applied to the additised diesel data. The soot

volume fraction can be estimated in the full 2D LII image (see Figure 24), nevertheless, these 2D data cannot be correlated to the point-wise data achieved by WALS and SMPS; consequently, for comparison purposes, only the area shown in Figure 34 (red rectangles) were considered for evaluation. For the comparison of the soot vertical trend between the various blends, the averaged f_V (obtained after calibration by extinction) of every measurement area (2 mm x 2.4 mm area) was considered. The comparison is shown in Figure 35 a, b and c. The soot volume fraction over the height above the burner for OME_2-, OME_{3-5}- and TPGME-diesel blend is always flanked by the baseline data measured at the same conditions. Generally, the f_V - height trends reflect the one already seen in Figure 28, i.e. a growth of soot concentration until 70 mm-80 mm HAB followed by a reduction in the oxidation zone. From Figure 35 the following observations can be made (the following remarks take into consideration the error bars which derive from the standard deviation of the 1000 LII images obtained after filtering):
1) a significant decrease of f_V results from the insertion of OME additives in the neat diesel. While OME_2 provokes a minimal reduction of soot volume fraction, the effect of OME_{3-5}, especially upper in the flame, is slightly more accentuated. Furthermore, the reduction effect of both additives increases by increasing the additive's concentration, i.e. the OMEs inserted in 3% vol. and 9% vol. in the baseline show higher soot abatement compared to the 1% blends.
2) TPGME exhibits a slight decreasing effect only at higher concentrations and in the higher part of the flame where a little drop of soot volume fraction for the 9% TPGME-diesel at 70 mm HAB and the 3% TPGME-diesel at 90 mm HAB is detected. Nevertheless, overall this additive has no significant impact on soot formation especially during the initial stages of the combustion and in the case of low additive concentration (i.e. lower than 3% vol.).

a.

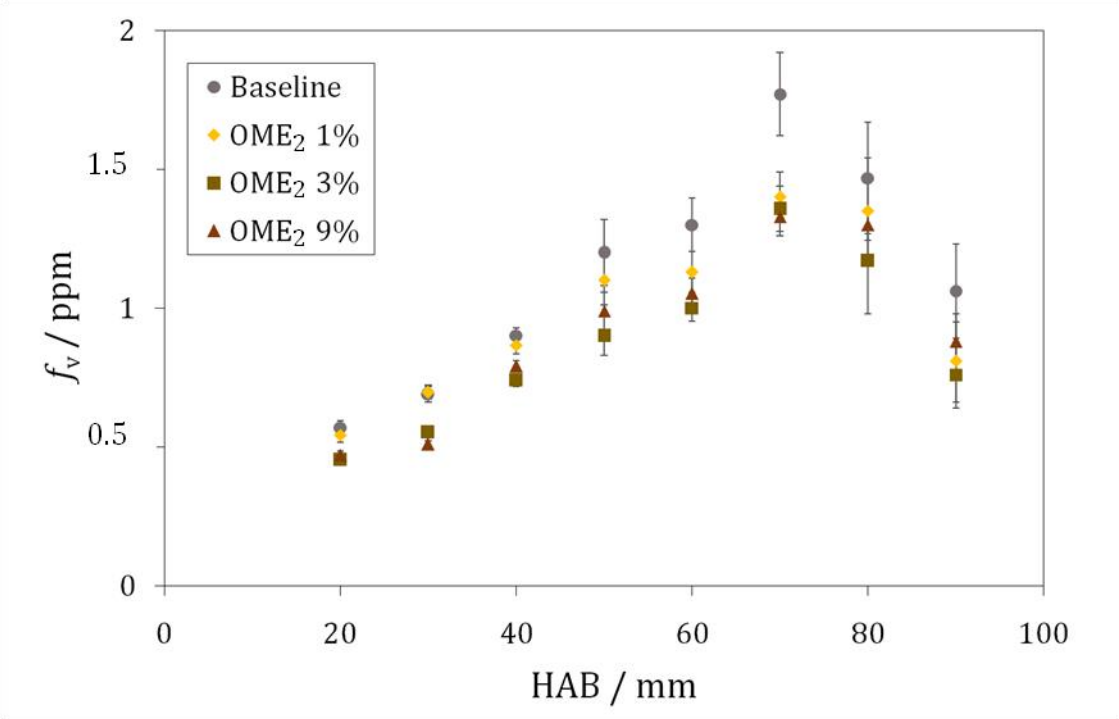
Baseline
OME2 1%
OME2 3%
OME2 9%
fv / ppm
HAB / mm
0
0.5
1
1.5
2
0
20
40
60
80
100

b.

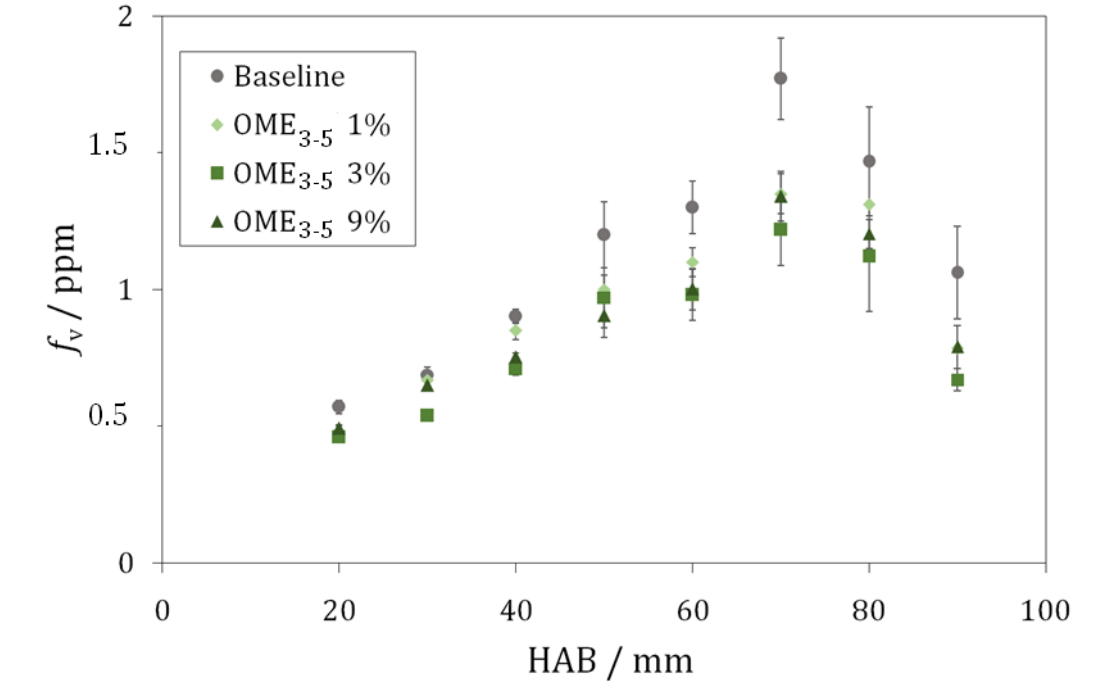
Baseline
OME3-5 1%
OME3-5 3%
OME3-5 9%
fv / ppm
HAB / mm
0
0.5
1
1.5
2
0
20
40
60
80
100

c.

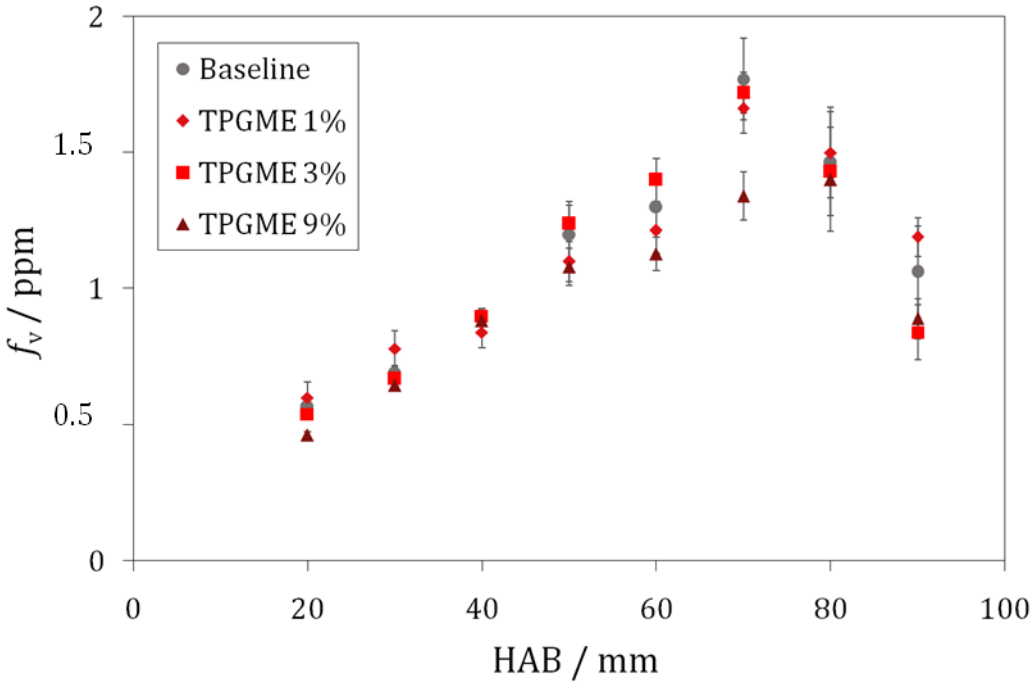

Figure 35. f_V *-HAB curves for pure baseline and* ***a.*** *OME_2-baseline blends (1% vol, 3%vol and 9% vol)* ***b.*** *$OME_{3\text{-}5}$-baseline blends (1% vol, 3% vol and 9% vol) and* ***c.*** *TPGME-baseline blends (1% vol, 3% vol and 9% vol). The error bars were calculated from the standard deviation of the 1000 LII images which passed the Matlab filter. (Figure from [96].)*

5.2.2 Radius of gyration

The soot aggregates' medium radius of gyration $\mu_{g,eff}$ was evaluated for all the additised diesels and also in this case compared with the $\mu_{g,eff}$ found for the baseline. The charts in Figure 36 a, b and c display the $\mu_{g,eff}$ vertical trend of OMEs- and TPGME-diesel blends. Generally, the increasing aggregation time by moving upper in the flame yields the generation of larger aggregate assembles at the end of the combustion process (see section 5.1.2). The comparison in Figure 36 reveals that the addition of OME_2 and $OME_{3\text{-}5}$ causes a slight reduction of $\mu_{g,eff}$, particularly evident for the additive's concentrations of 3% and 9%. We observe such a size diminution, compared to the baseline's soot aggregates, particularly between 60 mm and 80 mm HAB. Similarly, the soot aggregates produced by the 9% TPGME-diesel blend are smaller with respect to the baseline; this confirms the tendency of TPGME to be more effective on soot properties mainly at higher concentration (the same behaviour was observed for the effect of

TPGME on soot volume fraction). Nevertheless, no significant effect of the 1% and 3% TPGME-diesel blend on aggregates' size is detected.

a.

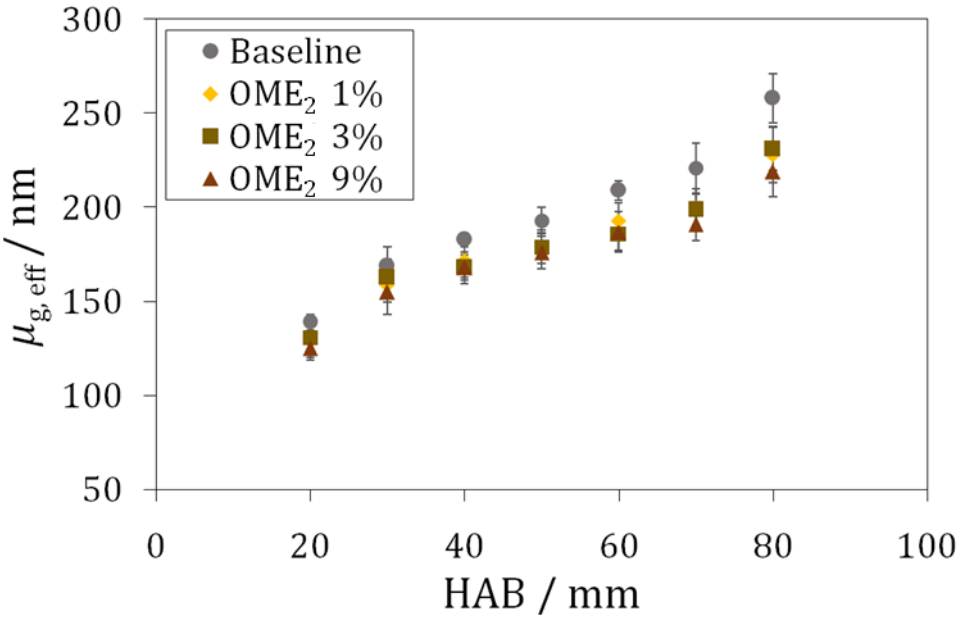

b.

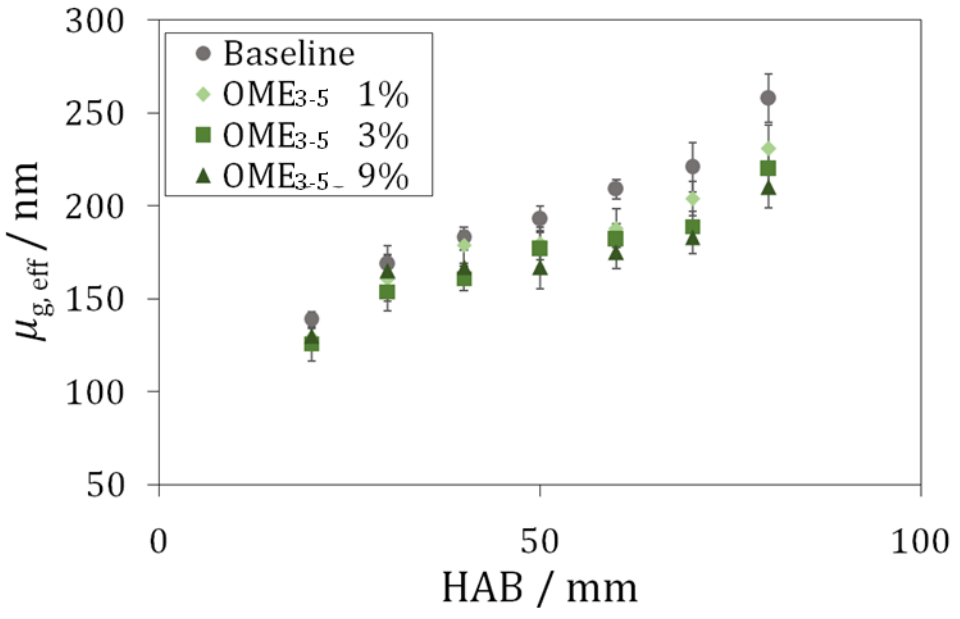

c.

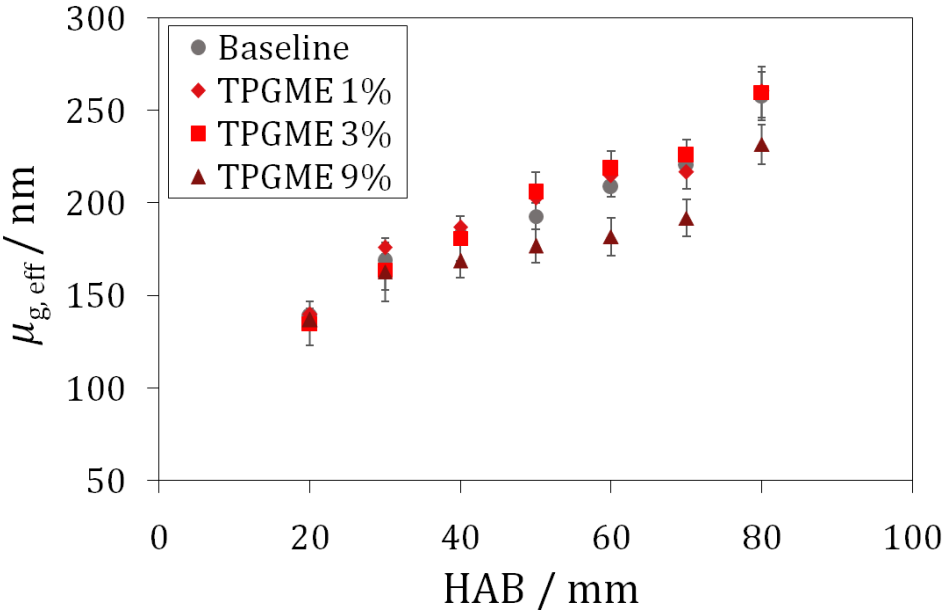

c.

Figure 36. *$\mu_{g,eff}$ vertical trends for neat baseline and **a.** OME_2-baseline blends (1% vol, 3%vol and 9% vol) **b.** $OME_{3\text{-}5}$-baseline blends (1% vol, 3%vol and 9% vol) and **c.** TPGME-baseline blends (1% vol, 3% vol and 9% vol). (Figure from [96].)*

5.2.3 Aerodynamic diameter and temperature

Two non-laser based methods were applied to complete the characterization of the particulate matter produced by the additised diesels: Scanning Mobility Particle Sizer (SMPS) and Two-color pyrometry. SMPS, the first technique considered, performs a scan of soot particles with different aerodynamic diameters (d_{ae}) and subsequently counts them. The size measured by SMPS is not the same physical quantity obtained by WALS. Indeed by WALS measurements the median value and the geometric standard deviation of the effective radii of gyration ($R_{g,eff}$) distribution (which usually exhibits a lognormal shape) is determined. The $R_{g,eff}$ results from the scattering signal generated by a multitude of aggregates (with a broad distribution of sizes) where larger aggregates influence more on the overall signal than smaller aggregates. The particle size found with WALS and SMPS experiments cannot be compared directly (the comparison could be possible only by taking into account some assumption [164]). Nevertheless, the general particle size trend in the flame as well as the tendency of an additised fuel to generate smaller/larger particles with respect to the neat diesel, which is of interest for

the purposes of the present study, is detectable by both methods. The aim of the application of both WALS and SMPS is to compare the particle size trend and the changes of particle size between the fuels. SMPS was basically applied to support the information achieved by WALS measurements and to complete the flame characterization by investigation of additive effect on initial soot formation.

In particular, the SMPS was employed for the investigation of the effect of OME_2,3% in volume in the baseline, on soot particle diameters. The measurements were carried out between 10 mm and 40 mm above the burner outlet. Due to flame's fluctuations, above 50 mm the sampling was inaccurate and, consequently, the measurements were not reliable. At every height of the flame three up- and down-scans (i.e. from smaller diameters to bigger diameters and the contrary) were performed and subsequently the number of particles found for every diameter was averaged. The glass capillary used for particles sampling was cleaned before and after every scan (i.e. in between the up/down scans) to remove the soot that accumulated on the capillary's walls and therefore obstructed the capillary. In Figure 37 the number of particles over the scanned particle's diameter for the baseline (Figure 37a.) and for the diesel-OME_2blend (Figure 37b.) is reported. At a first glance, considering initially the curves maxima, a shift to larger particle's diameter occurs when the height above the burner increases. Simultaneously, by increasing the height above the burner, the total number of soot particle decreases. This behaviour is expected as, according to WALS results (Figure 36 a.), soot particles agglomeration exhibits a significant progress between 10 mm and 40 mm HAB, leading contemporaneously to a lower number of (larger) particles. Furthermore, it is noticeable that the insertion of 3% vol. of OME_2 causes a significant reduction on particle diameters and a significant diminution of soot particles' quantity, i.e. the number of particles halves itself.

a.

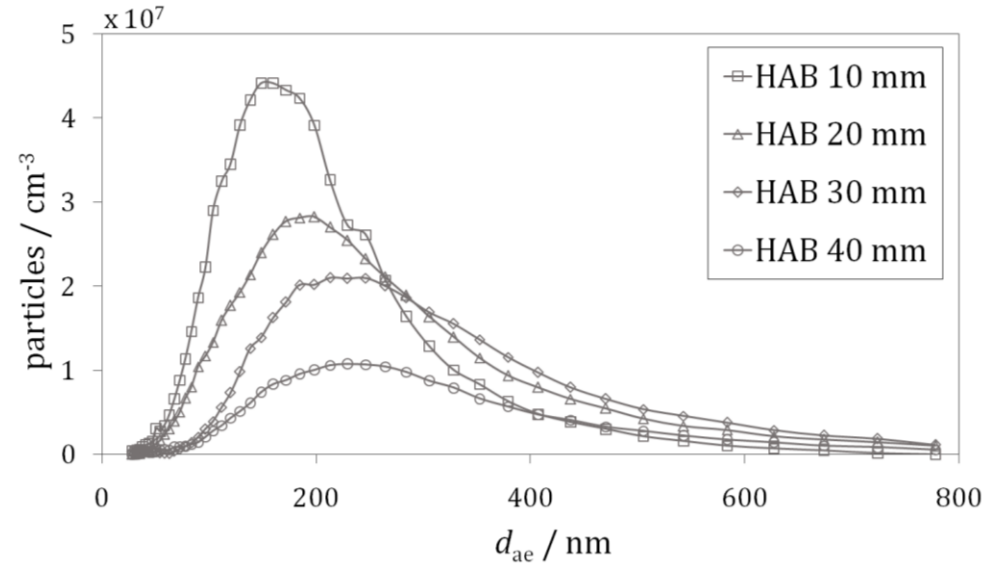

b.

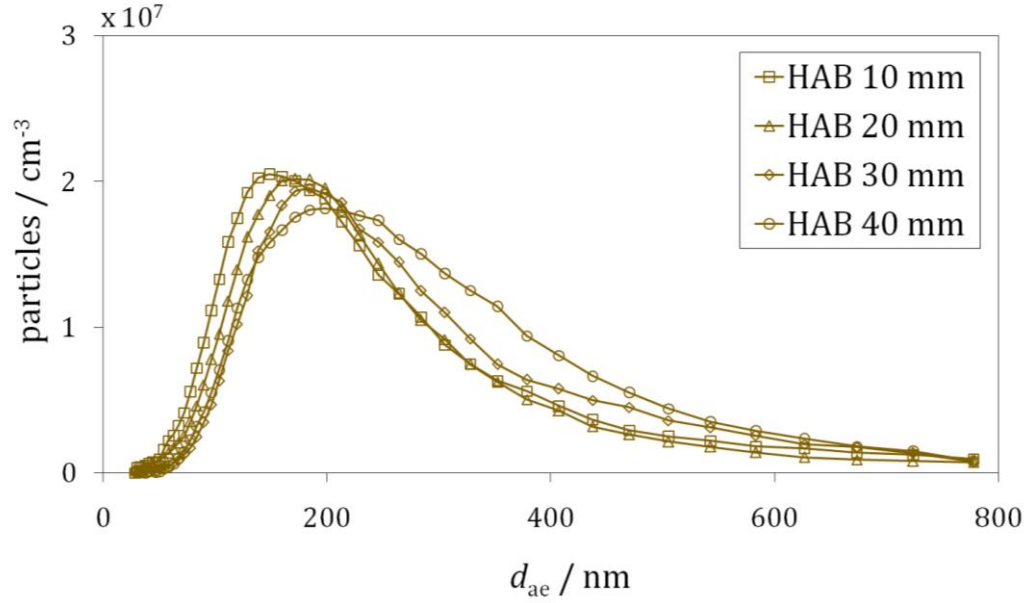

Figure 37. *Particle aerodynamic diameter (average) distribution from 10 mm to 40 mm HAB for* ***a.*** *neat baseline and* ***b.*** *OME_2-baseline blend (3% vol).*

The effect of OME_2 on particle size can be clearly visualized in Figure 38 where the median particles' diameter of the neat baseline and the one of the baseline-OME_2 blend are compared over the height above the burner. While at 10 mm HAB the size of the particles seems to not vary considerably between the fuels, higher in the flame (at 20 mm, 30 mm and 40 mm above the burner) the median aggregates' diameter of the OME_2-baseline blend is between 38 nm and

45 nm smaller compared to pure baseline. Precisely, the median diameters of the OME_2-baseline blend at 20 mm, 30 mm and 40 mm HAB are 160 nm, 172 nm and 184 nm respectively while the ones of the neat baseline are 198 nm, 213 nm and 229 nm respectively. The variation of the values may be partially due to measurement error. Errors are mostly caused by electromagnetic hysteresis, a typical high number of multiply charged particles in the aerosol (mainly corrected by the SMPS itself after the measurement) or a slight shift in the horizontal position of the probe after cleaning the glass capillary in between measurements. These phenomena are represented by the error bars (calculated from the standard deviation of the up- and down-scan performed at the same measurement point) shown in Figure 38. We find that the measurement error never exceeds 9%, therefore the size difference between the two fuels can be considered significant.

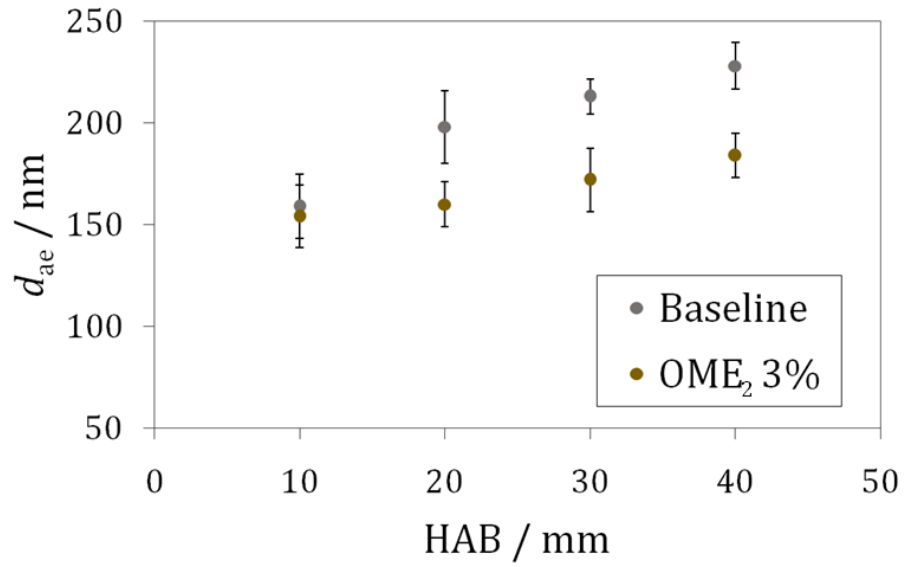

Figure 38. *Comparison of the average particles aerodynamic diameter (d_{ae}) over the height above the burner for pure baseline and OME_2-baseline blend (3% vol).*

Regarding the temperature measurements, we simultaneously acquired, for every fuel, 200 600 nm-750 nm couple of images of the flame. First, soot temperatureof every pair of images was determined from the ratio of the calibrated soot radiance detected at the two wavelengths. The temperature profiles achieved from the 200 couple of images were averaged in turn. The measurement point at 90 mm HAB did not show uniform flame conditions, due to flame flickering, therefore the data at this height was discarded. Figure 39 shows the temperature profiles of the pure baseline and the baseline additised with TPGME and OMEs. Soot

temperature generally rises smoothly by increasing the HAB until 60 mm HAB. Above 60 mm HAB the temperature drops slightly. Similar trends for diffusion flame have been found in literature [142].

If we compare the neat baseline soot temperature with the additives temperature profile, a minimal cooling effect of the additives can be noticed. The 3% OME_{3-5} – diesel blend and the 3% TPGME – diesel blend exhibit the highest soot temperature reduction which corresponds, in average, to 40 K and 45 K respectively. OME_{3-5} and TPGME have a major impact in the higher part of the flame, especially at 50 mm and 60 mm HAB where the difference between the baseline and the blends goes up to 70 K. Nevertheless, if we consider the error bars, calculated from the standard deviation of the 200 temperature values obtained from every pair of images, the measurement error corresponds to 20 K - 40 K (mainly due to the flame flickering). Since the error bars are comparable to the differences between the temperatures of the various additised and not additised fuels, a clear impact of the additives on soot temperature cannot be inferred.

a.

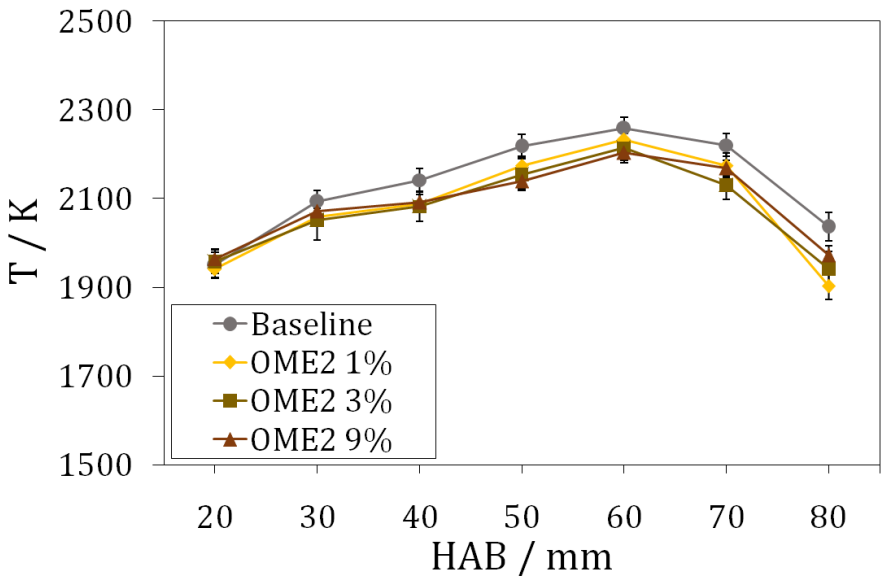

b.

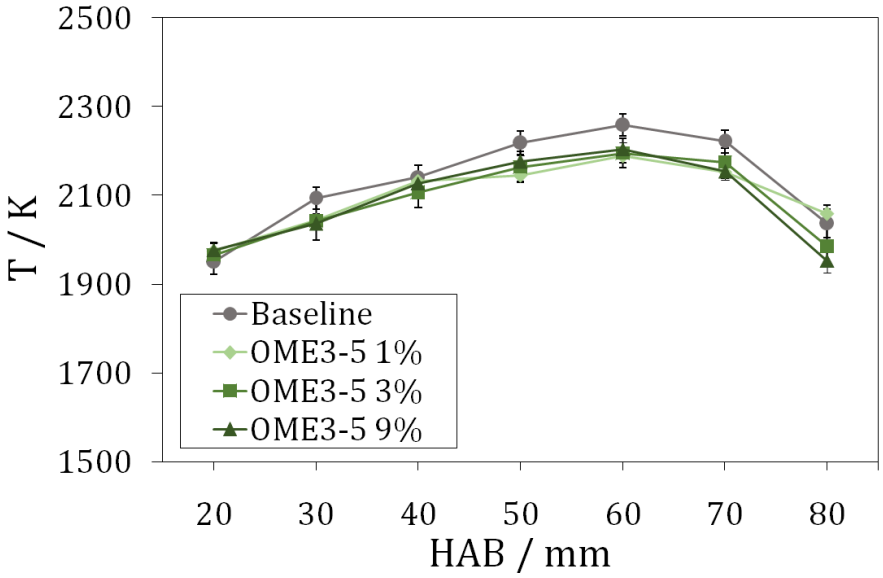

c.

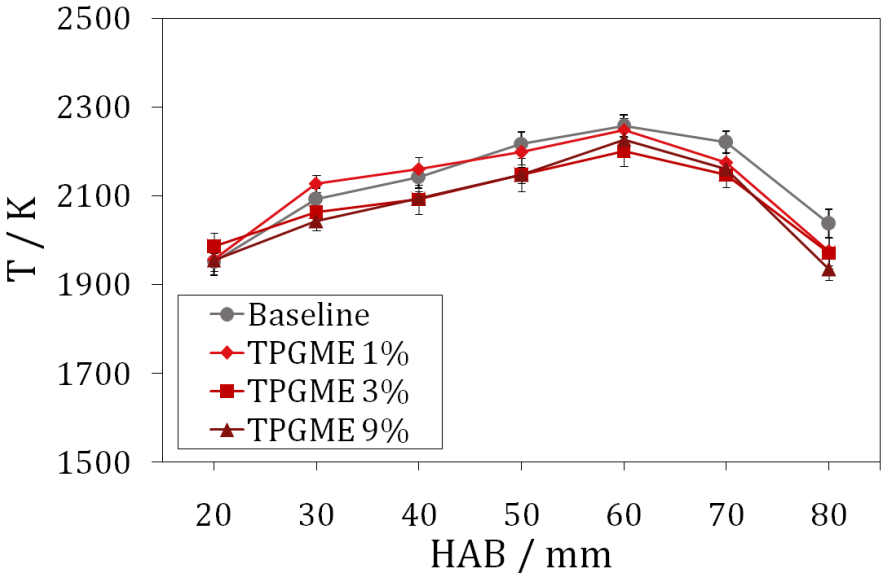

Figure 39. *Temperature vertical trends for neat baseline and* ***a.*** *OME_2-baseline blends (1% vol, 3%vol and 9% vol)* ***b.*** *OME_{3-5}-baseline blends (1% vol, 3%vol and 9% vol) and* ***c.*** *TPGME-baseline blends (1% vol, 3% vol and 9% vol). (Figure from [96].)*

5.3 Spray flame

The measurements performed in the constant volume chamber aimed to investigate the effect of diesel additives on soot production in the case of high (ambient) pressure and temperature, conditions more similar to real engines. The fuels studied were, beside the pure baseline, the OME_2-diesel blend 3% vol. and the TPGME-diesel blend 3% vol. The injection pressure and temperature were set to 120 MPa and 363 K, respectively. The ambient gas in the chamber was pure dehumidified air. The spray is constituted of three plumes with identical properties (only one plume was considered for the experiments). The measurement ambient conditions are listed in Table 4. For every pressure/temperature condition we collected ~ 1200 LII images during the entire soot visibility time, meaning ~ 150 LII images every 100 µs / 200 µsand precisely at 1200 µs, 1300 µs, 1400 µs, 1500 µs, 1700 µs, 1900 µs, 2100 µs and 2300 µs after start of injection. The 150 LII images were averaged afterwards. The laser fluence was adjusted to 0.35 J/cm^2 by following the same procedure described in paragraph 5.1.1. The laser sheet (50 mm height) intersected the entire plume for the whole soot luminosity time during the spray development and was positioned in the centre of the optical window that corresponds to the centre of the plume. For every measurement point, meaning every pressure/temperature/time after injection condition, 100 background images with the laser turned off, accounting for the soot luminosity, were collected. The averaged background image was subtracted to the corresponding averaged LII image. The soot luminosity signal resulted to be ~ 60% less intense than the maximum LII signal. In Figure 40 the development of the LII signal (representing the soot distribution in the spray flame) over time can be observed. The Figure shows the averaged images, obtained from the 150 collected, during the entire soot visibility time (1200 µs – 2300 µs after start of injection). In the images only the soot region is observable, i.e. the area where the LII signal was detected. This area is part of the plume but it does not correspond with the whole spray plume. In fact, the plume's external layer of soot, the one facing the window where the laser sheet comes from, is more visible than the internal ones. Since the soot in the external layer is hit earlier by the laser sheet, this layer absorbs the laser energy causing a strong extinction in the direction of the spray core, as shown in Figure 41.

Table 4. *Ambient pressure and temperature conditions of the constant volume combustion vessel "OptiVeP" during the LII measurements of the neat and additised baseline.*

Ambient Pressure / MPa	Ambient Temperature / K
4	*923*
4	*973*
6	*873*
6	*923*
6	*973*

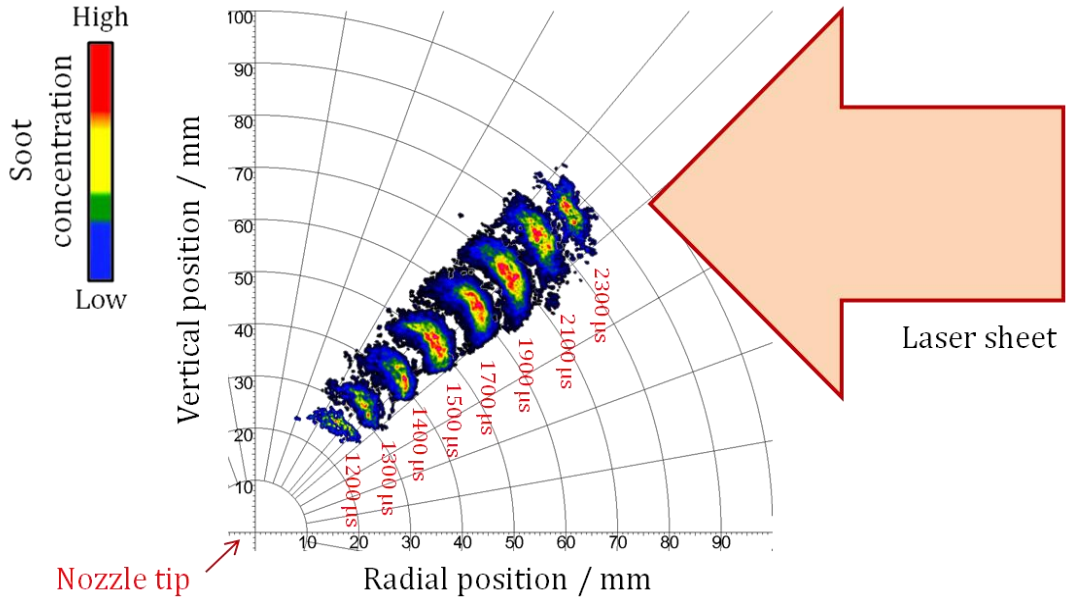

Figure 40. *Time development of the spray flame (averaged LII signal) in the combustion chamber during the soot visibility time (1200 µs to 2300 µs after injection), false colors image, 6 MPa, 923 K ambient conditions, baseline diesel.*

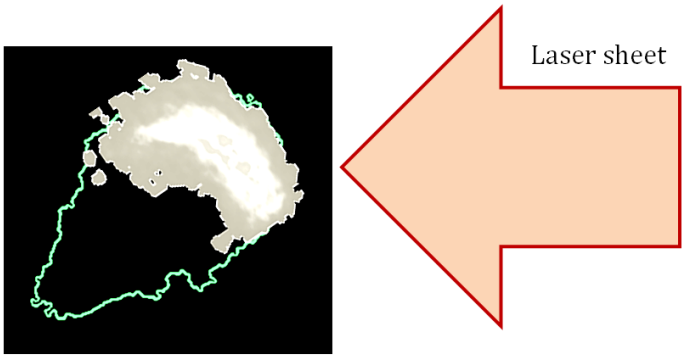

Figure 41. *Spray flame at 6 MPa, 973 K ambient conditions, 1700 µs after injection. The light green curve represents the contour of the plume while the white region is the LII signal from the soot.*

For evaluation of the LII signal the entire plume was considered. The area where the signal is evaluated is called region of interest (ROI). Basically, all the pixels of the plume (averaged image) containing the LII signal were summed up. The total intensity of the ROI versus the time after injection is reported in Figure 42 a-e. The charts in Figure 42 are grouped according to their measurement conditions. The comparison between the fuels during the soot visibility time is reported. The incandescence signal over time, which displays soot increasing from 1300 µs to ~ 2100 µs and decreasing afterward, reflects the spray flame development in the chamber involving flame ignition, expansion and quenching. This process is anticipated when the ambient temperature increases because the flame ignition starts earlier. Furthermore, it should be taken into account that a gain of the ambient temperature causes an increment of the LII signal, while by increasing the ambient pressure the incandescence signal decreases. The impact of OME_2 and TPGME depends on the time after injection and on the chamber ambient conditions. Generally, the LII signal of the different fuels exhibits comparable intensity/a minimal difference right after the flame ignition, at ~ 1200 µs - 1300 µs after the injection. When the combustion proceeds, the gap between the neat baseline and the additised ones increases significantly leading the curves to diverge. If we consider Figure 42 a., 4 MPa and 923 K ambient condition, in the initial part of the combustion process, i.e. between 1400 µs - 1700 µs, the soot suppression performed by the additives ranges between 10% and 35%, while later, from 1900 µs after injection, the soot reduction goes up to 55% -70%. At higher temperature (Figure 42 b.) the soot decreasing effect of additives is about 20% - 40% at the beginning of the combustion process (until 1700 µs) and around 70% at the end of the combustion. Moving to higher pressure, for example Figure 42 d. (same ambient temperature

of Figure 42 a., but ambient pressure 2 MPa higher) the initial soot reduction due to the additives is less than 30%; at the end of the process the additives are able to lessen soot up to 70% again. In some cases, like the measurements at 6 MPa and 873 K and the ones at 6 MPa and 973 K, during the first half of the combustion process the insertion of the additives seems to cause an increment of soot.

If we compare TPGME and OME_2, the last one results to be the most effective soot inhibitor, which is in agreement with the results found on the diesel burner at atmospheric pressure. The maximum soot drop is observable at 4 MPa, 973 K, 2100 µs after the injection: at this measurement point the LII signal of the baseline additised with 3% of OME_2is78% lower than the neat baseline's signal.

These results indicate that both OME_2 and TPGME are good soot reducers, especially in the later stages of the spray combustion, when mainly the soot oxidation takes place. In particular, we observe that OME_2 has the higher decreasing effect on soot emitted by spray flames. These findings are in agreement with the literature [6, 101, 165, 166] demonstrating that oxygenated additives play an important role in reducing soot emissions, most likely by enhancing the oxidation of soot.

a.

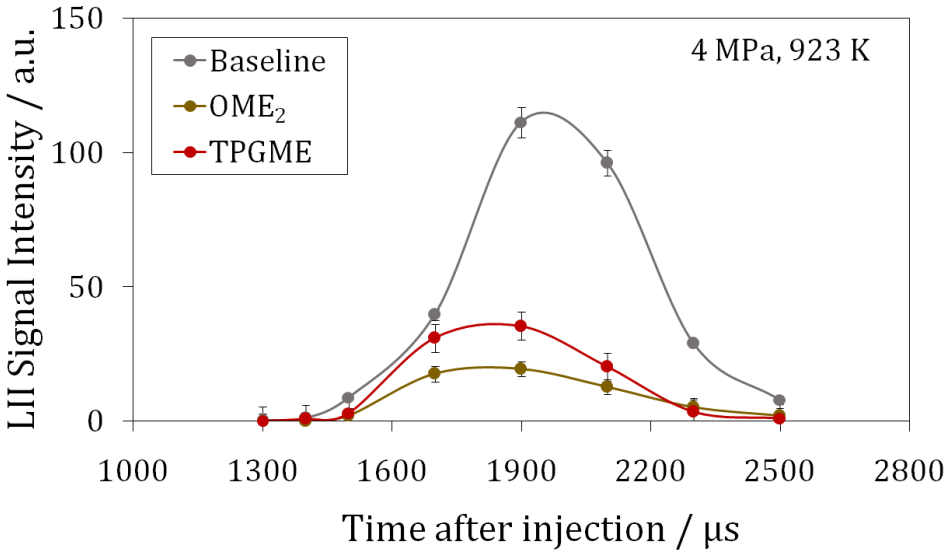

b.

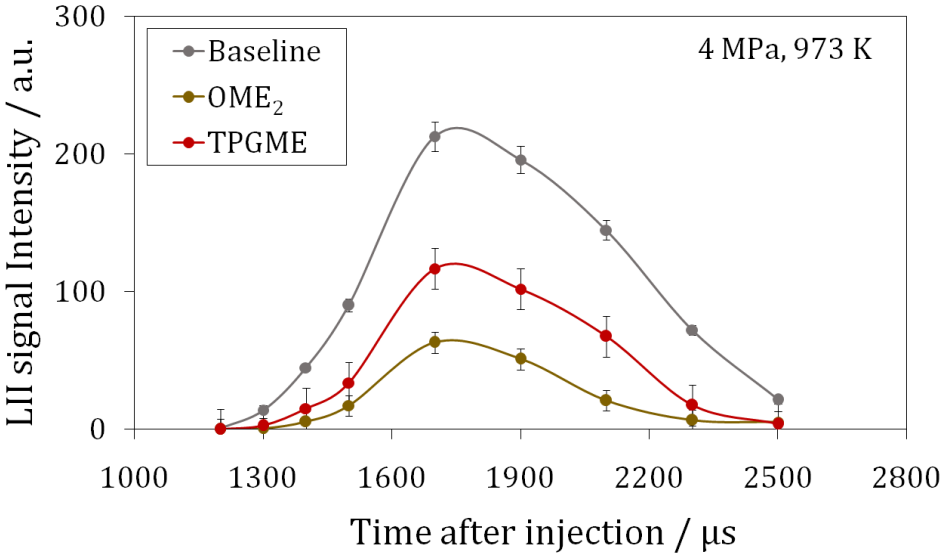
Baseline
OME2
TPGME
4 MPa, 973 K
LII signal Intensity / a.u.
300
200
100
0
1000
1300
1600
1900
2200
2500
2800
Time after injection / µs

c.

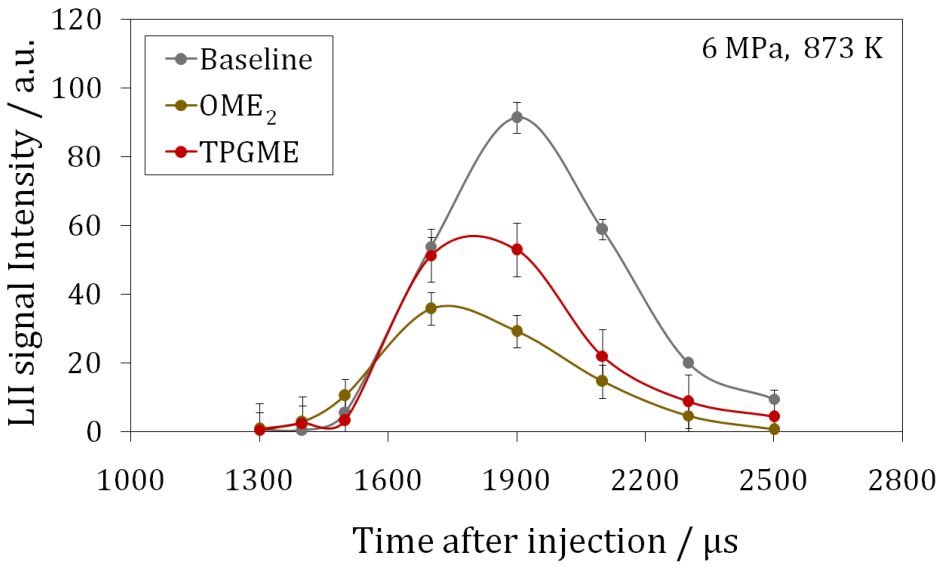
Baseline
OME2
TPGME
6 MPa, 873 K
LII signal Intensity / a.u.
120
100
80
60
40
20
0
1000
1300
1600
1900
2200
2500
2800
Time after injection / µs

d.

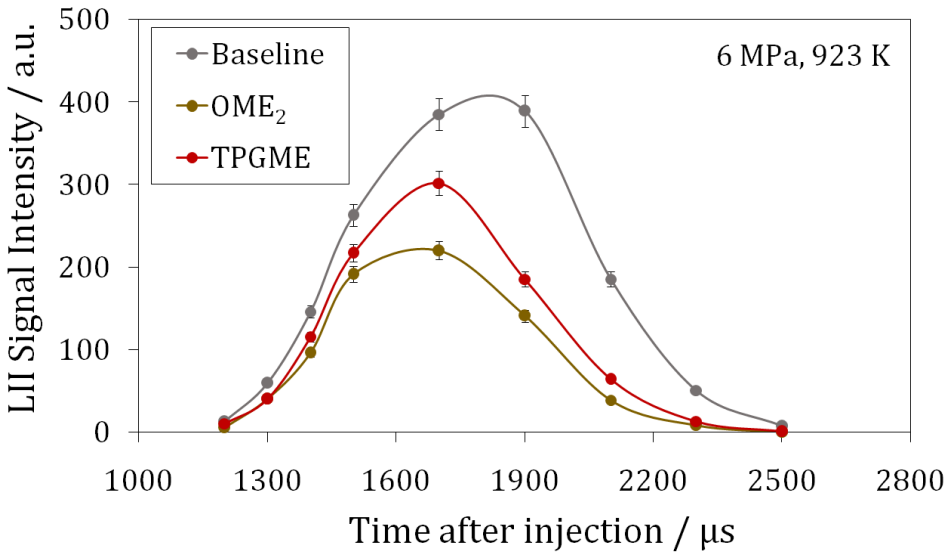

e.

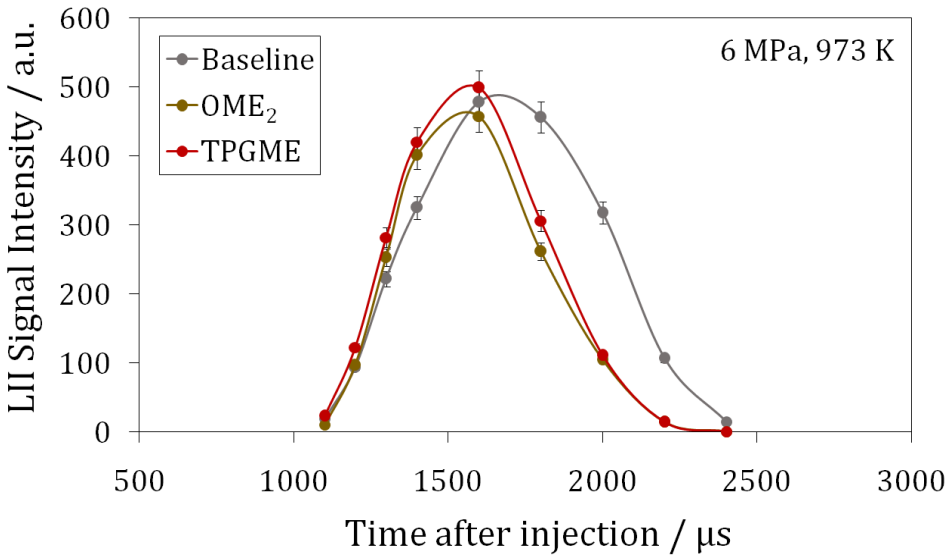

Figure 42. *Comparison of averaged LII signal intensity development over time after injection for pure baseline, OME_2-baseline blend (3% vol) and TPGME-baseline blend (3% vol) at* ***a.*** *4 MPa and 923 K* ***b.****4 MPa and 973 K* ***c.*** *6 MPa and 873 K* ***d.*** *6 MPa and 923 K* ***e.*** *6 MPa and 973 K. The error bars are obtained from the standard deviation of the 150 images of the plume collected.*

5.4 Overall comparison

Looking back to the initial purpose of this study, the principal questions we want to answer are: which is the actual influence of the oxygenated additives on soot emissions and which one of them is the most effective in soot reduction? Will the effect of fuel's chemical composition on soot, observed on the diesel burner, occur similarly under real engine conditions? Considering the measurements on the laminar diffusion flame first, to better quantify the impact of the additives, the percentage of reduction of the soot volume fraction displayed by the additised diesel was calculated with respect to the f_V determined in the pure baseline (Figure 43). In the same way, we calculated the percentage of reduction of the aggregate size induced by the additives with respect to the neat baseline (Figure 44). The capability of the OMEs, in particular $OME_{3\text{-}5}$, to lower soot concentration along all the flame is particularly evident in Figure 43.a. The diesels additised with just 1% of OME_2 and $OME_{3\text{-}5}$ show a significant reduction of the soot emitted, which ranges between 15% and 25% especially in the upper part of the flame. In the same Figure (43.a) it is observable that TPGME leads to an increment of soot f_V at 20 mm, 30 mm, 80 mm and 90 mm HAB, while for the others measurement points at different flame's heights the soot decreases. The changes observed have the same size of the measurement errors (see Figure 35), i.e. about 7% in the lower part of the flame and 11% in the upper part of the flame, meaning that the increment/decrement observed can be caused by a variation of the measurements' conditions. Consequently, the effect of TPGME 1% vol. in diesel cannot be stated clearly. If we have a look at Figure 43.b (3%), the OMEs' capacity to abate soot production is especially noticeable; a significant example is the measurement point at 90 mm HAB: here the soot produced by the diesel additised with 3% $OME_{3\text{-}5}$ is 36% less compared to the pure baseline. Regarding TPGME, this compound has, also in this case, a controversial behaviour. It shows a significant lowering effect only at 90 mm above the burner, where the soot is 20% less than the baseline, while for all the other heights the decreasing effect is not relevant or absent. In contrast, TPGME, like OMEs, exhibits a positive reduction effect on soot emission at 9% additive-diesel concentration (at all heights), as shown in Figure 43.c. About this last figure, we can observe that the soot decrement is higher in the upper part of the flame and the most effective additive is $OME_{3\text{-}5}$, although in this case the drop caused by TPGME goes up to 27%, therefore the additives' effect is quite comparable. The better performance of $OME_{3\text{-}5}$ compared to OME_2 and TPGME could be due to the presence of more CH_2-O groups inside the molecule, that means more oxygen content and therefore an enhancement of the oxidation process. This is confirmed by one detail: the additives' tendency to decrease soot

volume fraction mainly in the upper part of the diffusion flame where indeed the soot oxidation process is dominant. Nevertheless, more investigations are required, also involving soot precursor measurements, in order to ascertain the additive complete mechanism. Moreover, the results obtained underline another important aspect: while TPGME has an increasing effect by increasing the concentration, the OMEs show the highest soot reduction performance at the concentration of 3%. Several studies [88, 167-169] have already pointed out that OMEs' reduction performance does not increase when the concentration of the additive increases. Song et al. and Kocis et al. found that 2% and 4% OME_1 – diesel blends were able to lessen soot by 46% and 57%, respectively [168, 169]. In the same conditions 30% OME_1-diesel blend decreased PM of only 35% [88, 167].

a.

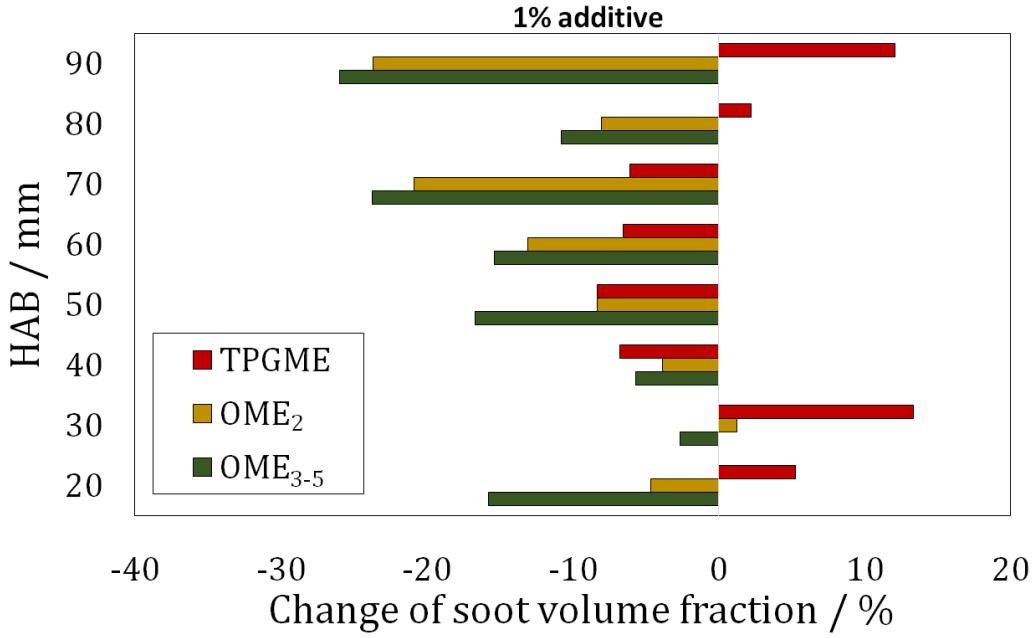

b.

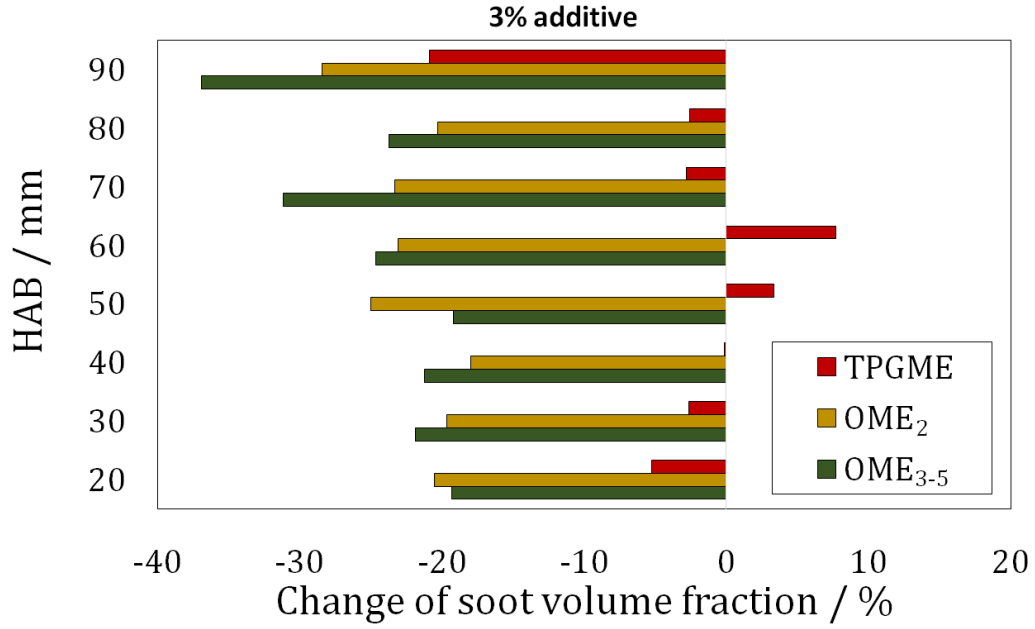

c.

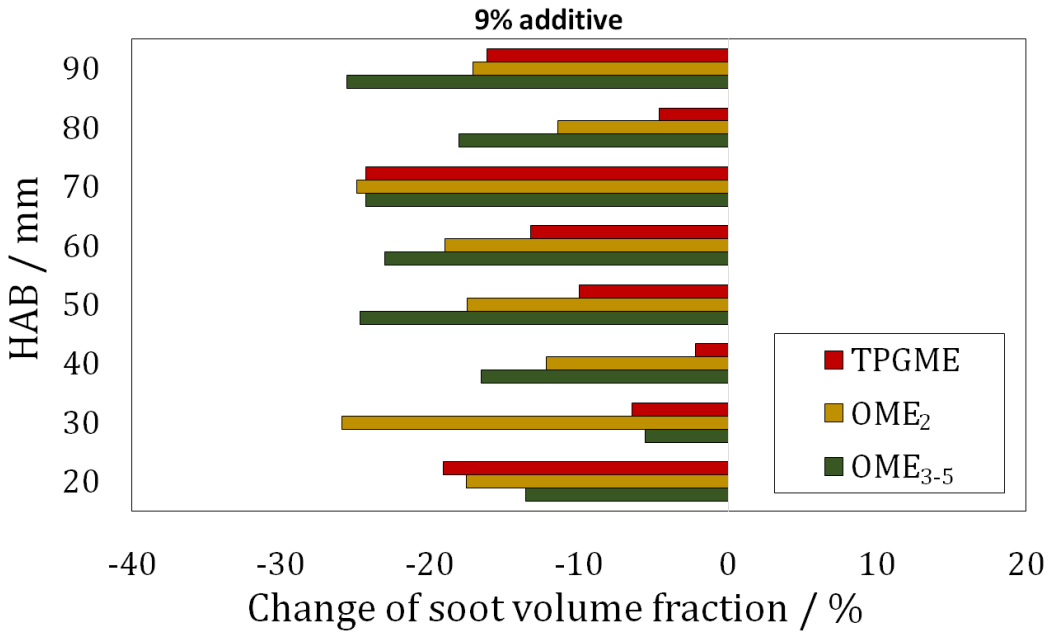

Figure 43. *Comparison of TPGME, OME_2 and OME_{3-5}effect on f_V with respect to the neat baseline with* ***a.****1% of additives,* ***b.*** *3% of additives and* ***c.*** *9% of additives. (Figure from [96].)*

OME_2 and OME_{3-5} affect slightly also soot size as shown in Figure 44. The change of soot aggregate size in the OME-diesel blends, compared to the neat baseline, ranges between 10% and 20% (measurement errors, obtained from the standard deviations, vary between 5% and

8%) depending on the compound's concentration and on the height above the burner. Indeed, the OMEs impact on R_g increases by increasing the concentration and the height above the burner. OME_2 exhibits a considerable decreasing effect on R_g at 3% and 9% vol. in baseline. Specifically, at 80 mm HAB the reduction shown by OME_2-diesel blend (9% concentration) on aggregate size, in percentage, is 16% (maximum reduction found for the OME_2 on aggregate size). Overall, also in this case OME_{3-5} show the best performance in decreasing soot aggregate size: the maximum size drop is observable for 9% OME_{3-5}-diesel blend at 80 mm above the burner. It corresponds to 20% reduction compared to the baseline diesel. Considering TPGME, it appears to affect the size of soot particles; namely it seems to increase particle size up to 6% at the concentration of 1% and 3% vol. Nevertheless, the growth is contained inside the measurement errors which goes up to 8%. The aggregate size (percentage reduction) trend of the 9% TPGME-diesel is comparable to OMEs. The effect of additives on soot aggregate size seems to be much lower than the one on soot volume fraction. We have to consider that, while by LII technique we estimate a volume (3D), by WALS technique we obtain the radius of gyration of the aggregates, that is a 1D value. When we want to draw a parallel between R_g and f_V we have to consider the "R_g^3" value or, better, we can use the fractal dimension. If we assume a fractal dimension of 1.8 [36] the reduction in aggregate size is comparable to the decrease of soot volume fraction. An example is the case of 3% of OME_{3-5}-diesel blend at 70 mm HAB: the additive induces a downsizing of ~ 16 % of $\mu_{g,eff}$, with respect to the baseline. This leads to a drop of aggregate mass of about 29% (supposing constant primary particle sizes), consistent with the f_V reduction under these conditions (31%).

a.

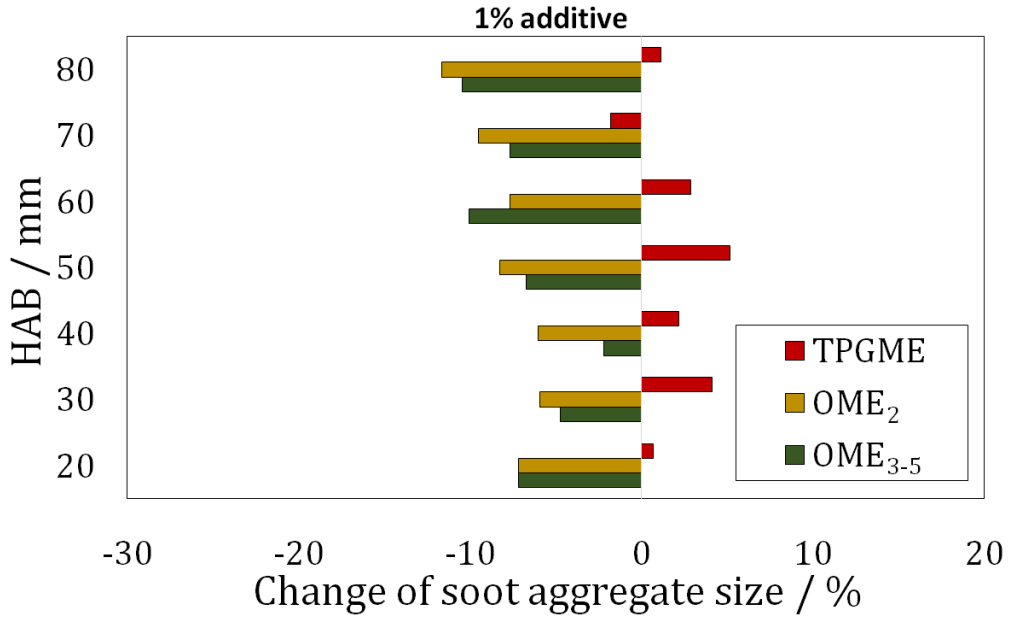
1% additive
HAB / mm
80
70
60
50
40
30
20
-30
-20
-10
0
10
20
Change of soot aggregate size / %
TPGME
OME2
OME3-5

b.

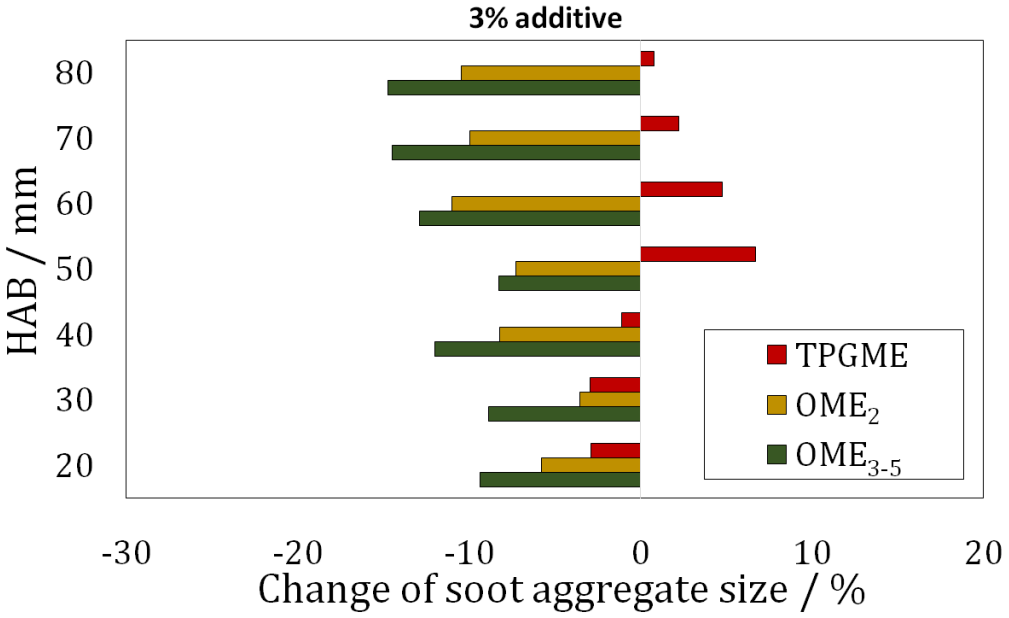
3% additive
HAB / mm
80
70
60
50
40
30
20
-30
-20
-10
0
10
20
Change of soot aggregate size / %
TPGME
OME2
OME3-5

c.

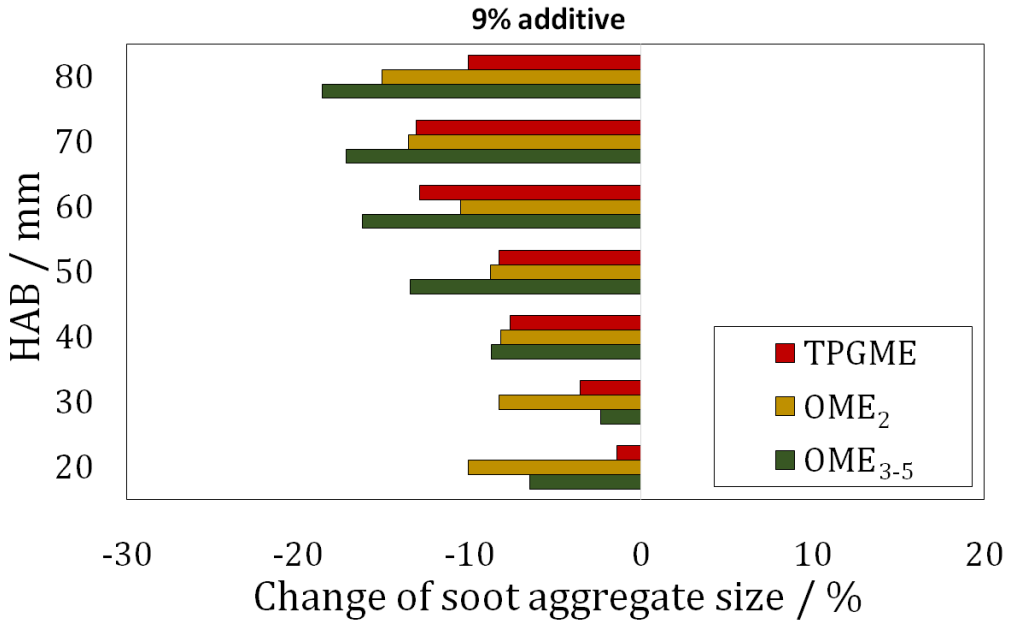

Figure 44. *Comparison of TPGME, OME_2 and OME_{3-5} effect on $\mu_{g,eff}$ with respect to the pure baseline with* ***a.****1% of additives,* ***b.*** *3% of additives and* ***c.*** *9% of additives. (Figure from [96].)*

Overall, regarding the laminar diffusion flame, it is clear that oxygenated additives play a meaningful role during the soot formation process by abating particles concentration and by lowering particles size. It arises from both LII and WALS measurements that OMEs cause the major soot concentration drop. For instance, both OME_2 and OME_{3-5}, 3% vol., are able to suppress about 20% more soot than TPGME, while the aggregates emitted are 10 % - 15 % smaller. The efficacy of OMEs is confirmed by SMPS measurements, concerning the particles dimensions. SMPS experiments showed that, in the lower part of the flame (20 mm - 40 mm HAB), OME_2, 3% vol., has the capability of decreasing particles diameter of ~ 15% - 18% compared to the neat diesel, similarly to the downsizing effect found by WALS measurements between 40 mm and 80 mm HAB. On the contrary, none of the additives has a significant impact on soot temperature in the laminar diffusion flame. Indeed, Two-Colour Pyrometry measurements show that the diesels additised with 3% of OMEs and TPGME exhibit a temperature reduction that ranges between 10 K and 45 K with respect to the neat baseline. These values are contained within the measurement error and correspond to 1 % - 2 % of reduction with respect to the pure baseline. This leads to the conclusion that, according to our

findings, the oxygenated molecules tested have mainly a chemical effect, i.e. they act as oxidizer, while physical effects on temperature are not relevant.

Finally, concerning the measurements performed in the constant volume chamber, the results obtained from the LII experiments on spray flame support the results achieved from LII measurements on the laminar diffusion flame, meaning that we observe the same trends, i.e. also in spray flames OME has more effect in decreasing soot than TPGME. The higher tendency of OME_2 (3% vol.) of decreasing soot concentration is observed at almost every temperature/pressure condition. Specifically, OME_2-diesel blend (3% vol.) emits between 10% and 40%less soot than TPGME-diesel blend, depending on the temperature/pressure condition. For instance, the soot produced by the OME_2-diesel blend at 6MPa, 923 K,1700 μs ignition delay, is about 30% less than the one found for the TPGME-diesel blend and about 40% less than the one measured for the neat diesel. These outcomes are in agreement with the results found in literature [94, 100, 101, 170]. Iannuzzi et al. [101] observed that OME_2 is a good soot suppressor and specifically 5%-10% OMEs-diesel blends suppress between 10% and 35% more soot with respect to commercial diesel (measurements carried out in a single cylinder heavy-duty diesel engine), that is comparable to our results. From our findings it seems that the reduction effect caused by OME_2 in spray flames is slightly enhanced (more evident) compared to the laminar diffusion flame. The additive effect can be enhanced by the ambient condition of the constant volume chamber, the spray structure, the fuel/air mixture, etc. more studies are required to understand this phenomenon.

6. Conclusion and outlook

The present dissertation aimed to investigate the impact of additives on soot emissions. To isolate chemical effects from the physical effects connected to spray's efficiency of nebulisation, liquid/vapour mixture, high pressure effects, etc. a novel combustion system was designed and manufactured. The new implemented diesel burner performs the complete vaporization of high boiling temperature liquid fuel at atmospheric pressure and the subsequent combustion in a laminar diffusion flame. The flame produced by the novel prototype has been initially characterised by using two different diesels, namely CEC RF-06-03 (called "reference" for simplicity) and CEC RF-79-07 (called "baseline"). These two fuels have similar properties but they slightly differ for the content of aromatic species. The concentration of soot produced, expressed as volume fraction f_V, and the size of the aggregates, expressed as radius of gyration R_g, have been studied by applying Laser-Induced Incandescence (LII) and Wide-Angle Light Scattering (WALS) technique respectively.

The diesel burner characterization proved the capability of the combustion system to efficiently vaporize and burn fuels with high boiling point at ambient conditions. The complete vaporization was guaranteed by the temperature at which the burner was operated, namely between 643 K and 653 K (higher than the diesel boiling point, 453 K – 633 K). Furthermore, self-ignition of diesel was avoided by using N_2 as carrier gas instead of air. The diesel complete vaporization allowed to limit the manifestation of physical effects. The creation of a stable laminar diffusion flame (diesel volume flow: 0.175 l/min, N_2 volume flow: 0.3 l/min, air co-flow: 20 l/min), with Reynolds Number ~ 100, facilitated the use of laser-based techniques for the investigation of soot properties.

The initial flame's characterization shows that soot is mainly distributed along the annular region of the flame, while the central part presents much less soot particles. Between 30 mm and 80 mm HAB soot concentration rises by increasing the height above the burner. After 80 mm HAB the soot volume fraction decreases because of oxidation processes. Although the behaviour just described is common to both diesels, the amount of soot emitted varies, resulting to be higher in the reference diesel. The maximum volume fraction measured for the reference is 1.76 ppm (80 mm HAB) while the maximum value found in the baseline flame, at 80 mm HAB, is 1.47 ppm. The minimum amount of soot was detected at the beginning of the combustion and corresponds to ~ 0.7 ppm for the reference and around 0.5 ppm for the baseline. The WALS measurements show a general, clear trend: the size of soot aggregates enlarges slightly by increasing the height above the burner, due to the increasing aggregation time. For

the reference the median $R_{g,eff}$ reaches its maximum at 70 mm HAB with a value of $\mu_{g,eff}$ = 211 nm; the maximum $\mu_{g,ff}$ for the baseline amounts to 207 nm. We found that the smallest radii of gyration were $\mu_{g,eff}$ = 178 nm and $\mu_{g,eff}$ = 169 nm, for the reference and baseline respectively, which were measured at 30 mm HAB. Overall, it can be stated that on one hand the soot concentration is clearly lower in the baseline diesel flame, while on the other hand, the particles' size does not change significantly between the two fuels. The reduction of soot volume fraction observed in the baseline, with respect to the reference, can be explained by the different chemical composition of the diesels: the reference contains about 3% more aromatic species, which are known as soot precursors. This promotes soot particle inception and consequently causes an increment of f_V; however, the aggregation process in not influenced. The characterization of the flame showed that we could isolate the impact of minor changes of the fuel chemical composition on soot, therefore the burner implemented can be applied to the study of additives' effects.

The work proceeded to the next phase, the study of soot produced by oxygenated-diesel blends. After review of the dedicated literature, three promising soot reducer additives were chosen: the Tripropylene Glycol Methyl Ether abbreviated TPGME (chemical structure CH_3-OC_3H_6-$(OC_3H_6)_2$-OH), the poly oxymethylene dimethyl ether OME_2 (chemical structure CH_3-O-$(CH_2$-$O)_2$-CH_3) and the poly oxymethylene dimethyl ether OME_{3-5} (a mixture of poly oxymethylene dimethyl ethers with chemical structure CH_3-O-$(CH_2$-$O)_{3-5}$-CH_3). These ether compounds are highly oxidized and contain very few/no C-C direct bond; these characteristics, according to the literature, make these molecule good soot reducer.

The additive's behaviour was investigated by four different techniques, i.e. Laser-Induced Incandescence, Wide-Angle Light Scattering, Scanning Mobility Particle Sizer and two-color pyrometry. The oxygenated compounds were inserted in the pure baseline with increasing concentration from 1%, 3%, up to 9% vol. and the effect of concentration changes was investigated. The results obtained from the measurements on the blends were compared with the ones of the neat baseline.

The LII experiments on the burner show that OME additives decrease soot at every concentration and height above the burner; their effect increases by increasing the height above the burner and moving from 1% vol. to 3% vol. The reduction effect of OMEs on soot is maximum at the concentration of 3% vol. in baseline, while the 9% OMEs-diesel blends exhibit lower or almost comparable reduction effect of the 3% OMEs-diesel blends, in agreement with the trends found in literature [168, 169]. OME_2 and OME_{3-5} are able to lower the soot volume fraction by up to ~ -28% and ~ -37% respectively (3% vol., 90 mm HAB) compared to the pure

baseline. TPGME shows a negligible decreasing effect on soot concentration at 1% vol. and 3% vol. in baseline while at 9% vol. in baseline this additive reduces soot f_V significantly. Also in this case the reduction effect increases by increasing the height above the burner. The maximum soot reduction caused by TPGME is ~ -24% when the additive is 9% concentrated (70 mm HAB).

Besides the influence on soot volume fraction, OME_2 and OME_{3-5} play a secondary role on the aggregation process. Indeed, the medium $R_{g,eff}$ measured for the OME_2-diesel blend is about 15% smaller than the one found for the pure baseline. For OME_{3-5} the decrement of $R_{g,eff}$ goes up to 18%. The effect on aggregate size rises by increasing the additive's concentration. For the TPGME-diesel blend (TPGME in a concentration lower than 9%) the medium $R_{g,eff}$ observed does not vary significantly compared to the pure baseline. The blend 9%TPGME-baseline exhibits a particles downsizing up to about 13%. A non laser-based device, SMPS, was employed to recheck the dimensional trend as well as the effectiveness of the OMEs. We found again that the particles' diameter enlarges by increasing the height above the burner and, in agreement with WALS measurements, the OME_2 was capable of reducing particle's size up to 20%.

Finally, two-colors pyrometry measurements have not highlighted a significant effect of the oxygenated additives on temperature. Although soot from additised diesel seems to be between 20 K and 50 K colder than the one emitted by the baseline, the measurements are affected by 20 K – 40 K standard deviation that makes the difference not significant.

The capability of the additives to decrease soot concentration was tested at high temperature and pressure, more similar to engine's conditions. LII was applied to study the soot produced by the same additive-diesel blends investigated on the burner (TPGME and OME_2, 3% vol.), this time on spray flames. The outcomes of these measurements confirmed that oxygenated additives reduce soot formation, in this case of about 60% - 80%, especially in the later phases of the combustion, supporting the theory that both TPGME and OMEs promote the formation of oxidant species enhancing the oxidation process of soot/soot precursors. Furthermore, the experiments on the spray flames displayed a higher efficiency of OME_2, with respect to TPGME, to reduce soot, in agreement with the measurements on the burner flame.

The results achieved in the present study lead to the major conclusions that:

- Tripropylene glycol methyl ether (TPGME) restrains soot emissions with increasing strength when its concentration increases. The influence on the aggregate size is also dependent on the amount of additive inserted.

- Long-chain oxymethylene dimethyl ethers (OMEs) have been proven to be the most effective compounds for soot abatement, both at normal temperature/pressure and high-temperature/pressure conditions. In particular,OME_{3-5} is capable to significantly lower soot concentration and aggregates size even when it is present in minimal concentration, i.e. 1% (in the laminar diffusion flame). To a less extent, but still with high efficacy, OME_2 also decreases soot emissions.

OME_{3-5} is a mixture of hydrocarbons characterized by three to five CH_2-O groups, i.e. a considerable quantity of oxygen (OME_2 and TPGME contain only 2 and 3 CH_2-O groups respectively). Generally, soot models indicate that soot formation and oxidation are correlated to the flame temperature and to the concentration of the reagents. In our experiments, soot temperature does not change significantly when an oxygenated agent is present in the combusting blend. Consequently, the reduction effect of OMEs and TPGME can be associated with the oxygen content of the additives: more oxygen in the molecule enhances the generation of oxidizing species such as OH, O and O_2 which yields to an acceleration of the oxidation process. The oxidation occurs during the entire combustion and influences also the soot formation process (we find that additives decrease soot also in the initial part of the flame). Both soot precursors (C_2H_2, benzene, PAH, etc.) and already formed soot could be oxidized. Our results suggest that the additives play an important role during the whole combustion, and their effect is more accentuated in the final stage of the combustion, i.e. the oxidation of already formed soot. Obviously, for a better comprehension of the mechanism behind soot formation from diesels and the role of oxygenated species in this process, further investigations, involving soot precursors and different combustion products are required.

Finally, this study has several applications, for example the results presented can constitute a database for validation of soot formation models from diesel's surrogates where usually the chemical structure of the fuel is a crucial input parameter. The outlook of the present work is wide and can include burner system applications and additives effect investigation. The burner system designed and implemented in the present study can be employed for online measurements of soot emitted by different kind of petroleum-based fuels with high boiling point (from gasoline to diesel and biodiesel) and their blends. The impact of various additive compounds, from organomettallic species to oxygenated organic species like detergents, esters or alcohols, can be also investigated in the laminar diffusion flame produced by the burner. The three oxygenated compounds studied in the present work (TPGME, OME_2, OME_{3-5}) showed a significant reduction effect on soot volume fraction, especially the OMEs additives. Further investigations can involve the development of soot precursors during the combustion of OMEs-

and TPGME-diesel blends, coupling optical /no optical/spectroscopic techniques. The research on additives can be also extended to different species, for example OMEs with longer chain, and the selection can be based on the results reported in the present study.

References

[1] Lee R, Pedley J, Hobbs C. Fuel quality impact on heavy duty diesel emissions:-a literature review. SAE Transactions 1998:1952-70.

[2] Krzyzanowski M, Kuna-Dibbert B, Schneider J. Health effects of transport related air pollution. In: World Health Organization ROfE, Copenhagen, editor.2005.

[3] Schwartz J. Air pollution and daily mortality: a review and meta analysis. Environmental Research 1994;64:36-52.

[4] Stöber W, Abel UR. Lung cancer due to diesel soot particles in ambient air? International Archives of Occupational and Environmental Health 1996;68:S3-S61.

[5] Mansurov Z. Soot formation in combustion processes. Combustion, Explosion and Shock Waves 2005;41:727.

[6] Lemaire R, Bejaoui S, Therssen E. Study of soot formation during the combustion of Diesel, rapeseed methyl ester and their surrogates in turbulent spray flames. Fuel 2013;107:147-61.

[7] Gairing M, Marriott J, Reders K, Reglitzky A, Wolveridge P. The effect of modern additive technology on diesel fuel performance. SAE Technical Paper 950252; 1995.

[8] Omidvarborna H, Kumar A, Kim D-S. Recent studies on soot modeling for diesel combustion. Renewable and Sustainable Energy Reviews 2015;48:635-47.

[9] Wu F, Wang J, Chen W, Shuai S. Effects of different biodiesels and their blends with oxygenated additives on emissions from a diesel engine. SAE Technical Paper 2008-01-1812; 2008.

[10] Schönborn A, Ladommatos N, Williams J, Allan R, Rogerson J. The influence of molecular structure of fatty acid monoalkyl esters on diesel combustion. Combustion and Flame 2009;156:1396-412.

[11] Haynes BS, Wagner HG. Soot formation. Progress in Energy and Combustion Science 1981;7:229-73.

[12] Haynes B, Wagner HG. The surface growth phenomenon in soot formation. Zeitschrift für Physikalische Chemie 1982;133:201-13.

[13] Bockhorn H. Soot formation in combustion: mechanisms and models: Springer Science & Business Media; 2013.

[14] Glassman I. Soot formation in combustion processes. Symposium (international) on combustion: Elsevier; 1989. p. 295-311.

[15] Frenklach M. Reaction mechanism of soot formation in flames. Physical Chemistry Chemical Physics 2002;4:2028-37.

[16] Wang H. Formation of nascent soot and other condensed-phase materials in flames. Proceedings of the Combustion Institute 2011;33:41-67.

[17] Chen W, Shuai S, Wang J. A soot formation embedded reduced reaction mechanism for diesel surrogate fuel. Fuel 2009;88:1927-36.

[18] Johansson K, Head-Gordon M, Schrader P, Wilson K, Michelsen H. Resonance-stabilized hydrocarbon-radical chain reactions may explain soot inception and growth. Science 2018;361:997-1000.

[19] Stanmore BR, Brilhac J-F, Gilot P. The oxidation of soot: a review of experiments, mechanisms and models. Carbon 2001;39:2247-68.

[20] Tree DR, Svensson KI. Soot processes in compression ignition engines. Progress in Energy and Combustion Science 2007;33:272-309.

[21] Calcote H, Manos D. Effect of molecular structure on incipient soot formation. Combustion and Flame 1983;49:289-304.

[22] Crossley SP, Alvarez WE, Resasco DE. Novel micropyrolyis index (mpi) to estimate the sooting tendency of fuels. Energy & Fuels 2008;22:2455-64.

[23] Glassman I, Yetter RA, Glumac NG. Combustion: Academic press; 2014.

[24] Takatori Y, Mandokoro Y, Akihama K, Nakakita K, Tsukasaki Y, Iguchi S, et al. Effect of hydrocarbon molecular structure on diesel exhaust emissions part 2: effect of branched and ring structures of paraffins on benzene and soot formation. SAE Technical Paper 982495; 1998.

[25] Das DD, John PCS, McEnally CS, Kim S, Pfefferle LD. Measuring and predicting sooting tendencies of oxygenates, alkanes, alkenes, cycloalkanes, and aromatics on a unified scale. Combustion and Flame 2018;190:349-64.

[26] Miyamoto N, Ogawa H, Shibuya M, Arai K, Esmilaire O. Influence of the molecular structure of hydrocarbon fuels on diesel exhaust emissions. SAE transactions 1994:1069-74.

[27] Tsurutani K, Takei Y, Fujimoto Y, Matsudaira J, Kumamoto M. The effects of fuel properties and oxygenates on diesel exhaust emissions. SAE Technical Paper 952349; 1995.

[28] Bertoli C, Del Giacomo N, Iorio B, Prati M. The influence of fuel composition on particulate emissions of DI diesel engines. SAE Technical Paper 932733; 1993.

[29] Bryce D, Ladommatos N, Xiao Z, Zhao H. Investigating the effect of oxygenated and aromatic compounds in fuel by comparing laser soot measurements in laminar diffusion flames with diesel-engine emissions. Journal of the Institute of Energy 1999;72:150-6.

[30] Böhm H, Hesse D, Jander H, Lüers B, Pietscher J, Wagner H, et al. The influence of pressure and temperature on soot formation in premixed flames. Symposium (International) on Combustion: Elsevier; 1989. p. 403-11.

[31] Hallgren BE, Heywood JB. Effects of oxygenated fuels on DI diesel combustion and emissions. SAE Technical Paper 2001-01-0648; 2001.

[32] Donahue RJ, Foster DE. Effects of oxygen enhancement on the emissions from a DI diesel via manipulation of fuels and combustion chamber gas composition. SAE Transactions 2000:334-50.

[33] Mueller CJ, Martin GC. Effects of oxygenated compounds on combustion and soot evolution in a DI diesel engine: broadband natural luminosity imaging. SAE Transactions 2002:518-37.

[34] Choi M, Hamins A, Mulholland GW, Kashiwagi T. Simultaneous optical measurement of soot volume fraction and temperature in premixed flames. Combustion and Flame 1994;99:174-86.

[35] Lee KO, Cole R, Sekar R, Choi MY, Zhu J, Kang J, et al. Detailed characterization of morphology and dimensions of diesel particulates via thermophoretic sampling. SAE Technical Paper 2001-01-3572; 2001.

[36] Sorensen C. Light scattering by fractal aggregates: a review. Aerosol Science & Technology 2001;35:648-87.

[37] Forrest S, Witten Jr T. Long-range correlations in smoke-particle aggregates. Journal of Physics A: Mathematical and General 1979;12:L109.

[38] Hausdorff F. Dimension und äuβeres Maβ. Mathematische Annalen 1919;79:157-79.

[39] Mandelbrot BB. The fractal geometry of nature. 1982. San Francisco, CA 1982.

[40] Meakin P. Models for colloidal aggregation. Annual Review of Physical Chemistry 1988;39:237-67.

[41] Meakin P. Effects of cluster trajectories on cluster-cluster aggregation: a comparison of linear and Brownian trajectories in two-and three-dimensional simulations. Physical Review A 1984;29:997.

[42] Weitz D, Huang J, Lin M, Sung J. Limits of the fractal dimension for irreversible kinetic aggregation of gold colloids. Physical Review Letters 1985;54:1416.

[43] Ku JC, Shim K-H. A comparison of solutions for light scattering and absorption by agglomerated or arbitrarily-shaped particles. Journal of Quantitative Spectroscopy and Radiative Transfer 1992;47:201-20.

[44] Ku J, Shim K-H. Optical diagnostics and radiative properties of simulated soot agglomerates. Journal of Heat Transfer 1991;113:953-8.

[45] Fuller KA, Malm WC, Kreidenweis SM. Effects of mixing on extinction by carbonaceous particles. Journal of Geophysical Research: Atmospheres 1999;104:15941-54.

[46] Flynn PF, Durrett RP, Hunter GL, zur Loye AO, Akinyemi OC, Dec JE, et al. Diesel combustion: an integrated view combining laser diagnostics, chemical kinetics, and empirical validation. SAE Transactions 1999:587-600.

[47] Dec JE. A conceptual model of Dl Diesel combustion based on laser-sheet imaging. SAE Transactions 1997:1319-48.

[48] Siebers DL. Scaling liquid-phase fuel penetration in diesel sprays based on mixing-limited vaporization. SAE Transactions 1999:703-28.

[49] Siebers DL. Liquid-phase fuel penetration in diesel sprays. SAE Transactions 1998:1205-27.

[50] Riess S, Weiss L, Peter A, Rezaei J, Wensing M. Air entrainment and mixture distribution in Diesel sprays investigated by optical measurement techniques. International Journal of Engine Research 2018;19:120-33.

[51] Peter A, Klima T, Riess S, Weiss L, Braeuer A, Wensing M. Quantitative mixture formation analysis of diesel sprays. ICLASS 2018, 14th Triennial International Conference on Liquid Atomization and Spray Systems, Chicago, IL, USA, July 22-26, 2018.

[52] Curran HJ, Fisher EM, Glaude P-A, Marinov NM, Pitz W, Westbrook C, et al. Detailed chemical kinetic modeling of diesel combustion with oxygenated fuels. Sae Transactions 2001:514-21.

[53] Siebers D, Higgins B, Pickett L. Flame lift-off on direct-injection diesel fuel jets: oxygen concentration effects. Sae Transactions 2002:1490-509.

[54] Dec JE, Kelly-Zion PL. The effects of injection timing and diluent addition on late-combustion soot burnout in a DI diesel engine based on simultaneous 2-D imaging of OH and soot. SAE Technical Paper 2000-01-0238; 2000.

[55] Hong Z, Davidson D, Vasu S, Hanson R. The effect of oxygenates on soot formation in rich heptane mixtures: a shock tube study. Fuel 2009;88:1901-6.

[56] Mathieu O, Chaumeix N, Paillard C-E. Soot formation from a distillation cut of a Fischer–Tropsch diesel fuel: A shock tube study. Combustion and Flame 2012;159:2192-201.

[57] Moss J, Aksit I. Modelling soot formation in a laminar diffusion flame burning a surrogate kerosene fuel. Proceedings of the Combustion Institute 2007;31:3139-46.

[58] de Andrade Oliveira M, Olofsson N-E, Johnsson J, Bladh H, Lantz A, Li B, et al. Soot, PAH and OH measurements in vaporized liquid fuel flames. Fuel 2013;112:145-52.

[59] Lapuerta M, Barba J, Sediako AD, Kholghy MR, Thomson MJ. Morphological analysis of soot agglomerates from biodiesel surrogates in a coflow burner. Journal of Aerosol Science 2017;111:65-74.

[60] Inal F, Senkan SM. Effects of equivalence ratio on species and soot concentrations in premixed n-heptane flames. Combustion and Flame 2002;131:16-28.

[61] D'Anna A, Alfe M, Apicella B, Tregrossi A, Ciajolo A. Effect of fuel/air ratio and aromaticity on sooting behavior of premixed heptane flames. Energy & Fuels 2007;21:2655-62.

[62] Solero G. Experimental analysis of the influence of inert nano-additives upon combustion of diesel sprays. Nanoscience and Nanotechnology 2012;2:129-33.

[63] Lemaire R, Faccinetto A, Therssen E, Ziskind M, Focsa C, Desgroux P. Experimental comparison of soot formation in turbulent flames of diesel and surrogate diesel fuels. Proceedings of the Combustion Institute 2009;32:737-44.

[64] Du C, Andersson S, Andersson M. Two-dimensional measurements of soot in a turbulent diffusion diesel flame: the effects of injection pressure, nozzle orifice diameter, and gas density. Combustion Science and Technology 2018;190:1659-88.

[65] Matti Maricq M. Physical and chemical comparison of soot in hydrocarbon and biodiesel fuel diffusion flames: A study of model and commercial fuels. Combustion and Flame 2011;158:105-16.

[66] Lemaire R, Maugendre M, Schuller T, Therssen E, Yon J. Original use of a direct injection high efficiency nebulizer for the standardization of liquid fuels spray flames. Review of Scientific Instruments 2009;80:105105.

[67] Tian B, Chong C, Fan L, Ng J-H, Zhang C, Hochgreb S. Soot volume fraction measurements over laminar pool flames of biofuels, diesel and blends. Proceedings of the Combustion Institute 2019;37:877-84.

[68] Gertsmann J, Demetri EP, Jacobs JN, Pickard DW. Vaporizing diesel burner. United States: Advanced Mechanical Technology, Inc., Newton, MA (USA) NOV; NOV-91-038080; EDB-92-060629; 1991.

[69] Bryce DJ, Ladommatos N, Zhao H. Quantitative investigation of soot distribution by laser-induced incandescence. Applied Optics 2000;39:5012-22.

[70] Khalife E, Tabatabaei M, Demirbas A, Aghbashlo M. Impacts of additives on performance and emission characteristics of diesel engines during steady state operation. Progress in energy and Combustion Science 2017;59:32-78.

[71] Wang X, Cheung C, Di Y, Huang Z. Diesel engine gaseous and particle emissions fueled with diesel–oxygenate blends. Fuel 2012;94:317-23.

[72] Batt RJ, McMillan JA, Bradbury I. Lubricity additives-performance and no-harm effects in low sulfur fuels. SAE Transactions, 1996, 1380-1389.

[73] Barbour R, Arters D, Dietz J, Macduff M, Panesar A, Quigley R. Diesel Detergent Additive Responses in Modern, High-Speed, Direct-Injection, Light-Duty Engines. SAE Technical Paper 2007-01-2001; 2007.

[74] Reid J, Burgess V. Fuel composition comprising detergent and quanternary ammonium salt additive. Google Patents; 2013.

[75] Cheung C, Zhu L, Huang Z. Regulated and unregulated emissions from a diesel engine fueled with biodiesel and biodiesel blended with methanol. Atmospheric Environment 2009;43:4865-72.

[76] Wang H, Reitz RD, Yao M, Yang B, Jiao Q, Qiu L. Development of an n-heptane-n-butanol-PAH mechanism and its application for combustion and soot prediction. Combustion and Flame 2013;160:504-19.

[77] Buyukkaya E, Benli S, Karaaslan S, Guru M. Effects of trout-oil methyl ester on a diesel engine performance and emission characteristics. Energy Conversion and Management 2013;69:41-8.

[78] Huang H, Zhou C, Liu Q, Wang Q, Wang X. An experimental study on the combustion and emission characteristics of a diesel engine under low temperature combustion of diesel/gasoline/n-butanol blends. Applied Energy 2016;170:219-31.

[79] Imtenan S, Masjuki H, Varman M, Kalam M, Arbab M, Sajjad H, et al. Impact of oxygenated additives to palm and jatropha biodiesel blends in the context of performance and emissions characteristics of a light-duty diesel engine. Energy Conversion and Management 2014;83:149-58.

[80] Sadeghinezhad E, Kazi S, Sadeghinejad F, Badarudin A, Mehrali M, Sadri R, et al. A comprehensive literature review of bio-fuel performance in internal combustion engine and relevant costs involvement. Renewable and Sustainable Energy Reviews 2014;30:29-44.

[81] Lapuerta M, Armas O, García-Contreras R. Effect of ethanol on blending stability and diesel engine emissions. Energy & Fuels 2009;23:4343-54.

[82] Herreros J, Schroer K, Sukjit E, Tsolakis A. Extending the environmental benefits of ethanol–diesel blends through DGE incorporation. Applied Energy 2015;146:335-43.

[83] Happonen M, Heikkilä J, Aakko-Saksa P, Murtonen T, Lehto K, Rostedt A, et al. Diesel exhaust emissions and particle hygroscopicity with HVO fuel-oxygenate blend. Fuel 2013;103:380-6.

[84] Patil A, Taji S. Effect of oxygenated fuel additive on diesel engine performance and emission: A review. IOSR Journal of Mechanical and Civil Engineering (IOSR-JMCE) 2013:30-5.

[85] López AF, Cadrazco M, Agudelo AF, Corredor LA, Vélez JA, Agudelo JR. Impact of n-butanol and hydrous ethanol fumigation on the performance and pollutant emissions of an automotive diesel engine. Fuel 2015;153:483-91.

[86] Zhang Z, Tsang K, Cheung C, Chan T, Yao C. Effect of fumigation methanol and ethanol on the gaseous and particulate emissions of a direct-injection diesel engine. Atmospheric Environment 2011;45:2001-8.

[87] Giakoumis EG, Rakopoulos CD, Dimaratos AM, Rakopoulos DC. Exhaust emissions with ethanol or n-butanol diesel fuel blends during transient operation: a review. Renewable and Sustainable Energy Reviews 2013;17:170-90.

[88] Cheng A, Dibble RW, Buchholz BA. The effect of oxygenates on diesel engine particulate matter. SAE Technical Paper 2002-01-1705; 2002.

[89] Beatrice C, Bertoli C, Del Giacomo N, Migliaccio Mn. Potentiality of oxygenated synthetic fuel and reformulated fuel on emissions from a modern DI diesel engine. SAE Transactions 1999:1905-12.

[90] Liotta FJ, Montalvo DM. The effect of oxygenated fuels on emissions from a modern heavy-duty diesel engine. SAE Technical Paper 932734; 1993.

[91] Yoon SH, Cha JP, Lee CS. An investigation of the effects of spray angle and injection strategy on dimethyl ether (DME) combustion and exhaust emission characteristics in a common-rail diesel engine. Fuel Processing Technology 2010;91:1364-72.

[92] Goto S, Oguma M, Suzuki S. Research and development of a medium duty DME truck. SAE Technical Paper 2005-01-2194; 2005.

[93] Mueller CJ, Pitz WJ, Pickett LM, Martin GC, Siebers DL, Westbrook CK. Effects of oxygenates on soot processes in DI diesel engines: experiments and numerical simulations. SAE Transactions 2003:964-82.

[94] Pellegrini L, Marchionna M, Patrini R, Beatrice C, Del Giacomo N, Guido C. Combustion behaviour and emission performance of neat and blended polyoxymethylene dimethyl ethers in a light-duty diesel engine. SAE Technical Paper 2012-01-1053; 2012.

[95] Westbrook CK, Pitz WJ, Curran HJ. Chemical kinetic modeling study of the effects of oxygenated hydrocarbons on soot emissions from diesel engines. The Journal of Physical Chemistry A 2006;110:6912-22.

[96] Palazzo N, Zigan L, Huber FJT, Will S. Impact of Oxygenated Additives on Soot Properties During Diesel Combustion. Energies 2021;14.

[97] Kenney TE, Gardner TP, Low SS, Eckstrom JC, Wolf LR, Korn SJ, et al. Overall results: Phase I ad hoc diesel fuel test program. SAE Transactions 2001:8-32.

[98] Sirman MB, Owens EC, Whitney KA. Emissions comparison of alternative fuels in an advanced automotive diesel engine. SAE Transactions 2000:2166-76.

[99] Pellegrini L, Marchionna M, Patrini R, Florio S. Emission performance of neat and blended polyoxymethylene dimethyl ethers in an old light-duty diesel car. SAE Technical Paper 2013-01-1035; 2013.

[100] Iannuzzi SE, Barro C, Boulouchos K, Burger J. Combustion behavior and soot formation/oxidation of oxygenated fuels in a cylindrical constant volume chamber. Fuel 2016;167:49-59.

[101] Iannuzzi SE, Barro C, Boulouchos K, Burger J. POMDME-diesel blends: Evaluation of performance and exhaust emissions in a single cylinder heavy-duty diesel engine. Fuel 2017;203:57-67.

[102] Arnal C, Alfè M, Gargiulo V, Ciajolo A, Alzueta MU, Millera Á, et al. Characterization of soot. Cleaner Combustion: Springer; 2013. p. 333-62.

[103] Huber FJ, Altenhoff M, Will S. A mobile system for a comprehensive online-characterization of nanoparticle aggregates based on wide-angle light scattering and laser-induced incandescence. Review of Scientific Instruments 2016;87:053102.

[104] Michelsen H, Schulz C, Smallwood G, Will S. Laser-induced incandescence: Particulate diagnostics for combustion, atmospheric, and industrial applications. Progress in Energy and Combustion Science 2015;51:2-48.

[105] Maffi S, De Iuliis S, Cignoli F, Zizak G. Investigation on thermal accommodation coefficient and soot absorption function with two-color Tire-LII technique in rich premixed flames. Applied Physics B 2011;104:357-66.

[106] Snelling DR, Liu F, Smallwood GJ, Gülder ÖL. Determination of the soot absorption function and thermal accommodation coefficient using low-fluence LII in a laminar coflow ethylene diffusion flame. Combustion and Flame 2004;136:180-90.

[107] Michelsen HA. Understanding and predicting the temporal response of laser-induced incandescence from carbonaceous particles. The Journal of Chemical Physics 2003;118:7012-45.

[108] Daun K, Smallwood G, Liu F. Investigation of thermal accommodation coefficients in time-resolved laser-induced incandescence. Journal of Heat Transfer 2008;130.

[109] Yon J, Ouf F-X, Hebert D, Mitchell JB, Teuscher N, Le Garrec J-L, et al. Investigation of soot oxidation by coupling LII, SAXS and scattering measurements. Combustion and Flame 2018;190:441-53.

[110] Liu F, Smallwood GJ. Relationship between soot volume fraction and LII signal in AC-LII: effect of primary soot particle diameter polydispersity. Applied Physics B 2013;112:307-19.

[111] Liu F, Smallwood GJ, Snelling DR. Effects of primary particle diameter and aggregate size distribution on the temperature of soot particles heated by pulsed lasers. Journal of Quantitative Spectroscopy and Radiative Transfer 2005;93:301-12.

[112] Liu F, Stagg BJ, Snelling DR, Smallwood GJ. Effects of primary soot particle size distribution on the temperature of soot particles heated by a nanosecond pulsed laser in an atmospheric laminar diffusion flame. International Journal of Heat and Mass Transfer 2006;49:777-88.

[113] Snelling D, Liu F, Smallwood G, Gülder Ö. Evaluation of the nanoscale heat and mass transfer model of LII: prediction of the excitation intensity. 34th National Heat Transfer Conference2000.

[114] Michelsen H, Liu F, Kock BF, Bladh H, Boïarciuc A, Charwath M, et al. Modeling laser-induced incandescence of soot: a summary and comparison of LII models. Applied Physics B 2007;87:503-21.

[115] Shaddix CR, Harrington JE, Smyth KC. Quantitative measurements of enhanced soot production in a flickering methane/air diffusion flame. Combustion and Flame 1994;99:723-32.

[116] Shaddix CR, Smyth KC. Laser-induced incandescence measurements of soot production in steady and flickering methane, propane, and ethylene diffusion flames. Combustion and Flame 1996;107:418-52.

[117] Bladh H, Johnsson J, Olofsson N-E, Bohlin A, Bengtsson P-E. Optical soot characterization using two-color laser-induced incandescence (2C-LII) in the soot growth region of a premixed flat flame. Proceedings of the Combustion Institute 2011;33:641-8.

[118] Eremin A, Gurentsov E, Popova E, Priemchenko K. Size dependence of complex refractive index function of growing nanoparticles. Applied Physics B 2011;104:285-95.

[119] Axelsson B, Collin R, Bengtsson P-E. Laser-induced incandescence for soot particle size measurements in premixed flat flames. Applied Optics 2000;39:3683-90.

[120] Bauer FJ, Daun KJ, Huber FJT, Will S. Can soot primary particle size distributions be determined using laser-induced incandescence? Applied Physics B 2019;125:109.

[121] Walsh KT, Fielding J, Smooke MD, Long MB. Experimental and computational study of temperature, species, and soot in buoyant and non-buoyant coflow laminar diffusion flames. Proceedings of the Combustion Institute 2000;28:1973-9.

[122] McEnally CS, Pfefferle LD. Improved sooting tendency measurements for aromatic hydrocarbons and their implications for naphthalene formation pathways. Combustion and Flame 2007;148:210–22.

[123] Vander Wal RL, Jensen KA, Choi MY. Simultaneous laser-induced emission of soot and polycyclic aromatic hydrocarbons within a gas-jet diffusion flame. Combustion and Flame 1997;109:399-414.

[124] Reimann J, Will S. Optical diagnostics on sooting laminar diffusion flames in microgravity. Microgravity Science and Technology 2005;16:333-7.

[125] Das DD, McEnally CS, Pfefferle LD. Sooting tendencies of unsaturated esters in nonpremixed flames. Combustion and Flame 2015;162:1489-97.

[126] Kock BF, Tribalet B, Schulz C, Roth P. Two-color time-resolved LII applied to soot particle sizing in the cylinder of a Diesel engine. Combustion and Flame 2006;147:79-92.

[127] Schraml S, Will S, Leipertz A. Simultaneous measurement of soot mass concentration and primary particle size in the exhaust of a DI diesel engine by time-resolved laser-induced incandescence (TIRE-LII). SAE Transactions, 1999, 82-89.

[128] Wiltafsky G, Stolz W, Köhler J, Espey C. The quantification of laser-induced incandescence (LII) for planar time resolved measurements of the soot volume fraction in a combusting diesel jet. SAE Transactions, 1996, 978-988.

[129] Samson R, Mulholland GW, Gentry J. Structural analysis of soot agglomerates. Langmuir 1987;3:272-81.

[130] Köylü UO, Faeth G. Optical properties of soot in buoyant laminar diffusion flames. Journal of Heat Transfer 1994;116:971-9.

[131] Huber FJT, Will S, Daun KJ. Sizing aerosolized fractal nanoparticle aggregates through Bayesian analysis of wide-angle light scattering (WALS) data. Journal of Quantitative Spectroscopy and Radiative Transfer 2016;184:27-39.

[132] Sorensen C, Cai J, Lu N. Light-scattering measurements of monomer size, monomers per aggregate, and fractal dimension for soot aggregates in flames. Applied Optics 1992;31:6547-57.

[133] Altenhoff M, Aßmann S, Perlitz JF, Huber FJ, Will S. Soot aggregate sizing in an extended premixed flame by high-resolution two-dimensional multi-angle light scattering (2D-MALS). Applied Physics B 2019;125:176.

[134] Santoro R, Semerjian H, Dobbins R. Soot particle measurements in diffusion flames. Combustion and Flame 1983;51:203-18.

[135] Puri R, Richardson T, Santoro R, Dobbins R. Aerosol dynamic processes of soot aggregates in a laminar ethene diffusion flame. Combustion and Flame 1993;92:320-33.

[136] Hull P, Shepherd I, Hunt A. Modeling light scattering from diesel soot particles. Applied Optics 2004;43:3433-41.

[137] Oltmann H, Reimann J, Will S. Wide-angle light scattering (WALS) for soot aggregate characterization. Combustion and Flame 2010;157:516-22.

[138] Sorensen C, Wang G. Size distribution effect on the power law regime of the structure factor of fractal aggregates. Physical Review E 1999;60:7143.

[139] Oltmann H, Reimann J, Will S. Single-shot measurement of soot aggregate sizes by wide-angle light scattering (WALS). Applied Physics B 2012;106:171-83.

[140] Kuhn PB, Ma B, Connelly BC, Smooke MD, Long MB. Soot and thin-filament pyrometry using a color digital camera. Proceedings of the Combustion Institute 2011;33:743-50.

[141] Levendis YA, Estrada KR, Hottel HC. Development of multicolor pyrometers to monitor the transient response of burning carbonaceous particles. Review of Scientific Instruments 1992;63:3608-22.

[142] Lee W, Na YD. Soot study in laminar diffusion flames at elevated pressure using two-color pyrometry and Abel inversion. JSME International Journal Series B Fluids and Thermal Engineering 2000;43:550-5.

[143] Cignoli F, De Iuliis S, Manta V, Zizak G. Two-dimensional two-wavelength emission technique for soot diagnostics. Applied Optics 2001;40:5370-8.

[144] Musculus MP, Singh S, Reitz RD. Gradient effects on two-color soot optical pyrometry in a heavy-duty DI diesel engine. Combustion and Flame 2008;153:216-27.

[145] Dreyer JA, Slavchov RI, Rees EJ, Akroyd J, Salamanca M, Mosbach S, et al. Improved methodology for performing the inverse Abel transform of flame images for color ratio pyrometry. Applied Optics 2019;58:2662-70.

[146] Huang Q-x, Wang F, Liu D, Ma Z-y, Yan J-h, Chi Y, et al. Reconstruction of soot temperature and volume fraction profiles of an asymmetric flame using stereoscopic tomography. Combustion and Flame 2009;156:565-73.

[147] Best P, Chien P, Carangelo R, Solomon P, Danchak M, Ilovici I. Tomographic reconstruction of FT-IR emission and transmission spectra in a sooting laminar diffusion flame: species concentrations and temperatures. Combustion and Flame 1991;85:309-18.

[148] Daun KJ, Thomson KA, Liu F, Smallwood GJ. Deconvolution of axisymmetric flame properties using Tikhonov regularization. Applied Optics 2006;45:4638-46.

[149] Wiedensohler A. An approximation of the bipolar charge distribution for particles in the submicron size range. Journal of Aerosol Science 1988;19:387-9.

[150] Hinds WC. Aerosol technology: properties, behavior, and measurement of airborne particles: John Wiley & Sons; 1999.

[151] Cunningham E. On the velocity of steady fall of spherical particles through fluid medium. Proceedings of the Royal Society of London Series A, Containing Papers of a Mathematical and Physical Character 1910;83:357-65.

[152] Allen MD, Raabe OG. Slip correction measurements of spherical solid aerosol particles in an improved Millikan apparatus. Aerosol Science and Technology 1985;4:269-86.

[153] Pei Y, Mehl M, Liu W, Lu T, Pitz WJ, Som S. A multicomponent blend as a diesel fuel surrogate for compression ignition engine applications. Journal of Engineering for Gas Turbines and Power 2015;137:111502.

[154] Roubaud A, Lemaire O, Minetti R, Sochet L. High pressure auto-ignition and oxidation mechanisms of o-xylene, o-ethyltoluene, and n-butylbenzene between 600 and 900 K. Combustion and Flame 2000;123:561-71.

[155] Palazzo N, Kögl M, Bauer P, Mannazhi MN, Zigan L, Huber FJT, et al. Investigation of soot formation in a novel diesel fuel burner. Energies 2019;12:1993.

[156] Di Blasi C. Modeling chemical and physical processes of wood and biomass pyrolysis. Progress in Energy and Combustion Science 2008;34:47-90.

[157] Zhao B, Yang Z, Wang J, Johnston MV, Wang H. Analysis of soot nanoparticles in a laminar premixed ethylene flame by scanning mobility particle sizer. Aerosol Science & Technology 2003;37:611-20.

[158] Anselmi-Tamburini U, Campari G, Spinolo G, Lupotto P. A two-color spatial-scanning pyrometer for the determination of temperature profiles in combustion synthesis reactions. Review of Scientific Instruments 1995;66:5006-14.

[159] Haltermann G. Certificate 100000106008.

[160] Olofsson N-E, Simonsson J, Török S, Bladh H, Bengtsson P-E. Evolution of properties for aging soot in premixed flat flames studied by laser-induced incandescence and elastic light scattering. Applied Physics B 2015;119:669-83.

[161] De Iuliis S, Cignoli F, Zizak G. Two-color laser-induced incandescence (2C-LII) technique for absolute soot volume fraction measurements in flames. Applied Optics 2005;44:7414-23.

[162] Tran MK, Dunn-Rankin D, Pham TK. Characterizing sooting propensity in biofuel–diesel flames. Combustion and Flame 2012;159:2181-91.

[163] Flower W, Bowman C. Soot production in axisymmetric laminar diffusion flames at pressures from one to ten atmospheres. Symposium (International) on Combustion: Elsevier; 1988. p. 1115-24.

[164] Sorensen C. The mobility of fractal aggregates: a review. Aerosol Science and Technology 2011;45:765-79.

[165] Frusteri F, Spadaro L, Beatrice C, Guido C. Oxygenated additives production for diesel engine emission improvement. Chemical Engineering Journal 2007;134:239-45.

[166] Pepiot-Desjardins P, Pitsch H, Malhotra R, Kirby S, Boehman A. Structural group analysis for soot reduction tendency of oxygenated fuels. Combustion and Flame 2008;154:191-205.

[167] Vertin KD, Ohi JM, Naegeli DW, Childress KH, Hagen GP, McCarthy CI, et al. Methylal and methylal-diesel blended fuels for use in compression-ignition engines. SAE Technical Paper 1999-01-1508; 1999.

[168] Song KH, Litzinger TA. Effects of dimethyoxymethane blending into diesel fuel on soot in an optically accessible DI diesel engine. Combustion Science and Technology 2006;178:2249-80.

[169] Kocis D, Song K, Lee H, Litzinger T. Effects of dimethoxymethane and dimethylcarbonate on soot production in an optically-accessible DI diesel engine. SAE Transactions 2000:2299-308.

[170] Popp T, Lechner R, Becker M, Hebauer M, O'Connell N, Brautsch M. Potentials of OME/diesel blends for stationary power production–improving emission characteristics of a diesel CHP unit. Applied Thermal Engineering 2019;153:483-92.